
# 2018 STIC Incentive Project 12 Month Report - BFRP-RC Standardization

## Fed Project No: STIC-0004-00A; FPID 443377-1

This is the second report for the Basalt Fiber-Reinforced Polymer (BFRP) Bar Standardization for Reinforced Concrete (RC) with the FHWA allocation memorandum dated March 1, 2018. This report covers a slightly extended period from November 2018 until May 2019, since there were a number of key work products completed in April/May 2019.

## Description of the proposed work

Develop standard (guide) design specification, and standard material and construction specifications for basalt fiber-reinforced polymer (BFRP) bars for the internal reinforcement of structural concrete. Tasks involve *(highlighted tasks are completed or partially completed)*:

i. Establishing design and durability parameters using current state-of-the-art BFRP test data with ***ACI 440.1R*** as a design model framework, supplemented with ***AASHTO's LRFD Bridge Design Guide Specification for GFRP Reinforced Concrete - 2nd Edition (BDGS-2)*** - *published December 2018;*

ii. Develop FDOT design modifications to ***BDGS-2*** for inclusion of BFRP reinforcing - *see BDV30 986-01 Deliverable #3 (**Attachment 3**) to be expanded into the Structures Manual by July 17 cutoff;*

iii. Develop FDOT material specification for acceptance based on the 2017 ***ASTM D7957: Standard Specification for Solid Round Glass Fiber Reinforced Polymer Bars for Concrete Reinforcement*** - *see BDV30 986-01 Deliverable #4 April 2019 (**Attachment 4**), and FDOT **Materials Manual** 12.1 revisions May 2019 (**Attachment MM**);*

iv. Develop FDOT Construction Specifications based on ***BDGS-2*** and ***FDOT Specification Section 415 & 932*** GFRP reinforcing specifications - *Prepared for Internal/Industry review, see **Attachment CS**.*

v. Develop BFRP Reinforcing Database for collection of current and future test results based on FDOT GFRP reinforcing test library developed under ***BDV30 977-18*** and new research project ***BE694*** *"Testing Protocol and Material Specification for BFRP Rebars". Initial test data from **BDV30 986-01** in Deliverable #2 (**Attachment 2**);*

vi. Deliver a designer focus live workshop at the end of the STIC project in central Florida (and national event if funding permits). Post the delivered training material on ***FDOT FRP Innovation*** website for broader access and future updating - (a) BFRP-RC Designer Training schedule for 3 sessions at the FDOT Transportation Symposium (FTS2019) on June 4th; (b) Mini-symposium on BFRP-RC for coastal and marine structures is organized for the Bridge Engineering Institute conference (***BEI2019***) July 23-25, additionally several papers on BFRP-RC have been accepted for presentation by the

STIC project participants; (c) The ***FTS2019*** BFRP-RC Designer Training is also being offered to Hawaii DOT Bridge Office on July 22, 2019;

vii. Demonstration Project - Plans developed and contract awarded for BFRP-RC link-slab on pedestrian bridge in Port Charlotte, FL (along US 41). Construction delayed until September 2019 due to utility coordination issues. Monitoring contract executed with University of North Florida under ***BDV29 986-02***, to instrument link-slab and BFRP rebar to monitor initial and longer-term response. see Deliverable #1 (**Attachment 5**) for literature review, and draft Deliverable #2 (**Attachment 6**) for preliminary instrumentation plan.

## Project Breakdown and Schedule

The project is broken into several phases with distinct tasks some of which were not completely scoped, pending progress and findings in the early Phases. **Table 1** shows a summary of the project Phases. It is anticipated that there will be at least two services contracts with Florida Universities for the various tasks of: Existing information collection and curation (Phase 1a); Development of model specifications and standards (Phase 1b); Provision of supplemental test data and analysis (Phase 2a); Development of Materials Database (Phase 2b); Technology Transfer (Phase 3).

| **PROJECT PHASE** | **1** | **2** | **3** |
| --- | --- | --- | --- |
| **PROJECT WORK TASKS** | Develop Standards: ***(BDV30 986-01)***<br>• Design Spec.<br>• Materials Qualification and Verification Test Procedures<br>• Construction Spec. | • Full-scale Link-Slab Demo and Monitoring ***(BDV34 986-02)***<br>• Supplemental Bar Testing<br>• BFRP Database Completion ***(BDV30 986-01)*** | • Technology Transfer ***(FTS2019 & BEI2019)***<br>• Final Report |
| **PROJECT DELIVERABLES** | • LRFD Guide Design Spec. *(in AASHTO format)*<br>• Testing Spec. *(in ASTM format)*<br>• Construction Spec. *(in FDOT format)* | • Test Reports<br>• Electronic Database of physical and mechanical properties | $T^2$ Workshop in central Florida for information dissemination and training |
| | • | • | |
| **PROJECT TIMELINE** | Month 1-11 | Month 7-15 | Month 17 |

***Table 1- Project Summary*** ***(update 3/28/19)***

### *Activities March-September 2018*:

1. 04/05/2018 - Funding authorization from Division FHWA approved under 2018 STIC Incentive Proposal: STIC-004-00A / FPID 443377-1;

2. 05/21/2018 - Procurement completed for Principle Investigator of Phase 1 & 2b: Technology Review, Specifications & Database Development. Research Task Work Order (TWO) issued under FDOT research project ***BDV30-986-01***;
3. 05/30/2018 - Kickoff meeting held for ***BDV30-986-01***;
4. 09/11/2018 - ***BDV30-986-01***, Task 1 completed and Deliverable 1 (BFRP Technology Review Report) approved;
5. 09/14/2018 - Collaboration meeting on design of Full-Scale demonstration of BFRP-RC element for testing and monitoring.

***Activities October-May 2019*:**

1. 12/7/2018 - ***BDV30-986-01***, Task Work Order Amendment#1 executed for time extension due to manufacturer delays in providing BFRP rebar samples for testing.
2. 1/11/2019 - Procurement completed for Principle Investigator of Phase 2a BFRP-FRC Link-Slab Demonstration Project. Research Task Work Order issued under FDOT research project ***BDV34-986-02***. See **Appendix A** for the scope.
3. 2/6/2019 - ***BDV30-986-02***, (BFRP-FRC Link-Slab Demonstration Project) Kickoff Meeting held. See **Appendix B** for the meeting presentation.
4. 2/4/2019 - ***BDV30-986-01***, Draft Deliverable 2 (BFRP Testing Procedure and Results) submitted. Revisions requested by PM.
5. 2/28/2019 - ***BDV30-986-01***, Task 2 completed and Deliverable 2 (BFRP Testing Procedure and Results) approved. See **Appendix C** for the full report
6. 2/28/2019 - ***BDV30-986-01***, Draft Deliverable 3 (BFRP Material Specification Recommendation Report) submitted. Revisions requested by PM.
7. 3/26/2019 - ***BDV30-986-01***, Task 3 completed and Deliverable 3 (BFRP Material Specification Recommendations) approved. See **Appendix D** for the full report
8. 3/4/2019 - ***BDV30-986-02***, Draft Deliverable 1 (BFRP-FRC Link-Slab Demonstration Project - Literature Review) submitted. Revisions requested by PM.
9. 3/24/2019 - ***BDV30-986-02***, Task 1 completed and Deliverable 1 (BFRP-FRC Link-Slab Literature Review) approved. See **Appendix E** for the full report.
10. 5/4/2019 - ***BDV30-986-01***, Draft Deliverable 4 (BFRP Design Specification Recommendations) submitted. Revisions requested by PM.
11. 5/13/2019 - ***BDV30-986-02***, Draft Deliverable 2 (BFRP-FRC Link-Slab Demonstration Project: Instrumentation and Monitoring Plan) submitted and under review.
12. ***BEI-2019*** Mini-Symposium organization with Prof. Jimmy Kim (TRB co-sponsored event June 22-25: *http://www.beibridge.org/BEI2019.html* ). Two Abstracts accepted for presentation See **Appendix F**:
    a. *Basalt FRP-RC Standardization for Florida DOT Structures*
    b. *Evaluation of Bond-to-Concrete Characteristic of Basalt Fiber-Reinforced Polymer Rebars for Design Code Implementation*

## Planned Activities for May 2018-November 2019

*Phase 1:*

1. Complete some minor outstanding water absorption testing characterization for one BFRP bar manufacturers (BDV30-986-01, Task 2)
2. Develop Material & Construction Specifications in FDOT format (BDV30-986-01, Task 3)

3. Provide Design Recommendations for ***FDOT Structures Manual*** - FRPG Guide Specifications (BDV30-986-01, Task 4)
4. Prepare Draft Final Report BDV30-986-01

*Phase 2:*

5. Develop mockup testing specimen for Link-Slab Field Demonstration BFRP-RC element (Phase 2a)
6. Coordinate with District 1 EOR on final design, instrumentation, and monitoring for full-scale FRP-RC Link-Slab under FPID 435390-1-52-01: US 41 from Midway Blvd to Enterprise project.
7. February 27, 2019 construction letting of FPID 435390-1-52-01: US 41 from Midway Blvd to Enterprise project.
8. Complete initial database for BFRP characterization (***BDV30-986-01***, Task 2 results)

*Phase 3*:

9. Conduct Designer training of BFRP-RC Design at FDOT Transportation Symposium in Orlando on 6/4/2019.
10. Present two papers at BEI-2019 Mini-Symposium on BFRR for marine and coastal structures.
11. Update ***FRP-Innovation*** webpage with final reports, papers and presentation

## Budget

| Project Line Item | FHWA STIC Contribution | FDOT In-Kind Match (20%) | Total Budget |
|---|---|---|---|
| **Phase 1** *(100% BDV30 986-01)* | $48,000 | $12,000 | $60,000 |
| **Phase 2** *(50% BDV30 986-01; 50% SRC/U Testing)* | $36,000 | $9,000 | $45,000 |
| **Phase 3** | $16,000 | $4,000 | $20,000 |
| **Total Project** | **$100,000** | **$25,000** | **$125,000** |

***Table 2- Project Phase Funding Distribution*** ***(update 5/21/18)***

## Project Schedule

| Work Phase | Month | | | | | | | | | | | | | | | | |
|---|---|---|---|---|---|---|---|---|---|---|---|---|---|---|---|---|---|
| | 1 | 2 | 3 | 4 | 5 | 6 | 7 | 8 | 9 | 10 | 11 | 12 | 13 | 14 | 15 | 16 | 17 |
| 1. Develop Design, Materials and Construction Specifications | | | | | | | | | | | | | | | | | |
| 2a. Mockup testing at SRC and/or Full-scale slab instrumentation and monitoring | | | | | | | | | | | | | | | | | |

| | | | | | | | | | | | | | | | | | |
|---|---|---|---|---|---|---|---|---|---|---|---|---|---|---|---|---|---|
| 2b. BFRP Supplemental bar testing and Database development | | | | | | | | | | | | | | | | | |
| 3. Technology Transfer Workshop and Final Report | | | | | | | | | | | | | | | | | |

***Table 3- Project Timeline (update 3/14/18 – Month 1 = April 2018)***

## Appendices include:

Appendix A - University Task Work Order: BDV30 986-02 (BFRP-FRC Link Slab Instrumentation and Monitoring)
Appendix B - Presentation: BDV30 986-02 Kickoff Meeting
Appendix C - Deliverable 2: BDV30 986-01 BFRP Testing Procedure and Results
Appendix D - Deliverable 3: BDV30 986-01 BFRP Material Specification Recommendations
Appendix E - Deliverable 1: BDV30 986-02 BFRP-FRC Link Slab – Literature Review Report
Appendix F - BEI-2019 Accepted Abstracts for BFRP Mini-Symposium


# Appendix A

## University Task Work Order: BDV34 986-02 ((BFRP-FRC Link Slab Instrumentation and Monitoring)

(11 pages)

**EXHIBIT A – SCOPE OF SERVICE**

Project Title: **BRIDGE DECK WITH LINK-SLAB**
**for FPID: 435390-1-52-01: US 41 from Midway Blvd to Enterprise**


Submitted by
Principal Investigator: **Adel ElSafty**, Ph.D., P.E.
University of North Florida
Address: School of Engineering, 1 UNF Drive, Jacksonville, FL 32224-2645
Email Address: adel.el-safty@unf.edu
Phone Number: (904) 620-1398


Submitted to
c/o Steven Nolan
The Florida Department of Transportation
State Structures Design Office
605 Suwannee Street, MS 33
Tallahassee, FL 32399-0450


Dr. Cheresa Y. Boston
Director of Sponsored Research,
University of North Florida, Office of Research and Sponsored Programs
1 UNF Drive, Jacksonville, Florida 32224
Phone: (904) 620-2455, Fax: (904) 620-2457, Email: cheresa.boston@unf.edu


Project Manager: Steven Nolan
Florida Department of Transportation
State Structures Design Office
Email Address: Steven.Nolan@dot.state.fl.us
Phone: (850) 414-4272

December 19, 2018

**BACKGROUND STATEMENT**

***The need for this research:***

Bridge deck joints are costly to buy, install, and maintain. They have provided severe performance and maintenance problems as water and deck drainage contaminated with deicing chemicals leak through the superstructure and onto the pier caps below, thus damaging and eventually completely destroying some vital parts of bridges such as prestressing cable anchorage systems, beams and bearings. Also, debris accumulation in the joints may restrain deck expansion [ElSafty]. In addition, most joints leak posing a major reason for deficient bridges.

One of the best solutions is to adopt jointless bridges and elimination of expansion joints in bridge decks. That has been an effective method of constructing bridges. It corresponds to reduced maintenance and improved bridge-deck life expectancy. It is possible to replace bearing devices with simple elastomeric pads, or totally integrate the superstructure with the supports without any bearings. With the use of jointless bridge decks, there are no joints to purchase nor bearings to maintain, the riding surface is smoother, the initial and life-cycle cost are lower, and there will be a reduction in span bending moments. In conclusion, using a link-slab and making the bridge girders (partially continuous) continuous for live load provides lower cost, improved durability, longer spans, improved seismic performance, better resistance to wind loads, improved structural integrity, and improved riding quality. Current consensus seems to allow elimination of expansion joints on bridges as long as 650 feet. Much longer bridges have occasionally been constructed without reported distress. There is a need for simple guidelines for design and detailing of the popular continuous-for-live-load connection system. Options for jointless bridge deck link-slab are shown in the following figures.

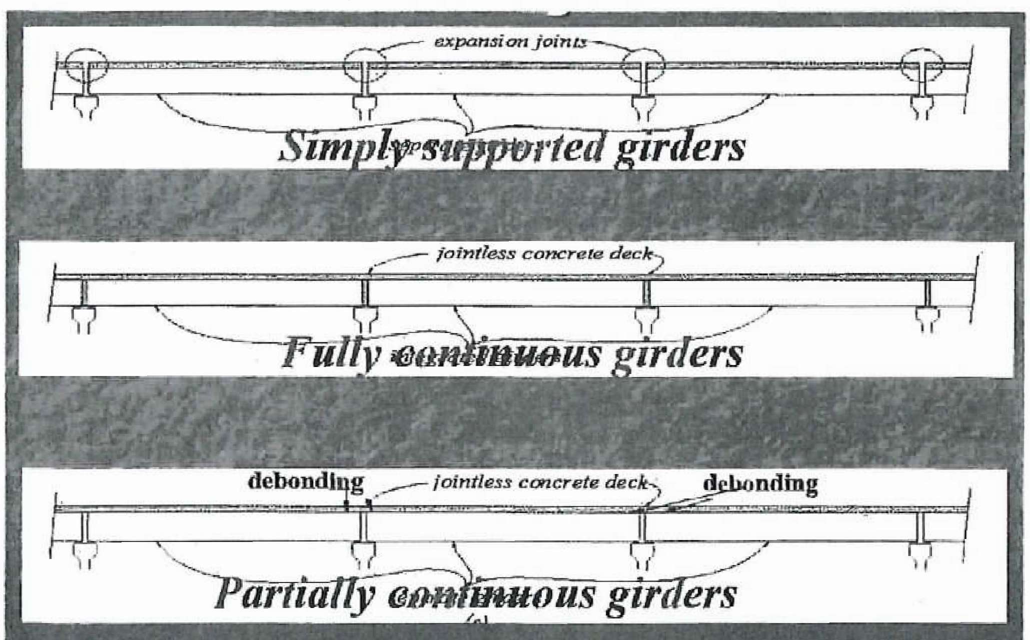


**Fig. 1 Some types of jointless bridge decks**

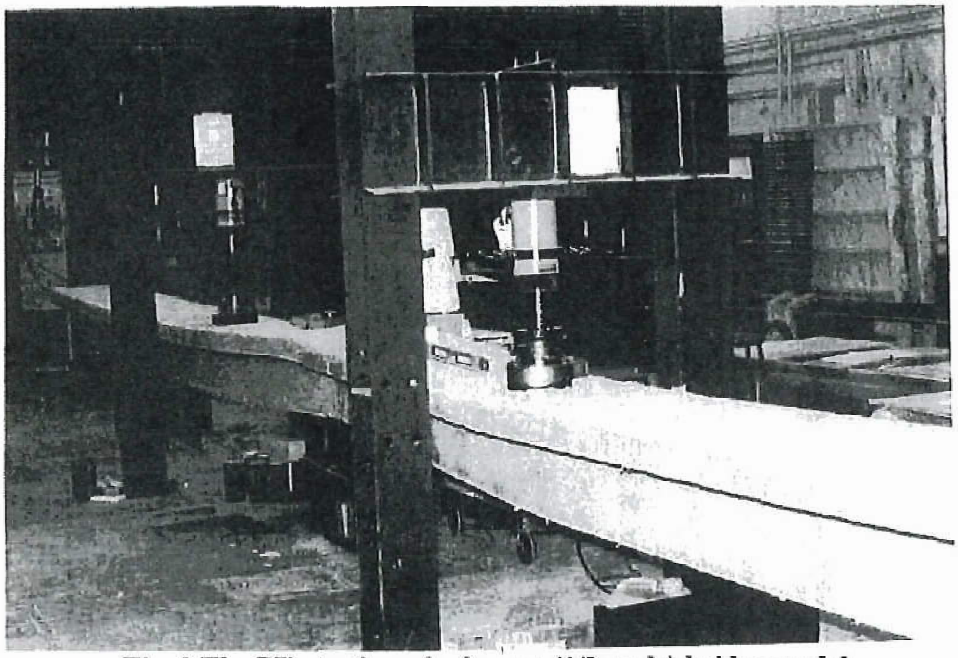
Fig. 2 The PI's testing of a 2-span (1/2-scale) bridge model

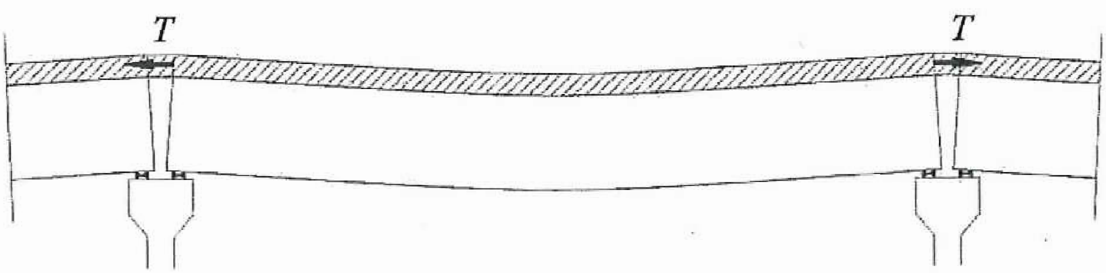


Fig. 3 Continuity caused by linking concrete decks in adjacent spans

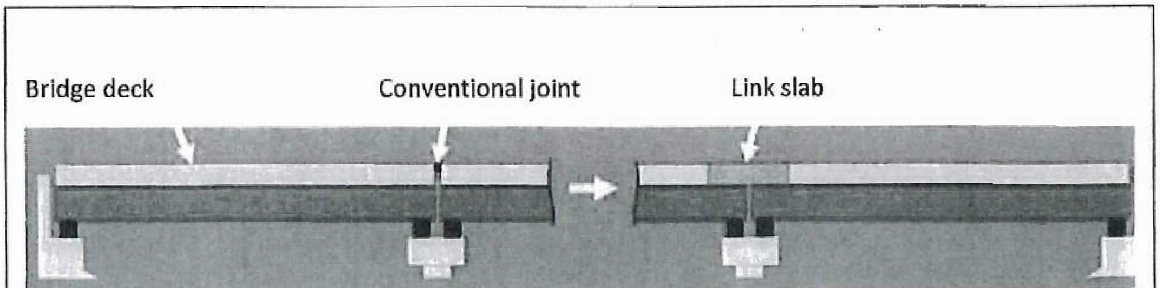


Fig. 4 Link-Slab Option

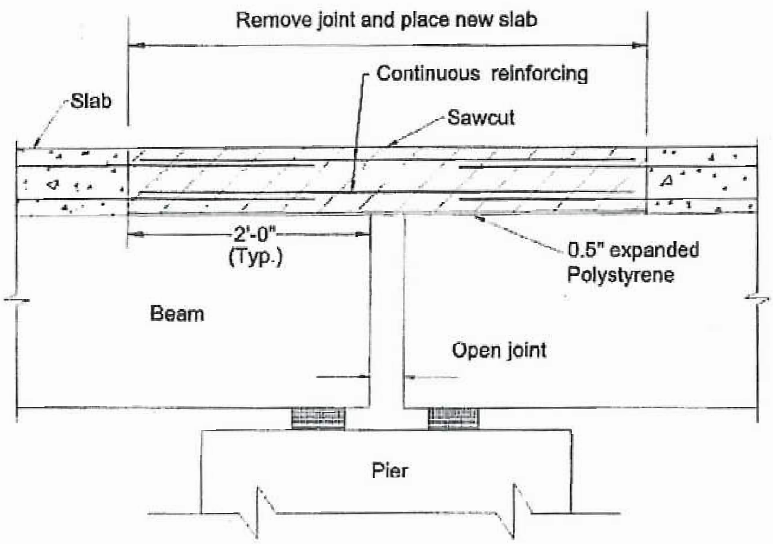


**Fig. 5- Use of link-slab by VDOT for rehabilitation work to eliminate expansion joint**

***Literature Review:***

One of the main factors affecting the durability of bridge structures is the presence of expansion joints at bridge support locations. The inability of current joint systems to provide reliable, long-term, leak-proof performance generally leads to early leakage of chloride- contaminated water through these joints, thereby causing premature corrosion in the deck elements below. This problem is particularly evident in older-type multi-span bridges in which the girders are simply supported at the piers and are separated by expansion joints or simple paved-over joints.

Trend in bridge design has been toward the elimination of joints and bearings in the bridge superstructure. Joints and bearings are expensive in both initial and maintenance costs and can get filled with debris, freeze up, and fail in their task to allow expansion and contraction of the superstructure. They are also a ''weak link'' that can allow deicing chemicals to seep down and corrode bearings and support components. Because the behavior is unknown and designs are cumbersome, jointless bridges are not widely used despite their enormous benefits. There are no standardized design procedures for these bridges, only a list of specifications and design recommendations are available.

In his study, ElSafty (1994) and Zia, Caner, and ElSafty (1998) investigated casting fully-continuous deck over simply supported girders with partial debonding of the deck from the girders ends at supports is investigated, using both numerical and experimental analysis. ElSafty and Okeil (2008) also investigated extending the service life of bridges using continuous decks. Caner and Zia (1998) presented the results of a test program to investigate the behavior of link-slabs connecting two adjacent simple-span girders, and proposes a simple method for designing the link-slab. To illustrate the proposed design method, three design examples were included. Based on the results of this investigation, it was concluded that within the elastic range, the measured deflections, the strains in the girders, and the strains in the link-slab reinforcement were not affected by the variations of support conditions (hinge vs. roller) at the exterior and interior supports. Because the stiffness of the link-slab was much smaller than that of the composite girders, the continuity introduced by the link-slab was negligible. Therefore, each of the two composite girders behaved like a simply supported girder. With the girders being treated as simply -supported, the predicted girder deflections compared closely with the measured deflections of the test specimens.

Li et al. 2003 conducted a research project with MDOT describing the development of durable link-slabs for jointless bridge decks based on strain hardening cementitious composite - engineered cementitious composite (ECC). A simple design guideline was presented. Li et al. 2005 conducted a research project with MDOT on the development of durable link-slabs for jointless bridge decks based on strain hardening cementitious composite - engineered cementitious composite (ECC). Specifically, the superior ductility of ECC was utilized to accommodate bridge deck deformations imposed by girder deflection, concrete shrinkage, and temperature variations, providing a cost-effective solution to a number of deterioration problems associated with bridge deck joints. Based on the findings within, the implementation of a durable ECC link-slab is possible in a standard bridge deck reconstruction scenario. This report includes development of theoretical guidelines for complete design of an ECC link-slab, example calculations, desk references, sample design drawings, material specifications, and contractual special provisions. Load tests conclude that the ECC link-slab functions as designed under bending loads.

To address this problem of bridges with joints, the Ministry of Transportation of Ontario (MTO) has recently rehabilitated a number of bridge decks using a debonded link-slab system to replace the deck joints at the pier locations. To get a better understanding of the performance and reliability of this new rehabilitative technique, MTO recently carried out an experimental research study of the long-term performance of the system on scale test models that were subjected to extensive cyclic loading in the laboratory. At the same time, it carried out a load test of a recently rehabilitated structure to study its structural behavior both before and after the link-slab was constructed. The test structure was instrumented with sensors that measured deflections and strains in the link-slab and girders. Au et al. 2013 described the experimental research study and the behavioral load tests that were carried out, and discusses the results obtained. The experimental study showed that the long-term performance of the link-slab was not affected by the extensive cyclic loading to which the model was subjected, whereas the load testing of the test structure showed that it satisfied the serviceability limit state requirements of the Canadian Highway Bridge Design Code, thus validating the design methodology of the system. Many researchers conducted studies to address link-slab design and performance issues.

**PROJECT OBJECTIVE(S)**

The purpose and objectives of the project are to:

A- Review and comment on the *design detail* of *link-slab options* using Basalt Fiber-Reinforced Polymer (BFRP) and Glass(G) FRP bars for a bridge US 41 (Project FPID: 435390-1-52-01), from Midway Blvd to Enterprise.

B- Identify appropriate instrumentation for monitoring and locations for sensors and instrumentations.
C- Conduct evaluation and organization of data collected from the field instrumentations on the bridge link-slab.

**PROJECT KICKOFF TELECONFERENCE**

The principal investigator will schedule a kickoff meeting that shall be held within the first 30 days of task work order execution. The kickoff meeting will consist of a webinar at least 30 minutes in length. The purpose of the meeting is to review the tasks, deliverables, deployment plan, timeline, and expected/anticipated project outcomes and their potential for implementation and benefits.

The principal investigator shall prepare a presentation following the template provided at http://www.fdot.gov/research/Program_Information/Research.Performance/kickoff.meeting.pdf The project manager, principal investigator, and research performance coordinator shall attend. Other parties may be invited, if appropriate.

**SUPPORTING TASKS AND DELIVERABLES**

**SCOPE:**

The following tasks will be performed to achieve the project goals. All deliverables must be submitted to the Project Manager at steven.nolan@dot.state.fl.us and must contain the contract number, task work order number, and deliverable number as identified in the scope.

**TASK 1 – REVIEW OF THE DESIGN OF THE LINK-SLAB**

The research team will evaluate the provided link-slab details. The team will review the provided design of the link-slab that has 2 options; Bridge No. 019004 using Ultra High Performance Concrete (UHPC) and GFRP; and the other Bridge No. 019003 using or BFRP-RC. The team will investigate and propose refinements to the planned link-slab options of both an UHPC/GFRP and BFRP-RC on an FSB pedestrian bridges under US41 project FPID 435390-1-52-10) in Charlotte county. These refinements may be incorporated into a recommended final system.

**Deliverable 1**: Upon completion of Task 1 the university will submit to the Project Manager steve.nolan@dot.state.fl.us, a written report detailing the review of the design of the proposed link-slab.

**TASK 2 – RECOMMENDATIONS FOR BRIDGE INSTRUMENTATIONS AND MONITORING OF LINK-SLAB:**

The researchers will identify appropriate instrumentation for monitoring and locations for sensors and instrumentations for the BFRP-RC link-slab on Bridge No. 019003 over Morning Star Waterway. The team will suggest monitoring plan and instrumentation system to monitor the temperature, strain, rotation, and elongation of link-slabs. The research team will inspect the instrumentations and sensor locations during construction.

**Deliverable 2**: Upon completion of Task 2 the university will submit to the Project Manager steve.nolan@dot.state.fl.us, a written report including the recommendation for the instrumentations of link-slabs, the suggested monitoring plan, and instrumentation system to monitor the temperature, strain, rotation, and elongation of different link-slabs.

**TASK 3 – INSTALL FIELD INSTRUMENTATION ON BRIDGE LINK-SLAB:**

Provide and install instrumentation to monitor the link-slab during concrete casting and periodically for the following 90 days

**Deliverable 3:** Upon completion of Task 3 the university will submit to the Project Manager, a written report documenting the instrumentation installation and monitoring activities.

**TASK 4 – EVALUATE THE DATA FROM FIELD INSTRUMENTATION ON BRIDGE LINK-SLAB:**

Investigate the performance of the link-slab using BFRP-RC. The team will evaluate the data from instrumentation and provide preliminary conclusions.

**Deliverable 4:** Upon completion of Task 4 the university will submit to the Project Manager, a written report including the review of the data provided by FDOT pertaining to the sensors and instrumentations used for monitoring the temperature, strain, rotation, and elongation readings.

**TASK 5 - DRAFT FINAL AND CLOSEOUT TELECONFERENCE:**

**Deliverable 5:** Ninety (90) days prior to the end date of the task work order, the university will submit a draft final report to the Project Manager. The draft final report will contain:

1. The evaluation of the link-slab design details for FSB pedestrian bridges No. 019003 and 019004 (FPID 435390-1) and proposed refinements for both link-slab options using UHPC with GFRP bars, and BFRP-RC;
2. A detailed account of the installed instrumentation used to monitor the link-slab during link-slab casting and the following 90 days;
3. A summary and evaluation of that data recorded under Task 4;
4. Final conclusions from the field observations and recommendations for any improvements to the demonstrated link-slab details.

The draft final and final reports must follow the Guidelines for University Presentation and Publication of Research available at http://www.fdot.gov/research/docs/T2/University.Guidelines.2016.pdf The report must be well-written and edited for technical accuracy, grammar, clarity, organization, and format.

**Deliverable 6:** Thirty (30) days prior to the end date of the task work order, the principal investigator will schedule a closeout teleconference. The principal investigator shall prepare a Powerpoint presentation following the template provided at http://www.fdot.gov/research/Program_Information/Research.Performance/closeout.meeting.reqs.pdf. At a minimum, the principal investigator, and demonstration project Engineer of Record shall attend. The purpose of the meeting is to review project performance, the deployment plan, and next steps.

**TASK 6 - FINAL REPORT**

**Deliverable 7:** Upon Department approval of the draft final report, the university will submit the Final Report in PDF and Word formats electronically to the Project Manager at steven.nolan@dot.state.fl.us. The Final Report is due by the end date of the task work order.

**USE OF SUBCONTRACTOR(S)**
No Subcontractor is needed

**USE OF GRADUATE STUDENT(S) AND OTHER RESEARCH ASSISTANTS**
The PI will request help and support of Dr. Jim Fletcher (UNF) to execute the instrumentation plans and implementations, along with help with the deliverables and final report.

**EQUIPMENT**
The project bridge will be instrumented with FDOT sensors and devices in the field and the results will be recorded by FDOT. No equipment purchase is needed.

**EXPENSES**
All the materials and instrumentations will be provided by the FDOT. That includes strain gages, LVDT, sensors, UHPC, and Basalt or FRP bars (donated or provided to FDOT at no cost)

**TRAVEL**
No budget is allocated for travel as the PI will not request reimbursement from FDOT for travel. Dr. ElSafty may travel to the job sites of bridges when needed; but no travel budget is needed. All travel shall be in accordance with Section 112.061, Florida Statutes. FDOT employees may not travel on research contracts. Travel must only be requested when teleconference and web meetings cannot achieve the purpose of the travel. The maximum amount of travel is limited to \$0. The maximum amount of indirect cost on travel is limited to \$0.

**PROJECT KICKOFF TELECONFERENCE**
The principal investigator will schedule a kickoff teleconference that shall be held within the first 30 days of execution. The project manager, principal investigator, and research performance coordinator shall attend. Other parties may be invited if appropriate. The purpose of the meeting is to review the tasks, deliverables, and deployment plan.

**PROJECT CLOSEOUT TELECONFERENCE**
The principal investigator will schedule a closeout teleconference that shall be held during the final 30 days of the task work order. The principal investigator, project manager, and research performance coordinator shall attend. Other parties may be invited, if appropriate. The purpose of the meeting is to review project performance, the deployment plan, and next steps.

**PERFORMANCE AND FINANCIAL CONSEQUENCES**
Work not identified and included in this scope of service is not to be performed and will not be subject to compensation by the Department.
Financial consequences for unsatisfactory performance are referenced in Section 10 and Section 11 of the Master University Agreement, Form No. 375-040-64.

**PUBLICATION PROVISION**
If at any time during a TWO the University desires to publish in any form any material developed under the TWO, the University must submit to the TWO Manager and the Research Center at research.center@dot.state.fl.us a written abstract and notification of intent to publish

the material and receive the TWO Manager's concurrence to publish. Such approval to publish shall not be unreasonably withheld. If the TWO Manager does not provide a written response within 30 days after receipt, the University may publish.

"The opinions, findings and conclusions expressed in this publication are those of the author(s) and not necessarily those of the Florida Department of Transportation or the U.S. Department of Transportation."

**Project Milestones**

| Tasks | Task | Deliverable Dates |
|---|---|---|
| Task 1 | Review of the Design of the Link-Slab | February 15, 2019 |
| Task 2 | Recommendations for Bridge Instrumentation and Monitoring of Link-Slab | March 15, 2019 |
| Task 3 | Install Field Instrumentation and Monitor on Bridge Link-Slabs | June - September 2019 *(dependent on contractor's schedule)* |
| Task 4 | Evaluate the Data from The Field Instrumentations on Bridge Link-Slabs | October 15, 2019 |
| Task 5 | Draft Final Report | November 15, 2019 |
| Task 6 | Final Report | February 14, 2020 |

The anticipated start date is January 15, 2018
Deliverable dates are subject to change
Budget is $20,000

**Deliverables Schedule**

| Deliverable # (Task #) | Deliverable Dates | Performance monitoring by Project Manager |
|---|---|---|
| Deliverable #1 (Task 1)<br>Review of the Design of the Link-Slab | February 15, 2019 | |
| Deliverable #2 (Task 2)<br>Recommendations for Bridge Instrumentation and Monitoring of Link-Slab | March 15, 2019 | |
| Deliverable #3 (Task 3)<br>Install Field Instrumentation and on Bridge Link-Slabs | September 2019 | |
| Deliverable #4 (Task 4)<br>Evaluate the Data from The Field Instrumentation on Bridge Link-Slabs | October 15, 2019 | |
| Deliverable #5 (Task 5)<br>Final Draft Report | November 15, 2019 | |
| Deliverable #6 (Task 5)<br>Final Draft Report | January 14, 2020 | |
| Deliverable #7 (Task 6)<br>Final Report | February 14, 2020 | |

Deliverable dates are subject to change

## Budget Sheet

**ElSafty / FDOT Bridge Deck with Link-Slab**

**Project Dates: December 1, 2018 - November 30, 2019**

| Account Code | Budget Items | | Year 1 12/1/2018-11/30/2019 | Total |
|---|---|---|---|---|
| | **Salaries (UNF Faculty and A&P)** | | | |
| 611002 | Faculty 9-month during summer 2019 (Adel ElSafty - FTE=.43) | | $ 15,000 | |
| 611002 | Faculty 9-month during summer 2019 (Jim Fletcher - FTE=.0584 ) | | $ 1,890 | |
| | | Sub-total | $ 16,890 | $ 16,890 |
| | **Employee Benefits - use one line per category** | | | |
| 629996 | Faculty Summer term @ 7.65% | | $ 1,292 | |
| | | Sub-total | $ 1,292 | $ 1,292 |

| | | | | |
|---|---|---|---|---|
| 771080 | **F&A at 10% total direct costs (TDC)** | Total Direct Costs | $ 18,182 | $ 18,182 |
| | | Indirect Costs | $ 1,818 | $ 1,818 |
| | | TOTAL COSTS | $ 20,000 | $ 20,000 |

Prepared by Cheresa B - v1 10/29/18; Cheresa B - v2 10/30/18

**Indirect Cost Base** $ 18,182

| Tasks | Task | Amount |
|---|---|---|
| Task 1 | Review of the Design of the Link-Slab | $5,000 |
| Task 2 | Recommendations for Bridge Instrumentation and Monitoring of Link-Slab | $3,000 |
| Task 3 | Install Field Instrumentation and Monitor on Bridge Link-Slabs | $3,000 |
| Task 4 | Evaluate the Data from The Field Instrumentations on Bridge Link-Slabs | $3,000 |
| Task 5 | Draft Final Report | $3,000 |
| Task 6 | Final Report | $3,000 |

**REFERENCES**

El-Safty, A. K., "Analysis of Jointless Bridge Decks with Partially Debonded Simple Span Beams," Ph.D. Dissertation, North Carolina State University, Raleigh, NC, 1994.

Paul Zia, Alp Caner, and Adel K. El-Safty, (September 1995), "Jointless Bridge Decks," Technical Report, FHWA/NC/95-006, North Carolina Department of Transportation (NCDOT).

Adel ElSafty, and Ayman M. Okeil, (November 2008), Extending the Service Life of Bridges Using Continuous Decks, PCI Journal - Precast/Prestressed Concrete Institute, PCI, Vol. 53, No. 6, pp. 96-111. 30.

A. El-Safty, (2006), The Behaviour of Bridges with Jointless Decks Subjected to Time-Dependent Effects, B.H.V. Topping, G. Montero, R. Montenegro, (Editors), CCP: 83 - Proceedings of the 8 th International Conference on Computational Structures Technology, Civil-Comp Press, Stirlingshire, UK, Paper 140, 2006.
doi:10.4203/ccp.83.140. http://www.ctresources.info/ccp/paper.html?id=3920, Civil- Comp Proceedings ISSN 1759-3433

Ayman M. Okeil and **Adel El-Safty,** (Nov. 2005), Partial Continuity in Bridge Girders with Jointless Decks, Practice Periodical on Structural Design and Construction, ASCE Journal, Vol. 10, No. 4, pp 229-238, doi:10.1061/(ASCE)1084-0680(2005)10:4(229).

El-Safty, Adel K., "Behavior of Jointless Bridge Decks ", North Carolina State University, Ph.D. Dissertation, May 1994.

Li, V.C., Lepech, M., and Li, M. (2005) "Field Demonstration of Durable Link Slabs for Jointless Bridge Decks Based on Strain-Hardening Cementitious Composites" Michigan Department of Transportation, Research Report RC- 1471.

Victor C. Li, V.C., Fischer, G., Kim, Y., Lepech, M., Qian, S., Weimann, M., and Wang, S. (2003) "Durable Link Slabs for Jointless Bridge Decks Based on Strain-Hardening Cementitious Composites" Michigan Department of Transportation, Research Report RC-1438.

# Appendix B

## Presentation: BDV34 986-02 Kickoff Meeting

(10 pages)

**FDOT Project:**
Contract Number: **BDV34 986-02**
Project Title: **BRIDGE DECK WITH LINK-SLAB**
**for FPID: 435390-1-52-01: US 41 from Midway Blvd to Enterprise**

Project Manager (PM): **Steven Nolan**
Florida Department of Transportation
State Structures Design Office
Email: Steven.Nolan@dot.state.fl.us , Phone: (850) 414-4272

Principal Investigator (PI): **Adel ElSafty**, Ph.D., P.E.
University of North Florida
School of Engineering, 1 UNF Drive, Jacksonville, FL 32224-2645
Email: adel.el-safty@unf.edu, Phone: (904) 620-1398

# ***PRESENTATION OUTLINE***

- **Project Benefits:** Qualitative Benefits & Quantitative Benefits
- **Implementation Items & Anticipated Issues**
  - Software, physical product/device, policy, procedure, etc.
  - Discussion of any additional stakeholders needed for implementation
- **Introduction**
- **Project Background**: problem/issue FDOT attempts to address with this project
- **Project Objectives**
- **Task Outline & Any Needs/Issues Associated With Tasks**
  - Task 1: research activities and any needs/issues
  - Task 2: research activities and any needs/issues
  - Task 3: research activities and any needs/issues
  - Task 4: research activities and any needs/issues
  - Task 5: research activities and any needs/issues
- **Anticipated Project Timeline**

# ***Project Benefits***

- ❑No joints to purchase nor bearings to maintain.
- ❑Smoother riding surface.
- ❑Lower initial & life-cycle cost. Reduction in maintenance
- ❑improved bridge-deck life expectancy
- ❑Reduction in span bending moments.
- ❑Casting fully continuous deck over simply supported girders and partially debonding the deck from the girders ends appear to be a promising solution for bridge deck joint maintenance problems.
- ❑A significant improvement in the deck-beam response is observed when the deck is partially debonded from the beams having a hinge at each side of the connection

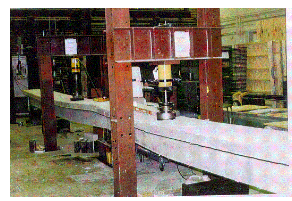

# ***Implementation Items & Anticipated Issues***

Software, physical product/device, policy, procedure, etc.

Discussion of any additional stakeholders needed for implementation

# ***Introduction***

- Most Joints Leak. And debris accumulate.
- Major reason for deficient bridges.
- Best solution is jointless bridges (link slab)
- Bridge deck joints are costly to buy, install & maintain.
- They have provided severe performance and maintenance problems as water and deck drainage contaminated with deicing chemicals leak through the superstructure and onto the pier caps below, thus damaging and eventually completely destroying some vital parts of bridges such as prestressing cable anchorage systems, beams and bearings.
- Link slab with BFRP provides a promising alternative.

## ***Project Background***:

problem/issue FDOT attempts to address with this project

- Bridge deck joints are costly to buy, install, and maintain.
- They have provided severe performance and maintenance problems as water and deck drainage contaminated with chemicals leak through the superstructure and onto the pier caps below, thus damaging and eventually completely destroying some vital parts of bridges such as prestressing cable anchorage systems, beams and bearings.
- Debris accumulation in the joints may restrain deck expansion.
- Most joints leak posing a major reason for deficient bridges.
- FDOT aims to adopt jointless bridges and elimination of expansion joints in bridge decks.
- FDOT intend to use a noncorrosive BFRP to eliminate corrosion problems.

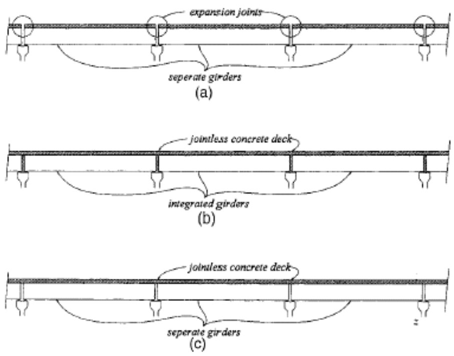


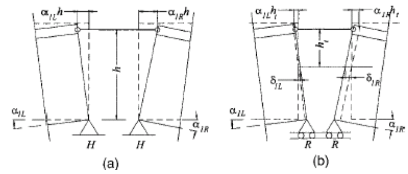


Support movement in a jointless system (a) hinged supports and (b) roller support

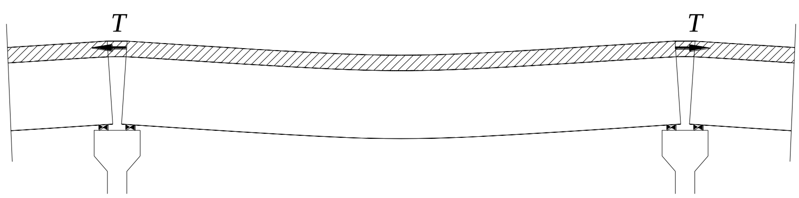


***Continuity caused by linking concrete decks in adjacent spans***

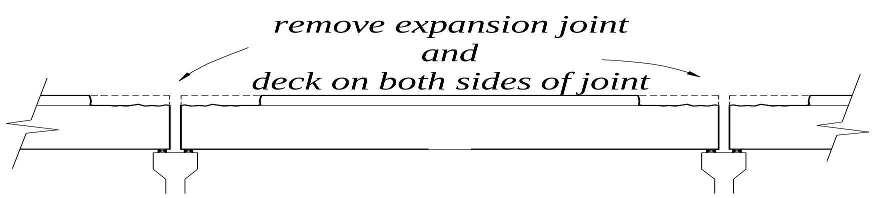


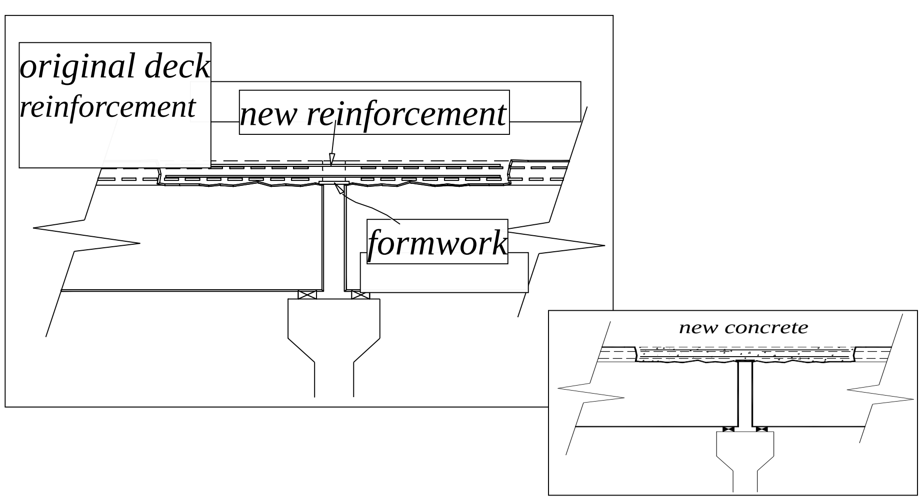

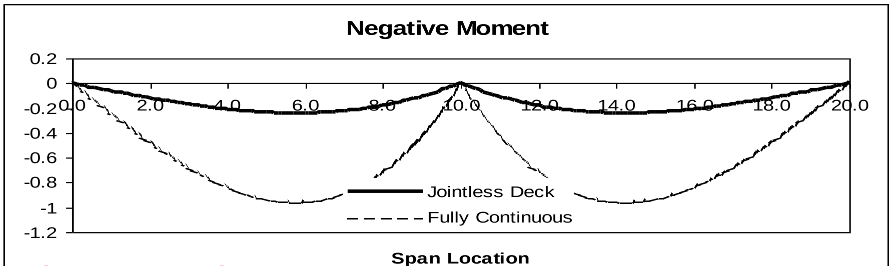


Influence Line for negative moment at the intermediate support

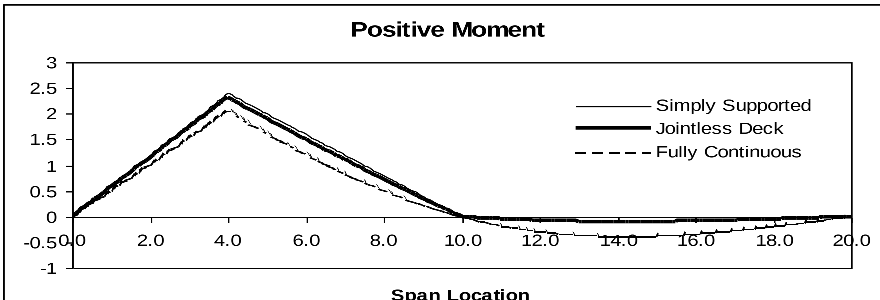


Influence Line for positive moment at $x/L1$ = 0.4 from LHS support

# ***Project Objectives***

- Review and comment on the *design detail* of *link-slab options* using Basalt Fiber-Reinforced Polymer (BFRP) and Glass(G) FRP bars for a bridge US 41 (Project FPID: 435390-1-52-01), from Midway Blvd to Enterprise.
- Identify appropriate instrumentation for monitoring and locations for sensors and instrumentations.
- Conduct evaluation and organization of data collected from the field instrumentations on the bridge link-slab.

## ***Task Outline*** **&**
## **Any Needs/Issues Associated With Tasks**

- **TASK 1 – REVIEW OF THE DESIGN OF THE LINK-SLAB**
- **TASK 2 – RECOMMENDATIONS FOR BRIDGE INSTRUMENTATIONS AND MONITORING OF LINK-SLAB**
- **TASK 3 – INSTALL FIELD INSTRUMENTATION ON BRIDGE LINK-SLAB**:
- **TASK 4 – EVALUATE THE DATA FROM FIELD INSTRUMENTATION ON BRIDGE LINK-SLAB**:
- **TASK 5 - DRAFT FINAL AND CLOSEOUT TELECONFERENCE**
- **TASK 6 - FINAL REPORT**

## **TASK 1 – REVIEW OF THE DESIGN OF THE LINK-SLAB**

- The research team will evaluate the provided link-slab details.
- The team will review the provided design of the link-slab that has 2 options; Bridge No. 019004 using Ultra High Performance Concrete (UHPC) and GFRP; and the other Bridge No. 019003 using or BFRP-RC.
- The team will investigate and propose refinements to the planned link-slab options of both an UHPC/GFRP and BFRP-RC on an FSB pedestrian bridges under US41 project FPID 435390-1-52-10) in Charlotte county.
- These refinements may be incorporated into a recommended final system.

**TASK 2 – RECOMMENDATIONS FOR BRIDGE INSTRUMENTATIONS AND MONITORING OF LINK-SLAB**

- The researchers will identify appropriate instrumentation for monitoring and locations for sensors and instrumentations for the BFRP-RC link-slab on Bridge No. 019003 over Morning Star Waterway.
- The team will suggest monitoring plan and instrumentation system to monitor the temperature, strain, rotation, and elongation of link-slabs.
- The research team will inspect the instrumentations and sensor locations during construction.

# Needed Sensors (tentative)

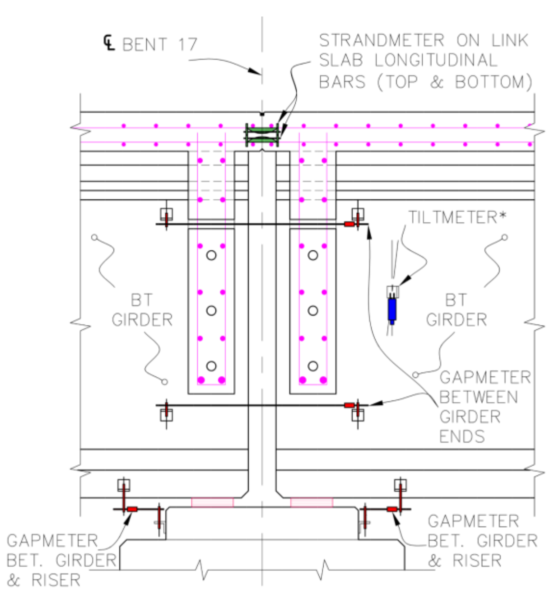


**TASK 3 – INSTALL FIELD INSTRUMENTATION ON BRIDGE LINK-SLAB**:

- Provide and install instrumentation to monitor the link-slab during concrete casting and periodically for the following 90 days
- FDOT/SRC will provide the data acquisition system/data logger, along with FDOT technicians' help to connect the data logger & record the data.
- FDOT/SRC will provide instrumentation and support for deflection and rotation measurements.

**TASK 4 – EVALUATE THE DATA FROM FIELD INSTRUMENTATION ON BRIDGE LINK-SLAB**:

- Investigate the performance of the link-slab using BFRP-RC.
- The team will evaluate the data from instrumentation and provide preliminary conclusions

## TASK 5 - DRAFT FINAL AND CLOSEOUT TELECONFERENCE

- **Deliverable 5:** Ninety (90) days prior to the end date of the task work order, the university will submit a draft final report to the Project Manager, containing:
- The evaluation of the link-slab design details for FSB pedestrian bridges No. 019003 and 019004 (FPID 435390-1) and proposed refinements for both link-slab options using UHPC with GFRP bars, and BFRP-RC;
- A detailed account of the installed instrumentation used to monitor the link-slab during link-slab casting and the following 90 days;
- A summary and evaluation of that data recorded under Task 4;
- Final conclusions from the field observations and recommendations for any improvements to the demonstrated link-slab details.
- **Deliverable 6:** Thirty (30) days prior to the end date of the task work order, the principal investigator will schedule a closeout teleconference. The principal investigator shall prepare a Powerpoint presentation following the template provided at http://www.fdot.gov/research/Program_Information/Research.Performance/closeout.meeting.reqs.pdf.

## TASK 6 - FINAL REPORT

- Submit the final report

# Anticipated Project Timeline

| Tasks | Task | Deliverable Dates |
|---|---|---|
| **Task 1** | Review of the Design of the Link-Slab | February 15, 2019 |
| **Task 2** | Recommendations for Bridge Instrumentation and Monitoring of Link-Slab | March 15, 2019 |
| **Task 3** | Install Field Instrumentation and Monitor on Bridge Link-Slabs | June - September 2019 (dependent on contractor's schedule) |
| **Task 4** | Evaluate the Data from The Field Instrumentations on Bridge Link-Slabs | October 15, 2019 |
| **Task 5** | Draft Final Report | November 15, 2019 |
| **Task 6** | Final Report | February 14, 2020 |

# Anticipated Project Timeline, *cont.*

| Deliverable # (Task #) | Deliverable Dates |
|---|---|
| Deliverable #1 (Task 1)<br>Review of the Design of the Link-Slab | February 15, 2019 |
| Deliverable #2 (Task 2)<br>Recommendations for Bridge Instrumentation and Monitoring of Link-Slab | March 15, 2019 |
| Deliverable #3 (Task 3)<br>Install Field Instrumentation and on Bridge Link-Slabs | September 2019 |
| Deliverable #4 (Task 4)<br>Evaluate the Data from The Field Instrumentation on Bridge Link-Slabs | October 15, 2019 |
| Deliverable #5 (Task 5)<br>Final Draft Report | November 15, 2019 |
| Deliverable #6 (Task 5)<br>Final Draft Report | January 14, 2020 |
| Deliverable #7 (Task 6)<br>Final Report | February 14, 2020 |

# Appendix C

## <u>Deliverable 2: BDV30 986-01 BFRP Testing Procedures and Results Report</u>

(39 pages)

**Deliverable 2**

# Performance evaluation, material and specification development for basalt fiber reinforced polymer (BFRP) reinforcing bars embedded in concrete

Contract Number BDV30 TWO 986-01
FSU Project ID: 042088

---

*Submitted to:*

**Florida Department of Transportation**
Research Center
605 Suwannee Street
Tallahassee, Florida 32399-0450

**Steven Nolan**
Project Manager
FDOT Structures Office

---


*Prepared by:*

**Raphael Kampmann, Ph.D.**
Principal Investigator
**Francisco De Caso, PhD, LEED A.P.**
Co-Principal Investigator
**Michelle Roddenberry, Ph.D., P.E.**
Co-Principal Investigator

FAMU-FSU College of Engineering
Department of Civil & Environmental Engineering
2525 Pottsdamer Street
Tallahassee, Florida 32310

University of Miami
Department of Civil, Architectural & Environmental Engineering
1251 Memorial Drive — McArthur Engineering Building 308
Coral Gables, Florida 33146


---

01/28/2019

# Table of Contents

# Chapter 1

# Introduction

It is the goal of this report to summarize the performance evaluation of basalt fiber reinforced polymer (BFRP) rebars. BFRP rebars are comparatively new material in the industry. Before using any new material in the infrastructure projects, the physical and mechanical properties of the material must be evaluated and compared to acceptance criteria (if applicable). In this report, physical properties such as cross-sectional dimensions, fiber content, and moisture absorption properties are described. In addition, physical properties, including the apparent horizontal shear strength, the transverse shear strength and the tensile properties were characterized. All tests were conducted according to the methods described by the American Society for Testing and Materials (ASTM) in line with the relevant test protocols. Data acquisition software, such as LabView and MTS TestWorks was used to collect the raw data with high data rates. The collected raw data were analyzed using R-statistics[1] and R-Studio[2] software packages.

For the purpose of this research, BFRP rebar from three different manufacturers were evaluated. Two different sizes were tested, which included # 3, and # 5 rebars. All tested materials were provided by the BFRP rebar manufacturers Galen Panamerica, No Rust Rebar, and Pultrall. One Manufacturer provide two sub-types of rebars, which were made from different resin types while all other production parameters were held constant (according to the manufacturer) All specimen types analyzed in this research are shown In the following figures 1.1 and 1.2. The surface enhancement properties of rebars are described in the table 1.1 It can be seen that all products featured

Table 1.1: Physical characteristics of tested BFRP rebars

| Name | Cross-Section | Surface Enhancement | Resin Type |
|---|---|---|---|
| A | Round (solid) | Sand coat | HP |
| B | Round (solid) | Surface lugs | Epoxy |
| C | Round (solid) | Helical Wraps | Epoxy |

sand coating as a surface enhancement to improve the bond-to-concrete properties. In addition to the surface sand, one product (No Rust Rebar) also had helical fibers made from polyethylene terephthalate, produced by Dacron®

[1] R.app GUI 1.70 (7434 El Capitan build), S. Urbanek & H.-J. Bibiko, R Foundation for Statistical Computing, 2016

[2] Version 1.1.383 2009-2017 RStudio, Inc.

(a) Galen Panamerica (b) No Rust Rebar (c) Pultrall

Figure 1.1: Sample pictures of tested BFRP # 3 Rebars

(a) Galen Panamerica (b) No Rust (c) Pultrall

Figure 1.2: Sample pictures of tested BFRP # 5 Rebars

# Chapter 2

# Test Procedures

## 2.1 Introduction

In this chapter, the test procedures of all the evaluated properties of rebar are described and detailed in individual sections.

## 2.2 Standard Test Methods for Density and Specific Gravity (Relative Density) of Plastics by displacement.

The test procedure to determine the density and specific gravity (relative density) of plastics by displacement methods is described in this paragraph to explain how the rebar diameter (or cross section) was specified for each product. The cross-sectional properties were measured according to ASTM D 792(ASTM-International, 2015), while the density of each specimen was calculated via the buoyancy principle. A clean specimen was conditioned for 40 h prior to testing in a temperature range from 21 °C to 25 °C (70 °F to 74 °F) at a relative humidity between 40 % and 60 %. The specimen was then cut to the desired length of 25 mm (1 in.) using an electric precision saw. The length of each curtailed specimen was measured 3 times, at 120° intervals perpendicular to the longitudinal axis of the FRP rebar, and the average value was noted for density calculations. Afterwards, the weight of dry and conditioned specimen was measured using an electronic balance, and recorded to the nearest 0.05 g (0.0017 oz.). The recorded weight of the curtailed specimen was measured to be no less than 10 g (0.352 oz.). and the value was used as the initial specimen weight, ($W_i$), needed for density calculations. A glass beaker of known volume was used as immersion vessel to hold the water in which the sample was submerged . However, the immersion vessel was tared from the weighing mechanism to obtain only the weight of the sample under buoyancy. The temperature of the water bath was monitored for each test and constant water temperatures of 21 °C to 25 °C (70 °F to 74 °F) were maintained throughout all experiments. A corrosion resistant copper wire was used as a sample holder and attached to the fixture that was independent of the water bath/vessel but introduced the forces into the scale and the specimen was carefully attached to one end of copper wire. The weight of the specimen along with the copper wire was measured and recorded as weight (Specimmen + wire) ($W_{s+w}$). The immersion vessel was placed on the support (independent of the weighing mechanism), and the specimen was completely submerged in the water with the help of the copper wire. To remove any entrapped air or air bubbles at the surface of the FRP rebar, the specimen was carefully rubbed with the wire across the surface and submerged in a rotating motion. Any water that was displaced onto the scale was wiped without disturbing the immersion vessel. The weight of the submerged specimen was measured and recorded as final weight ($W_f$). The density of the test specimen was determined via the buoyancy principle and the cross-sectional dimensions were calculated by dividing the determined volume by the measured specimen length. For reliability of test results and to obtain representative values for the BFRP rebar product as a whole, the test was repeated five times for specimens taken from different sections of the production lot and the average value was assigned. For the calculation of FRP rebar strength properties, the measured cross-sectional area is an important characteristic because the tensile strength of rebar is partially dependent on it's diameter. The cross-sectional area of the specimen must be determined in the laboratory because the cross-sectional properties may vary within an individual product due to imperfections in the manufacturing process. Stresses in the rebar depends on the cross sectional area, as stress is force divided by area. The stresses in the rebar changes with the change in the cross-sectional area. However, only bar strength based on nominal area is used in construction acceptance and structural calculations (actual measured area maybe used for volume fraction calculations).

## 2.3 Standard Test Method for Ignition Loss of Cured Reinforced Resins

The procedure for Ignition loss test for cured reinforced resins is explained in this paragraph to describe how the fiber content for the tested FRP rebars was determined. ASTM D 2584 -11(ASTM-International, 2011) outlines this procedure and details the required conditions. Similar to the specimen preparation for the cross-sectional dimension experiments, the specimens for this procedure were also conditioned in a temperature range from 21 °C to 25 °C (70 °F to 74 °F) at a relative humidity between 40 % and 60 %, for at least 40 hours prior to testing. The conditioned sample was then cut to the desired length of 25 mm (1 in.) with a precision of 0.05 mm (0.0019 in.). The weight of the conditioned sample ($W_s$), was then recorded to the nearest 0.05 g (0.0017 oz.) using an electronic balance. This weight was used as the 100 % reference value for calculating the fiber and resin contents (relative to the initial weight). Likewise, a clean and oven dried crucible was weighed ($W_c$),to the nearest 0.05 g (0.0017 oz.) to obtain the initial weight of the sample holder. The FRP rebar specimen was transferred to the crucible and the total weight of the specimen and the crucible ($W_i$), was recorded to the nearest 0.05 g (0.0017 oz.). To burn off all resin, the crucible (of known mass) along with the specimen were exposed to a temperature of 542 °C to 593 °C (1000 °F to 1100 °F) in a muffle furnace until the specimens reached a constant weight. The crucible was then carefully removed from the muffle furnace and allowed to cool down to room temperature, before the cooled crucible including the fibers (and sand for rebars that used surface enhancement made from sand) was weight using a precision electronic balance. This weight was recorded as final weight ($W_f$). For the rebar products made with sand at the surface for bond enhancement, the weight of the sand ($W_s$), was recorded and subtracted from the initial weight of the crucible and the specimen to obtain comparable and absolute fiber content percentages. Because fibers (and sand) are not susceptible to loss on ignition, the reduction in weight due to the burning process is equivalent to the weight of resin, and hence, the percentage of fibers was determined through the difference in weight before and after the burning process. For reliability of test results and to obtain representative values for the BFRP rebar product as a whole, the test was repeated five times for specimens taken from different sections of the production lot and the average value was assigned.

The fiber content percentage plays a key role in transferring the stresses through the cross section. The tensile stresses are transferred from one fiber to another during stressing. To increase the tensile strength of the rebar, to improve the ductility of the rebar, and to improve the overall quality of rebar production, it is important to understand the resin matrix and determine the fiber to resin ratio.

## 2.4 Moisture Absorption of Basalt FRP

The test procedure described in ASTM D 5229(ASTM, 2014) defines the standard method for determining the moisture absorption characteristics of FRP and is an indicator of porosity. This paragraph explains how the porosity of the tested rebars was calculated. ASTM D 5229 offers seven different test procedures (A through E,Y, and Z) to assign moisture absorption properties for FRP in different environments. Procedure A is most commonly used, and was used for this research project. Each specimen was first oven dried for 48 h to eliminate moisture entrapped in the pores or at the surface. The dried and conditioned specimens were placed in storage bags to ensure that no moisture contaminated the specimens. Three diameter measurements were taken at 120° intervals, perpendicular to the longitudinal axis of the FRP rebar, and those measurements were recorded to the nearest 0.001 mm ($\frac{4}{10\,000}$ in.). Then, each specimen was weighted with a precision of 0.05 g (0.0017 oz.) in its dry state and recorded as $W_i$. The specimens were then submerged in distilled water. The water along with the submerged specimens were stored in a air circulated oven to maintain the temperature of 50 °C (122 °F) throughout the entire duration of the conditioning. First weight measurements to record $W_1$ after water conditioning were taken after two weeks. To obtain additional measurements, the specimens were removed from the water bath in two week intervals (continuous conditioning) and surface dried with a fresh paper towel until no free water remained on the surface of the FRP rebar. The final weight of each specimen ($W_f$) was measured and recorded to the nearest 0.05 g (0.0017 oz.). This procedure was repeated and weight gains were monitored until three consecutive two-week measurement did not differ by more than 0.02 % from one another. For reliability of test results and to obtain representative values for the BFRP rebar product as a whole, the test was repeated five times for specimens taken from different sections of the production lot and the average value was assigned.

## 2.5 Horizontal Shear Test

The FRP rebar product was tested for horizontal shear properties. The horizontal shear test was conducted according to ASTM D 4475 (ASTM-International, 2012a) standards. This test alone does not relate to design properties, but the horizontal shear failure is an indicator for the strength of the resin to fiber bonding, and therefore, is a well suited quality control criteria and used for comparison among multiple specimens from the same manufacturer. First, the diameter at the center of the specimen was recorded and the specimens were conditioned at a temperature range from 21 °C to 25 °C and a moisture content between 40 % and 60 % before they were cut to a length of approximately 5 times the diameter. A minimum of 5 specimen were tested per sample. The horizontal shear strength was assessed through a three-point load test over a span length that is short enough to avoid bending failure. The load was applied at the center of specimen with a displacement rate of 1.3 $\frac{\text{mm}}{\text{min}}$ until the shear failure was reached via horizontal delamination (failure of the resin or resin-fiber interface). The ultimate load and the break type (number of fracture surfaces) were recorded and analyzed.

## 2.6 Transverse Shear Test

The transverse shear strength is an important characteristic if the bars are used as dowels in concrete pavement, stirrups in concrete beams, or as general shear reinforcement elements. ASTM D 7617 (ASTM-International, 2012b) was used in the process of testing and analyzing the data. Before testing, the specimens were conditioned according to the ASTM D 5229 (ASTM, 2014). The conditioned specimen were then cut to a minimum length of 225 mm so that they fit in the shearing apparatus which is a device that produces double shear on the FRP rebar specimen. This device has two bar seats, two lower plates, and two guides machined from steel which are connected with two threaded rods using bolts, and nuts. The conditioned and curtailed bars were placed inside the shear test device and loaded with a displacement rate such that the test is continuous for at least 1 minute, but not more than 10 minutes until the force reaches 70 % of the ultimate load. The transverse shear strength was determined using the ultimate load and the cross sectional area of the specimen measured as per nominal diameter of the rebar.

## 2.7 Tensile Strength Tests

The rebars were tested according to the ASTM D 7205, which describes a specific test method for specimen preparation and testing. It details how to protect the rebar ends via steel pipe anchors at both ends. Because of the low shear and crushing strength of FRP rebars this method is necessary to prevent the rebar from failing in shear before reaching the ultimate tensile strength. The grips of the testing machine would lead to a premature failure of the specimen. The anchors are potted with expansive grout which transfers the force from the testing machine into the rebar through compression and friction of the rebar surface and the grout. The dimensions of the anchors relate to the rebar diameter and the free specimen length between the anchors is described with 40 times the rebar diameter.

## 2.8 Acceptance Criteria

While acceptance criteria for basalt FRP rebars are not fully established yet, criteria for other fiber based rebars have been adopted. One of the most established composite rebar materials is the glass fiber reinforced polymer (GFRP) rebar. For reference, the data in the Tables 2.1 and 2.2 shows common acceptance criteria for (GFRP) rebars. The results obtained by testing BFRP rebars

Table 2.1: Acceptance criteria for GFRP rebar # 3

| | | | FDOT 932-3/2017 | AC454 | ASTM D 7957 |
|---|---|---|---|---|---|
| Test Method | Test Description | Unit | Criteria | Criteria | Criteria |
| ASTM D 792 | Measured Cross Sectional Area | in.$^2$ | 0.104 – 0.161 | 0.104 – 0.161 | 0.104 – 0.161 |
| ASTM D 2584 | Fiber Content | % wt. | $\geqslant 70$ | $\geqslant 70$ | $\geqslant 70$ |
| ASTM D 570 | Moist. Absorption short term @50 °C | % | $\leqslant 0.25$ | $\leqslant 0.25$ | $\leqslant 0.25$ |
| ASTM D 570 | Moist. Absorption long term @50 °C | % | $\leqslant 1.0$ | n/a | $\leqslant 1.0$ |
| ASTM D 7205 | Min. Guaranteed Tensile Load | kip | $\geqslant 13.2$ | $\geqslant 13.2$ | $\geqslant 13.2$ |
| ASTM D 7205 | Min. Guaranteed Tensile Strength | ksi | n/a | n/a | n/a |
| ASTM D 7205 | Tensile Modulus | ksi | $\geqslant 6,500$ | $\geqslant 6,500$ | $\geqslant 6,500$ |
| ASTM D 7205 | Max. Strain | % | n/a | n/a | n/a |
| ASTM D 7617 | Min. Guaranteed Transverse Shear | ksi | $\geqslant 22$ | $\geqslant 22$ | $\geqslant 19$ |
| ASTM D 4475 | Horizontal Shear Stress | ksi | n/a | $\geqslant 5.5$ | n/a |
| ACI440. 3 R,B.3 | Bond-to-concrete strength | ksi | $\geqslant 1.1$ | $\geqslant 1.1$ | $\geqslant 1.1$ |

Table 2.2: Acceptance criteria for GFRP rebar # 5

| | | | FDOT 932-3/2017 | AC454 | ASTM D 7957 |
|---|---|---|---|---|---|
| Test Method | Test Description | Unit | Criteria | Criteria | Criteria |
| ASTM D 792 | Measured Cross Sectional Area | in.$^2$ | 0.288 – 0.388 | 0.288 – 0.388 | 0.288 – 0.388 |
| ASTM D 2584 | Fiber Content | % wt. | $\geqslant 70$ | $\geqslant 70$ | $\geqslant 70$ |
| ASTM D 570 | Moist. Absorption short term @50 °C | % | $\leqslant 0.25$ | $\leqslant 0.25$ | $\leqslant 0.25$ |
| ASTM D 570 | Moist. Absorption long term @50 °C | % | $\leqslant 1.0$ | n/a | $\leqslant 1.0$ |
| ASTM D 7205 | Min. Guaranteed Tensile Load | kip | $\geqslant 29.1$ | $\geqslant 32.2$ | $\geqslant 29.1$ |
| ASTM D 7205 | Min. Guaranteed Tensile Strength | ksi | n/a | n/a | n/a |
| ASTM D 7205 | Tensile Modulus | ksi | $\geqslant 6,500$ | $\geqslant 6,500$ | $\geqslant 6,500$ |
| ASTM D 7205 | Max. Strain | % | n/a | n/a | n/a |
| ASTM D 7617 | Min. Guaranteed Transverse Shear | ksi | $\geqslant 22$ | $\geqslant 22$ | $\geqslant 19$ |
| ASTM D 4475 | Horizontal Shear Stress | ksi | n/a | $\geqslant 5.5$ | n/a |
| ACI440. 3 R,B.3 | Bond-to-concrete strength | ksi | $\geqslant 1.1$ | $\geqslant 1.1$ | $\geqslant 1.1$ |

are compared to GFRP rebar acceptance criteria because BFRP acceptance criteria in the US are yet to be established. Accordingly, the listed criteria (while established for glass) serve as reference points and are used for comparison and initial benchmark data.

# Chapter 3

# Results

## 3.1 Introduction

The following results were obtained at the FAMU-FSU College of Engineering in the High Performance Materials Institute (HPMI). All tests were conducted in accordance with the relevant American Society for Testing and Materials (ASTM) test protocol. The collected raw data were analyzed with the engineering software R-statistics[1] and R-Studio[2]. The results are presented throughout this chapter in tables and graphs for visual representation. For clarity, each property was individually studied and presented seperately. At the end of the chapter, a summary of the test results is provided to comprehensively present each specific product, document its performance, and to compare it to the acceptance criteria in FDOT 932, AC 454, and ASTM D 7957 (for glass based FRP rebars).

## 3.2 Cross Sectional Properties

The effective rebar diameter was measured according to the ASTM D 792-13. Due to the variety of FRP rebars on the market and depending on the proprietary production methods, rebars from different manufacturers with different surface enhancement vary from to the stated nominal diameter. Table 3.1 below lists the results of water displacement method according to the ASTM D 792-13 of the Galen Panamerica products.

[1] R.app GUI 1.70 (7434 El Capitan build), S. Urbanek & H.-J. Bibiko, © R Foundation for Statistical Computing, 2016

[2] Version 1.1.383 © 2009-2017 RStudio, Inc.

Table 3.1: Results from diameter measurements for rebar size # 3 and # 5

| Specimen | | Specimen Length | | | | Weight | | | | |
|---|---|---|---|---|---|---|---|---|---|---|
| | | $L1$ | $L2$ | $L3$ | $Average$ | $a$ | $a+s$ | $b$ | $s$ | $\Delta M$ |
| | | $cm$ | $cm$ | $cm$ | $cm$ | $g$ | $g$ | $g$ | $g$ | $g$ |
| Galen HP No. 3 | HP1 | 2.550 | 2.527 | 2.512 | 2.530 | 3.976 | 11.774 | 9.768 | 7.798 | 1.970 |
| | HP2 | 2.514 | 2.519 | 2.527 | 2.520 | 3.979 | 11.775 | 9.760 | 7.796 | 1.964 |
| | HP3 | 2.558 | 2.533 | 2.521 | 2.537 | 3.977 | 11.783 | 9.769 | 7.806 | 1.963 |
| | HP4 | 2.513 | 2.512 | 2.527 | 2.517 | 3.942 | 11.739 | 9.742 | 7.797 | 1.945 |
| | HP5 | 2.570 | 2.536 | 2.523 | 2.543 | 3.932 | 11.730 | 9.756 | 7.798 | 1.958 |
| Galen HE No. 3 | HE1 | 2.511 | 2.529 | 2.506 | 2.515 | 4.056 | 11.868 | 9.723 | 7.812 | 1.911 |
| | HE2 | 2.509 | 2.521 | 2.511 | 2.514 | 4.161 | 11.958 | 9.743 | 7.797 | 1.946 |
| | HE3 | 2.564 | 2.559 | 2.560 | 2.561 | 4.226 | 12.023 | 9.791 | 7.797 | 1.994 |
| | HE4 | 2.539 | 2.539 | 2.569 | 2.549 | 4.200 | 11.995 | 9.768 | 7.795 | 1.973 |
| | HE5 | 2.504 | 2.503 | 2.527 | 2.511 | 4.144 | 11.972 | 9.752 | 7.828 | 1.924 |
| Galen HP No. 5 | HP1 | 2.557 | 2.535 | 2.538 | 2.543 | 11.410 | 19.019 | 13.636 | 7.609 | 6.027 |
| | HP2 | 2.530 | 2.547 | 2.569 | 2.549 | 11.145 | 18.940 | 13.589 | 7.795 | 5.794 |
| | HP3 | 2.539 | 2.558 | 2.549 | 2.549 | 11.147 | 18.965 | 13.601 | 7.791 | 5.810 |
| | HP4 | 2.535 | 2.536 | 2.541 | 2.537 | 11.253 | 19.050 | 13.652 | 7.797 | 5.855 |
| | HP5 | 2.534 | 2.548 | 2.534 | 2.539 | 11.154 | 18.951 | 13.600 | 7.797 | 5.803 |
| Galen HE No. 5 | HE1 | 2.505 | 2.502 | 2.524 | 2.510 | 11.097 | 18.890 | 13.450 | 7.793 | 5.657 |
| | HE2 | 2.511 | 2.525 | 2.510 | 2.515 | 11.154 | 18.954 | 13.476 | 7.800 | 5.676 |
| | HE3 | 2.515 | 2.521 | 2.532 | 2.523 | 11.174 | 18.975 | 13.501 | 7.801 | 5.700 |
| | HE4 | 2.520 | 2.577 | 2.546 | 2.548 | 11.266 | 19.062 | 13.544 | 7.796 | 5.748 |
| | HE5 | 2.581 | 2.545 | 2.550 | 2.559 | 11.181 | 18.978 | 13.482 | 7.797 | 5.685 |

## 3.3 Fiber Content

The measured fiber content results are plotted in the Figure 3.1. The bar chart compares rebars

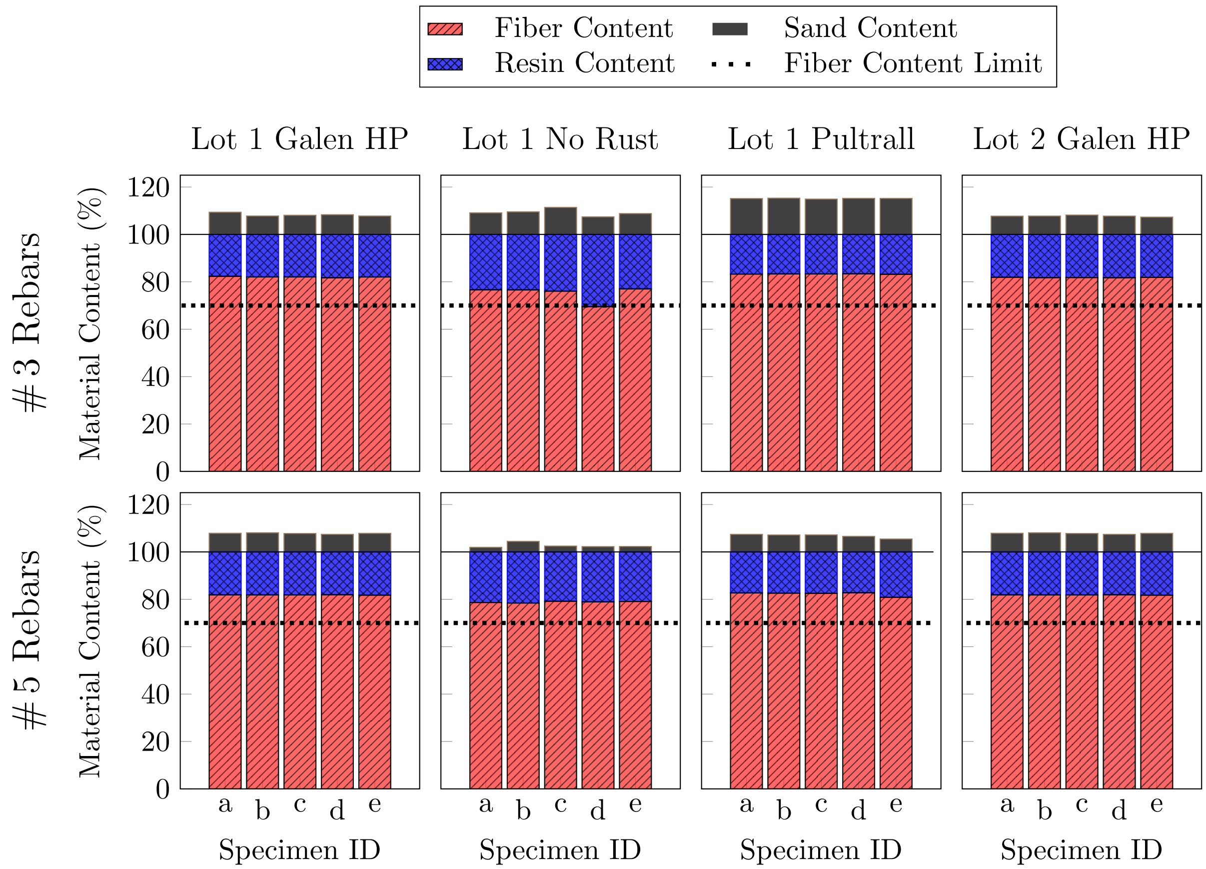


Figure 3.1: Fiber content percentage of rebars from Galen, No Rust, and Pultrall manufacturers

from different manufacturers, both the bar sizes and both the lots. All the rows in the plot indicate rebar sizes and all the columns indicate different manufacturers. Each individual column represents one specimen. The red hatched part of each column indicates fiber content percentage of the rebar specimen, the blue part represents the resin content percentage and the black part represents sand content percentage. The surface of the rebar specimens were sand coated to increase the bond to concrete. The 100% value of rebars are based on total specimen weight minus the sand content. All the rebar specimen easily met the minimum requirement of 70% fiber content. The only marginal exception was specimen d of # 3 rebar from No Rust Rebar. Overall, the measured fiber content results show the production consistency for all rebar manufacturers, lots, and sizes.

The following Figure 3.2 exemplifies the rebar appearance after the loss on ignition test procedure. While the specimens shown in the figure were material samples from Galen Panamerica, the

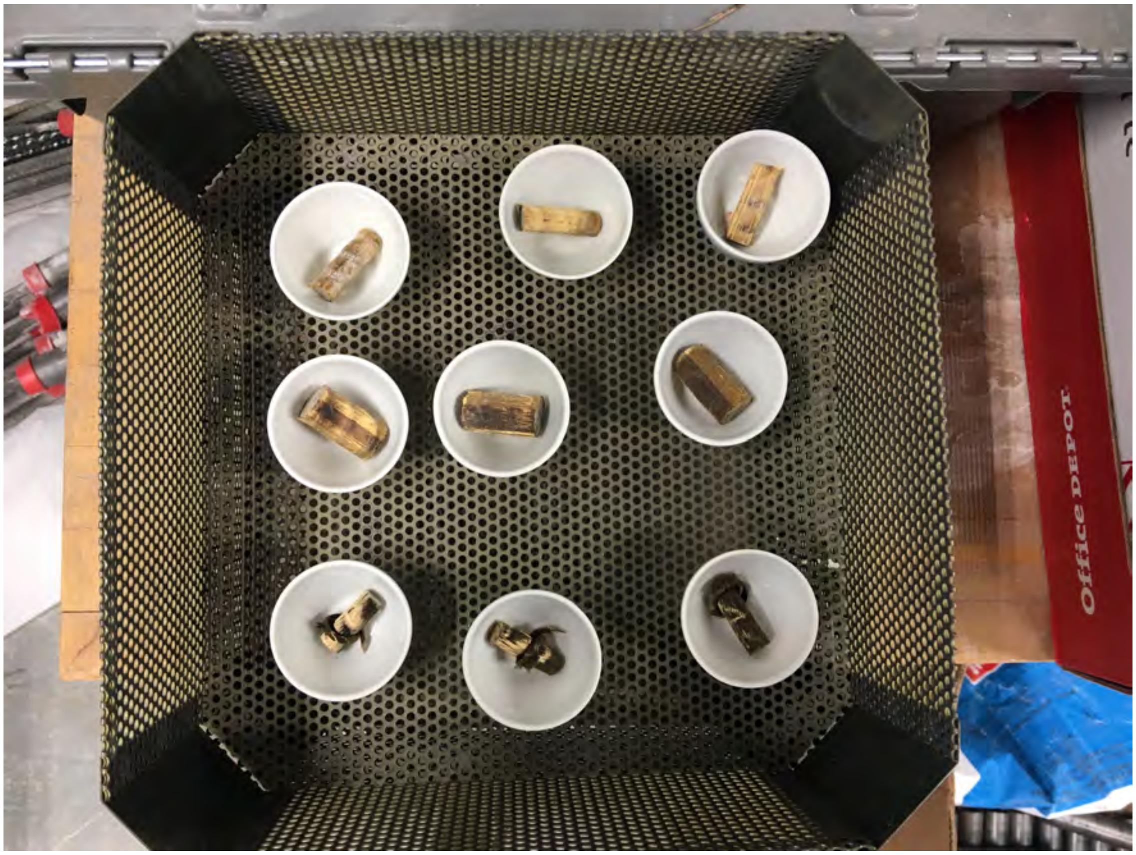


Figure 3.2: Fiber content specimen of GP HP # 3, 5 after test

appearance of the rebars after the test were similar for all rebar types.

## 3.4 Moisture Absorption

The graph plotted in Figure 3.3 represents weight change of the rebar specimen stored in distilled water over the entire test period. All the rebar yielded a comparable results except # 3 rebar from Galen with HP resin. All the rebar types did not satisfy the AC454 limitations for the absorption limit of 0 25% in first 24 hours of exposure.

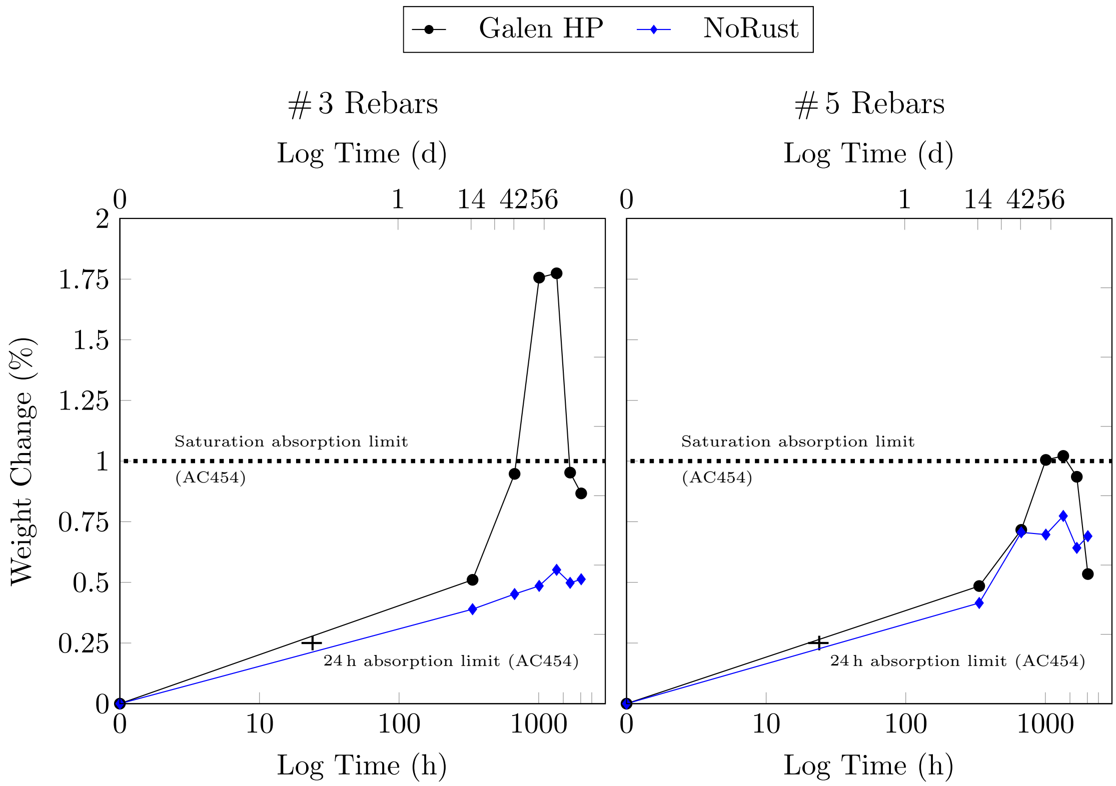


Figure 3.3: Moisture Absorption results of rebars from Galen and No Rust rebar manufacturers

## 3.5 Horizontal Shear

### 3.5.1 Load vs. Displacement

The graphs in Figure 3.4, 3.5, and 3.6 compares the load vs. displacement behavior of short span 3 point bending for # 3 and # 5 rebars from all manufacturer. The x-axis of the graph represents the cross-head extension and the y-axis represents the applied load.

The graph in Figure 3.4 show a nearly linear behavior until it reached the ultimate failure load.

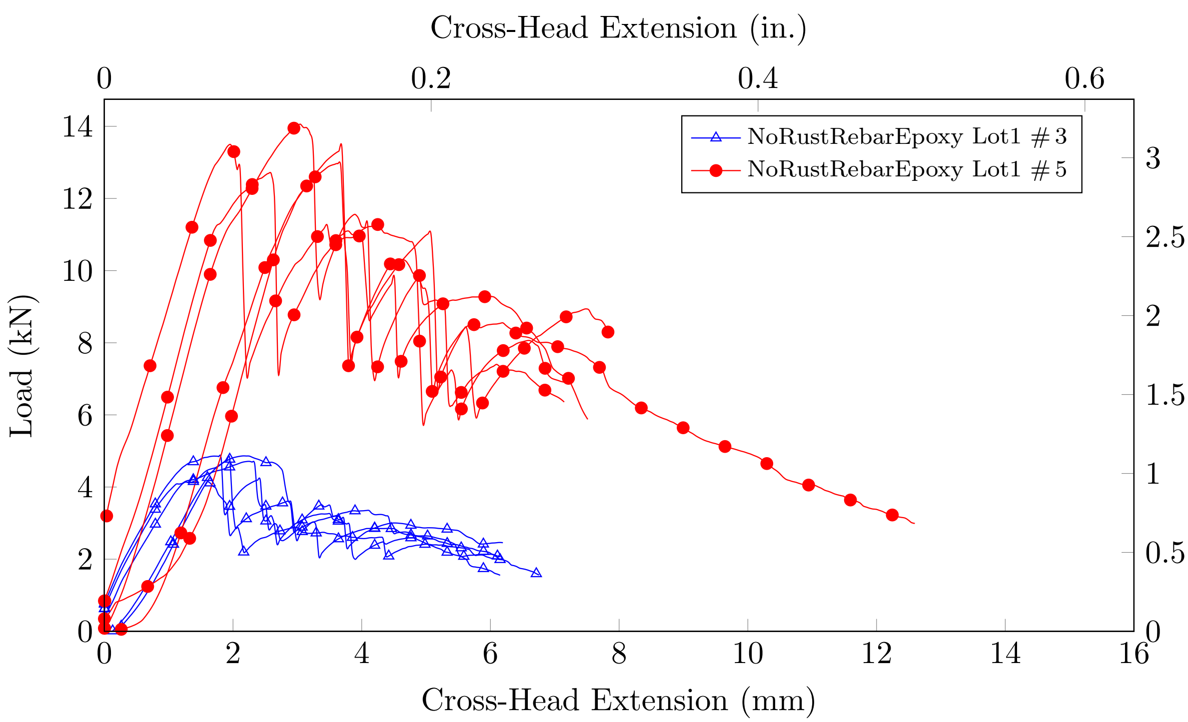


Figure 3.4: Extension vs. Horizontal Shear Load behavior of No Rust rebar Lot 1 size 3 and 5

The graphs shown in Figures 3.5 compares the load vs. displacement behavior of short span 3 point bending of # 3 and # 5 rebars from lot 1 from Galen Panamerica. The graphs show a linear behavior until it reached 90 % of the ultimate failure load.

The graph in Figure 3.5 compares the load vs. displacement behavior of short span 3 point bending of # 3 and # 5 rebars from lot 2 from Galen Panamerica. The graphs show a linear behavior until it reached 90% of the ultimate failure load.

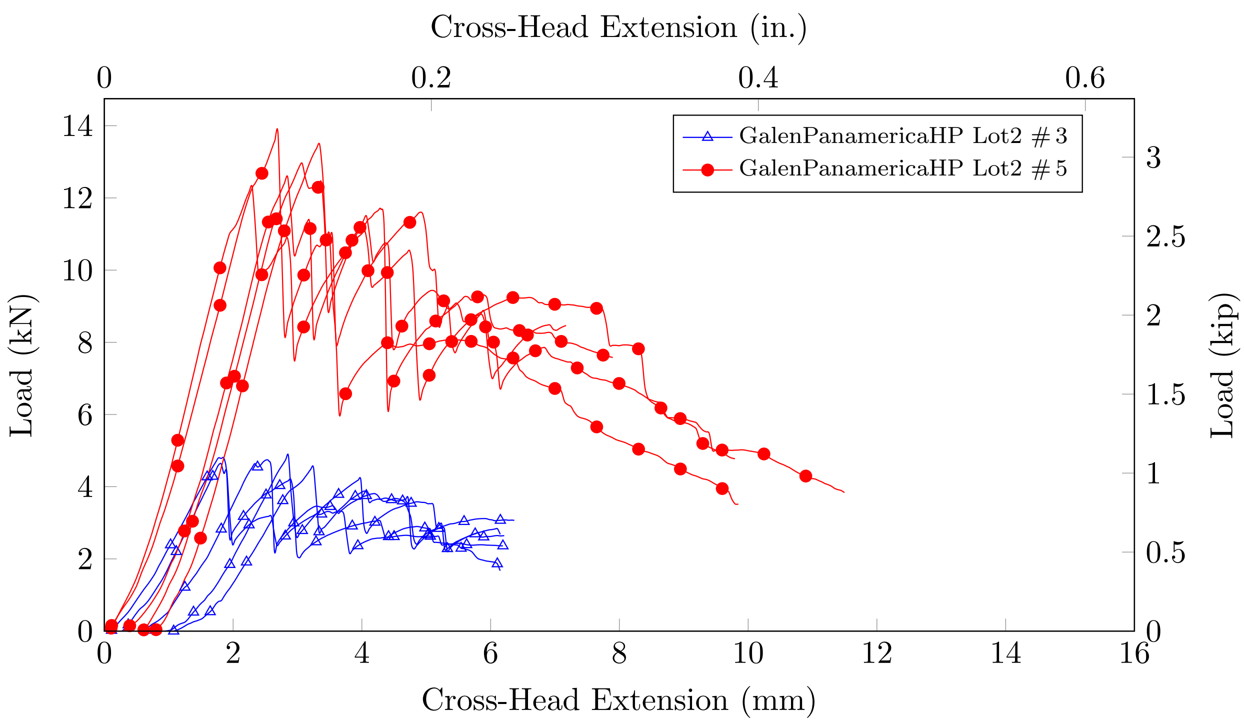


Figure 3.5: Extension vs. Horizontal Shear Load behavior of Galen Panamerica Lot 1 HP rebar size 3 and 5

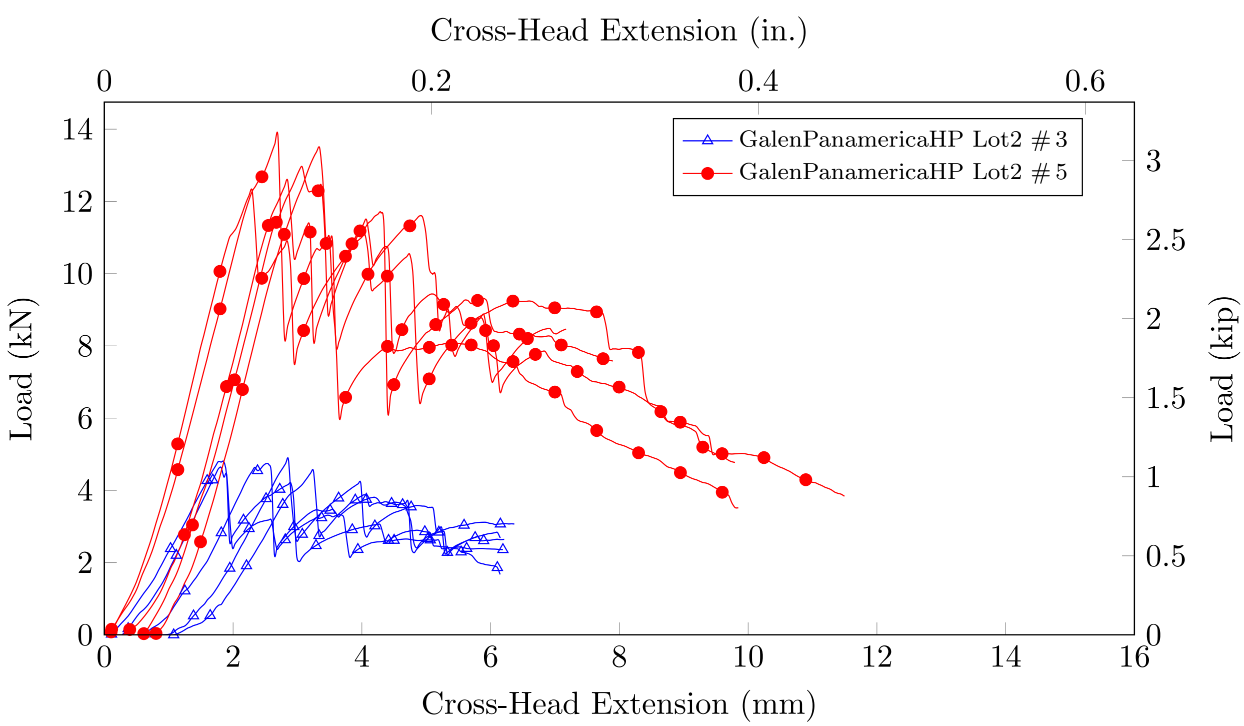


Figure 3.6: Extension vs. Horizontal Shear Load behavior of Galen Panamerica Lot 2 HP rebar size 3 and 5

### 3.5.2 Stress vs. Displacement

The following graphs in Figures 3.7, 3.8, and 3.9 show the comparison of the stress vs. displacement behavior of short span 3 point bending of # 3 and # 5 rebars from all manufacturer. The x-axis of graph represents the cross-head extension and the y-axis represents the shear stress.

The graph in figure 3.7 show a linear behavior until it reached the ultimate failure load. The

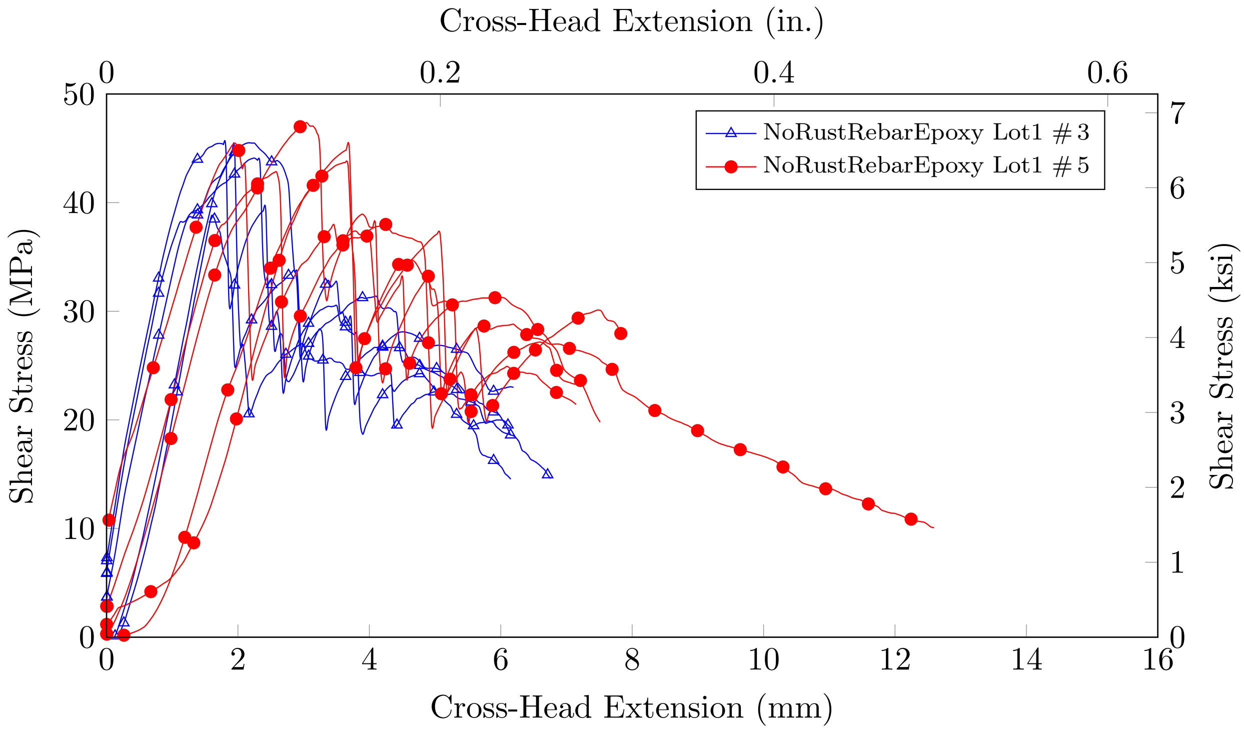


Figure 3.7: Horizontal shear stress vs. Extension behavior of No Rust rebar Lot 1 size 3 and 5

graph in Figure 3.8 compares the stress vs. displacement behavior of short span 3 point bending of # 3 and # 5 rebars from lot 1 from Galen Panamerica. The graph in Figure 3.9 compares the stress vs. displacement behavior of short span 3 point bending of # 3 and # 5 rebars from lot 1 from Galen Panamerica.

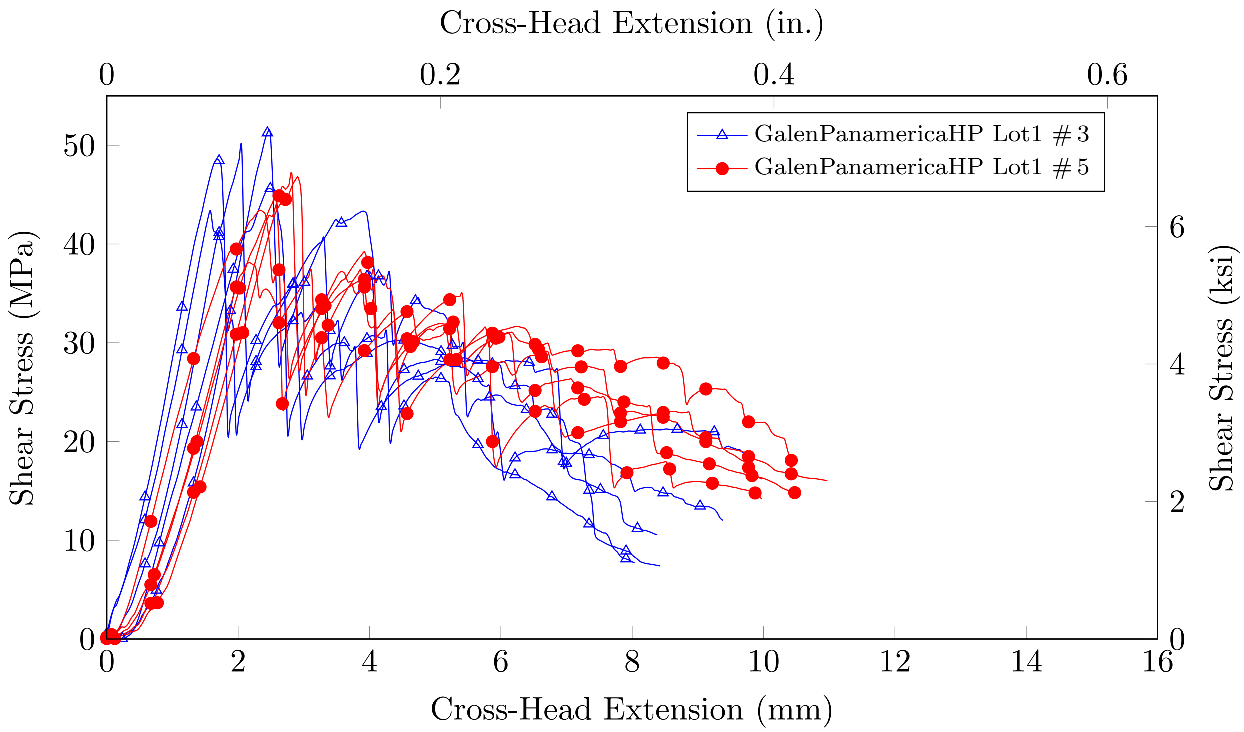


Figure 3.8: Horizontal shear stress vs. Extension behavior of Galen Panamerica Lot 1 HP rebar size 3 and 5

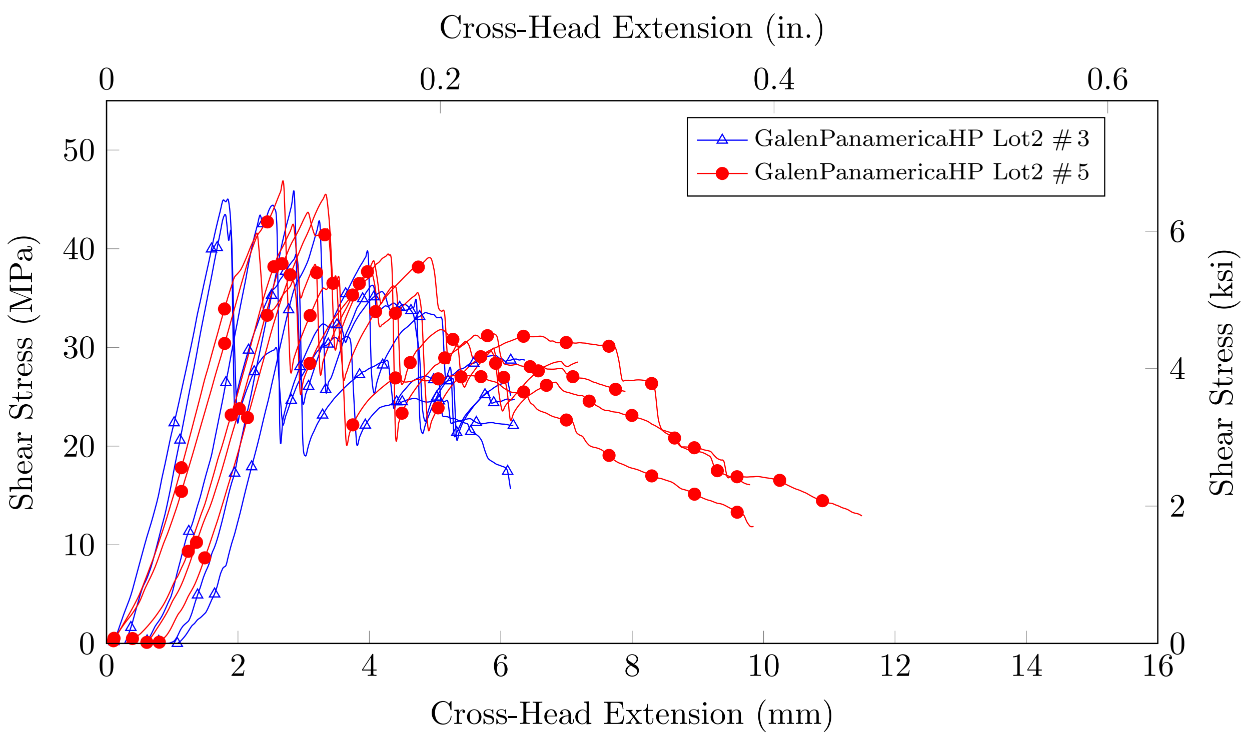


Figure 3.9: Horizontal shear stress vs. Extension behavior of Galen Panamerica Lot 2 HP rebar size 3 and 5

## 3.6 Modes of Failure

Figure 3.10 shows the failed BFRP specimen after completion of the horizontal shear test.

(a) Galen Panamerica HP # 3,

(b) Galen Panamerica HP # 5

(c) No Rust # 3

(d) No Rust # 5

Figure 3.10: Failure pattern for tested rebar after horizontal shear test

## 3.7 Summary of Horizontal Shear Strength Properties

The statistical values for the horizontal shear strength properties of the tested products are listed in the following Table 3.2. A total 30 specimen, five per each manufacture and each size were tested in total. An average of five specimen was calculated and shown in the table. All the BFRP rebar samples are satisfying the minimum GFRP criteria for horizontal shear strength which is shown in Tables 2.1, and 2.2.

Table 3.2: Horizontal Shear test statistical values for each sample group (US Customary Units)

| Exposure | | Sample Group | | | | Statistical Values | | | | |
|---|---|---|---|---|---|---|---|---|---|---|
| | | | | | | Shear Stress | | | | |
| Age | T | Manuf. | Resin | Size | Lot | $\wedge$ | $\vee$ | $\mu$ | $\sigma$ | CV |
| d | °C | Type | Type | # | No. | ksi | ksi | ksi | ksi | % |
| 0 | 23 | GalenPanamerica | HP | 3 | 1 | 6.4 | 7.5 | 7.0 | 0.5 | 6.57 |
| 0 | 23 | GalenPanamerica | HP | 3 | 2 | 6.2 | 6.7 | 6.5 | 0.2 | 2.79 |
| 0 | 23 | GalenPanamerica | HP | 5 | 1 | 5.6 | 6.8 | 6.4 | 0.5 | 7.98 |
| 0 | 23 | GalenPanamerica | HP | 5 | 2 | 6.0 | 6.8 | 6.4 | 0.3 | 4.99 |
| 0 | 23 | NoRustRebar | Epoxy | 3 | 1 | 5.8 | 6.7 | 6.4 | 0.4 | 5.90 |
| 0 | 23 | NoRustRebar | Epoxy | 5 | 1 | 6.2 | 6.9 | 6.5 | 0.3 | 3.89 |

## 3.8 Transverse Shear

### 3.8.1 Load vs. Displacement

The graphs plotted in Figures 3.11, 3.12, and 3.13 compares the load vs. displacement behavior of short span 3 point bending of # 3 and # 5 rebars from all manufacturer. The x-axis of graph represents the cross-head extension and the y-axis represents the applied load.

The graph in figure 3.11 shows a linear behavior until it reached the ultimate failure load.

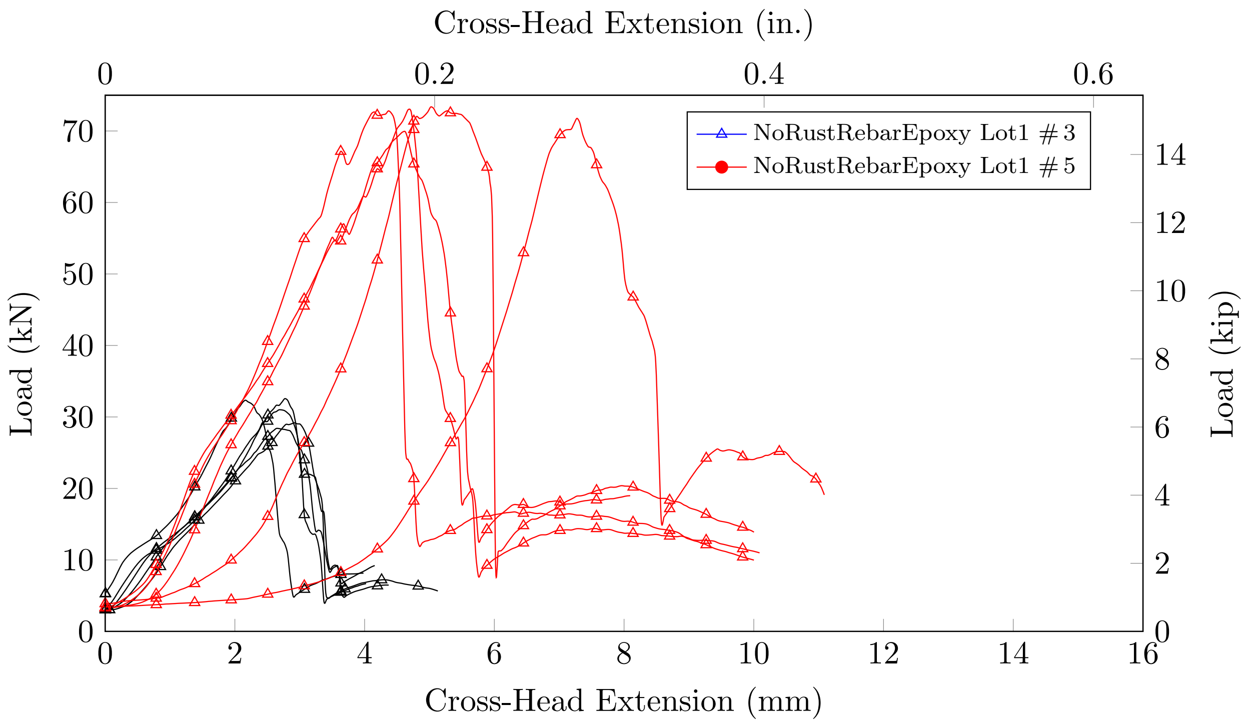


Figure 3.11: Extension vs. Transverse Shear Load behavior of No Rust rebar Lot 1 size 3 and 5

The graph in Figure 3.12 compares the load vs. displacement behavior of short span 3 point bending of # 3 and # 5 rebars from lot 1 from Galen Panamerica. The graphs show a linear behavior until it reached 90% of the ultimate failure load.

The graph in Figure 3.13 compares the load vs. displacement behavior of short span 3 point bending of # 3 and # 5 rebars from lot 2 from Galen Panamerica. The graphs show a linear behavior until it reached 90% of the ultimate failure load.

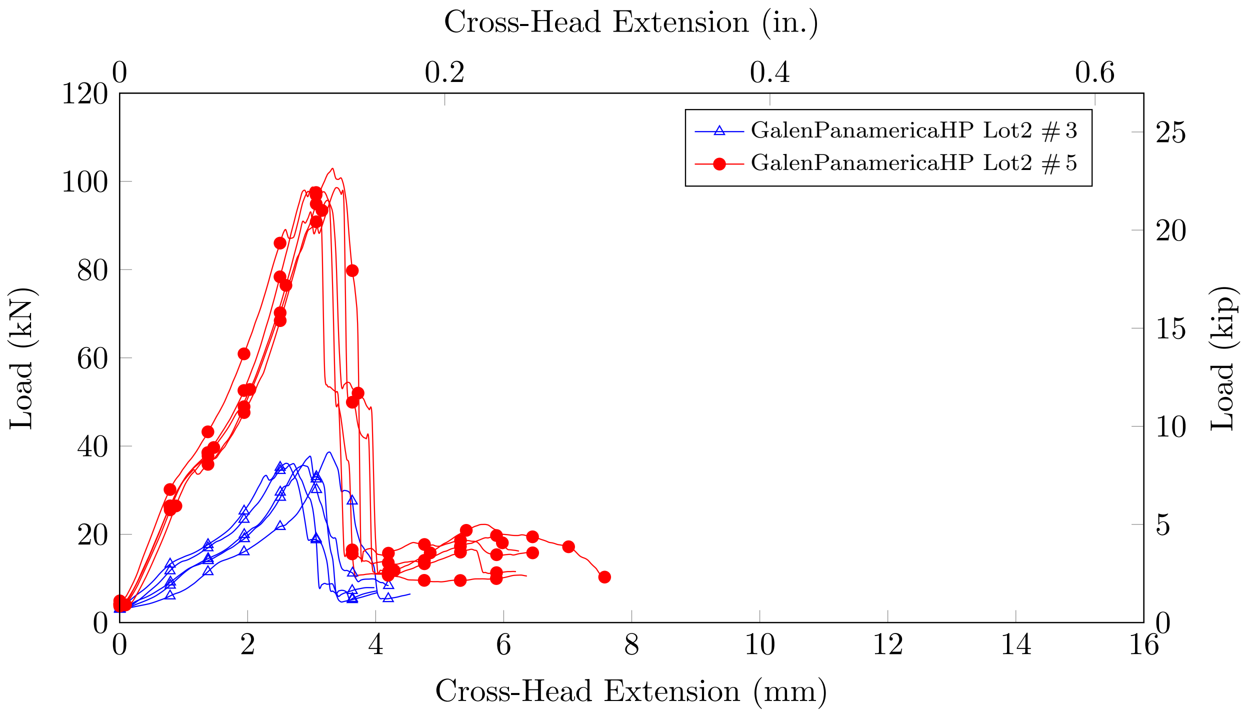


Figure 3.12: Extension vs. Transverse Shear Load behavior of Galen Panamerica Lot 1 HP rebar size 3 and 5

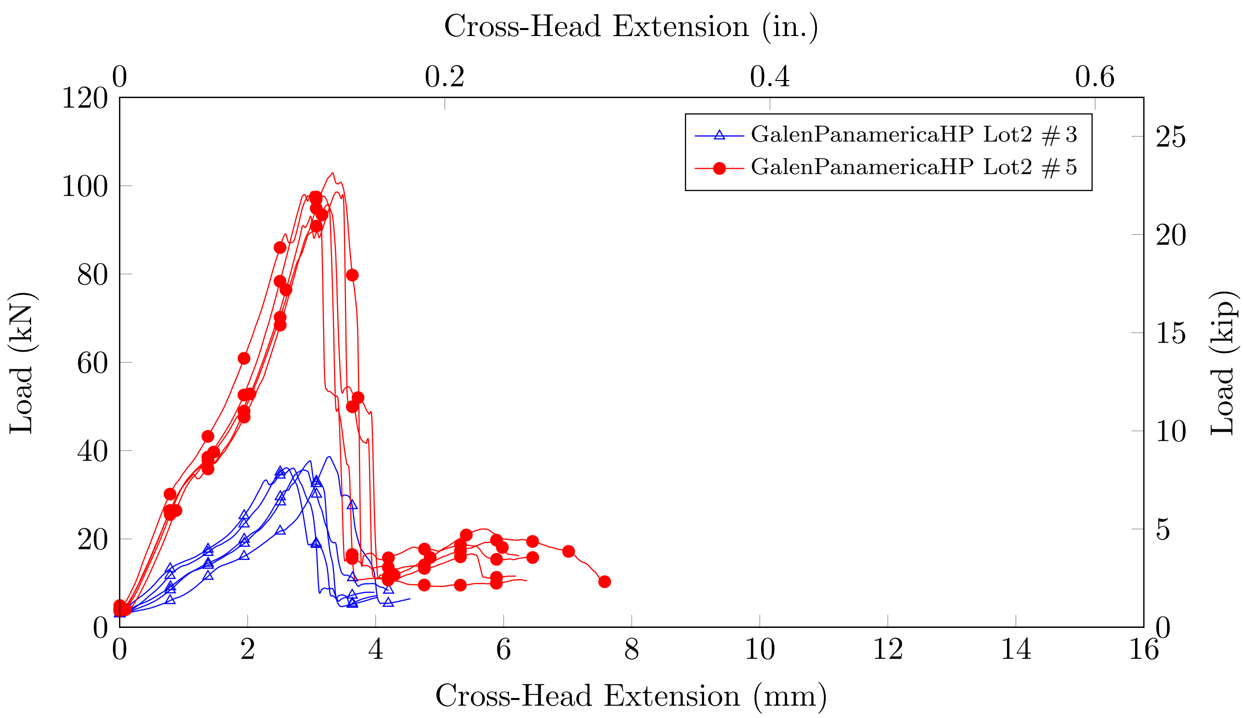


Figure 3.13: Extension vs. Transverse Shear Load behavior of Galen Panamerica Lot 2 HP rebar size 3 and 5

### 3.8.2 Stress vs. Displacement

The graphs in Figures 3.14, 3.15, and 3.16 compares the stress vs. displacement behavior of short span 3 point bending of #3 and #5 rebars from all rebar manufacturer. The x-axis of graph represents the cross-head extension and the y-axis represents the shear stress.

The graph in Figure 3.14 show a linear behavior until it reached the ultimate failure load.

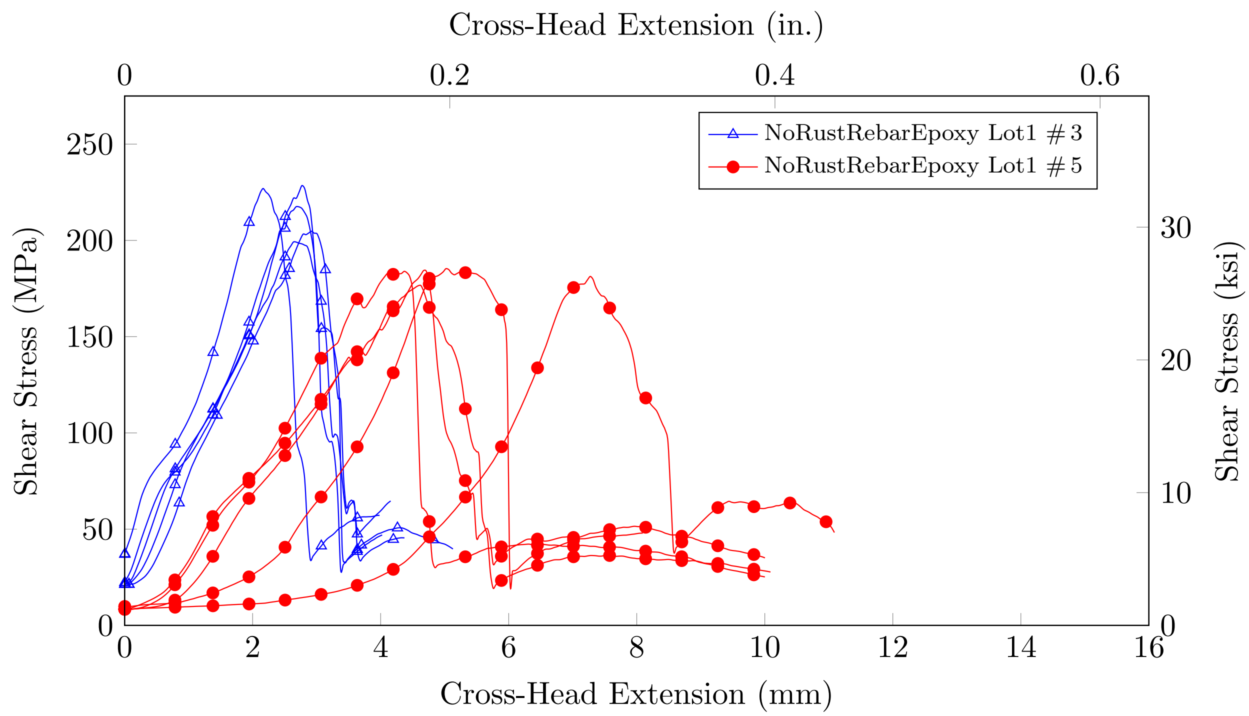


Figure 3.14: Transverse shear stress vs. Extension behavior of No Rust rebar Lot 1 size 3 and 5

The graph in Figure 3.15 compares the stress vs. displacement behavior of short span 3 point bending of #3 and #5 rebars from lot 1 from Galen Panamerica. The graphs show a linear behavior until it reached the ultimate failure load.

The graph in Figure 3.16 compares the stress vs. displacement behavior of short span 3 point bending of #3 and #5 rebars from lot 2 from Galen Panamerica. The graphs show a linear behavior until it reached the ultimate failure load.

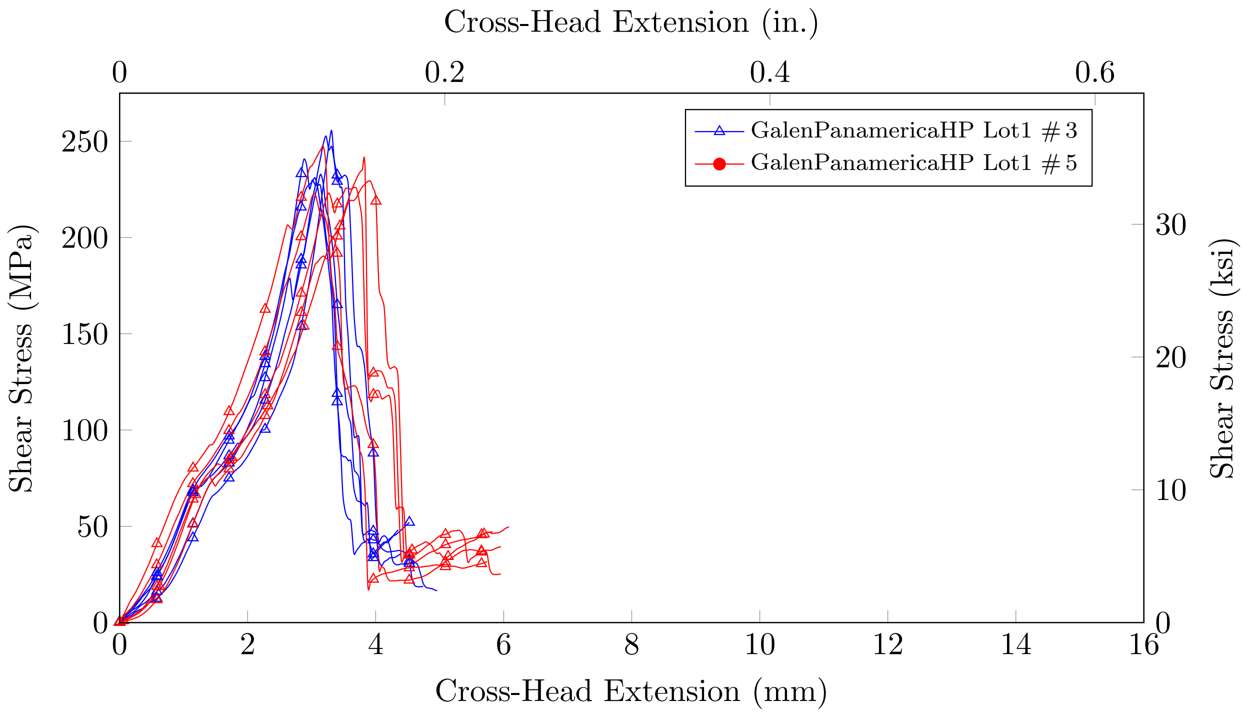


Figure 3.15: Transverse shear stress vs. Extension behavior of Galen Panamerica Lot 1 HP rebar size 3 and 5

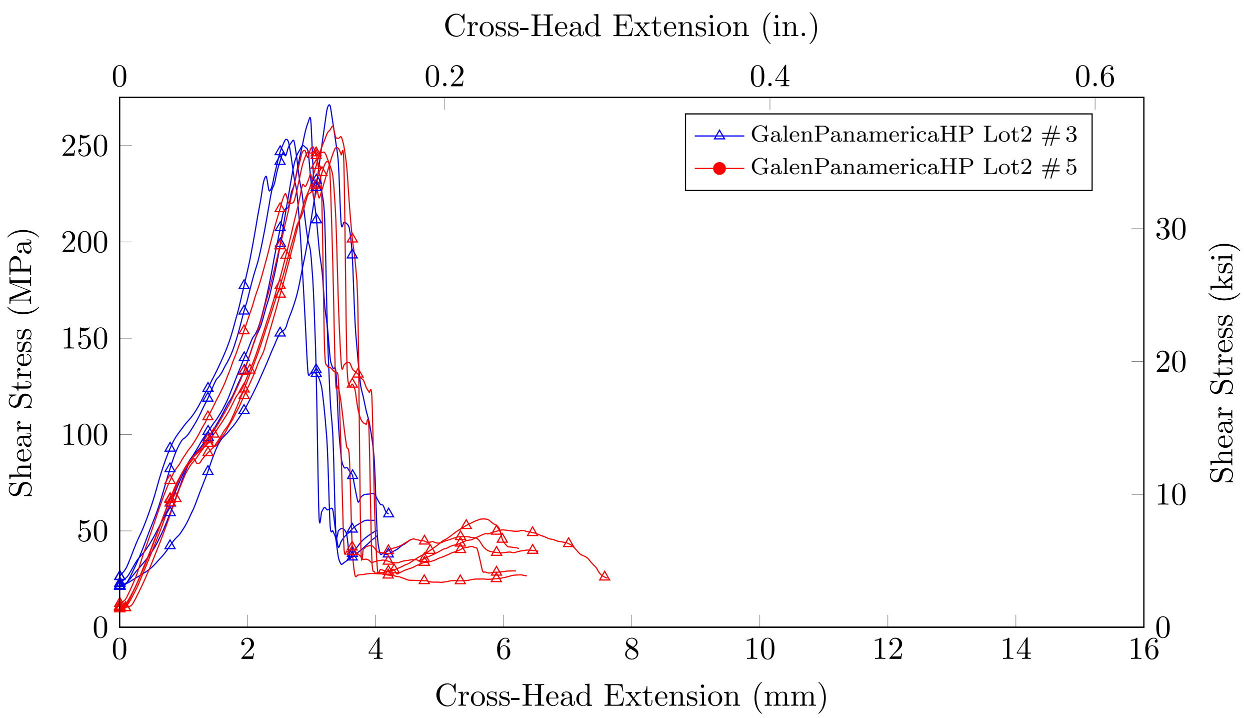


Figure 3.16: Transverse shear stress vs. Extension behavior of Galen Panamerica Lot 2 HP rebar size 3 and 5

## 3.9 Modes of Failure

The Figure 3.17 in this section shows the pictures of failed BFRP specimen due to transverse shear load.

(a) Galen Panamerica HP # 3

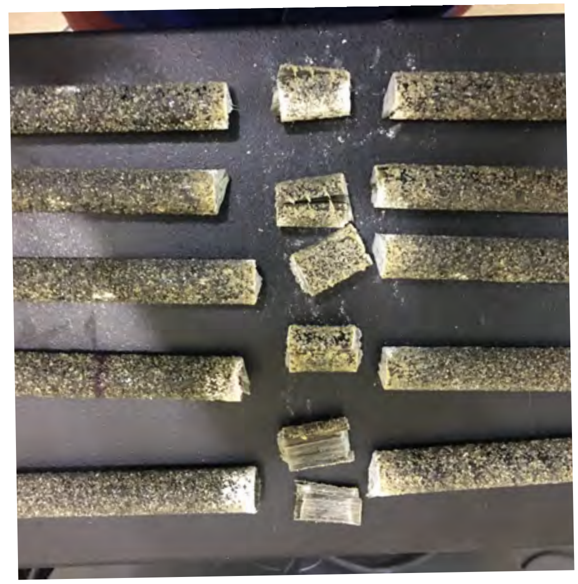

(b) Galen Panamerica HP # 5

(c) No Rust # 3

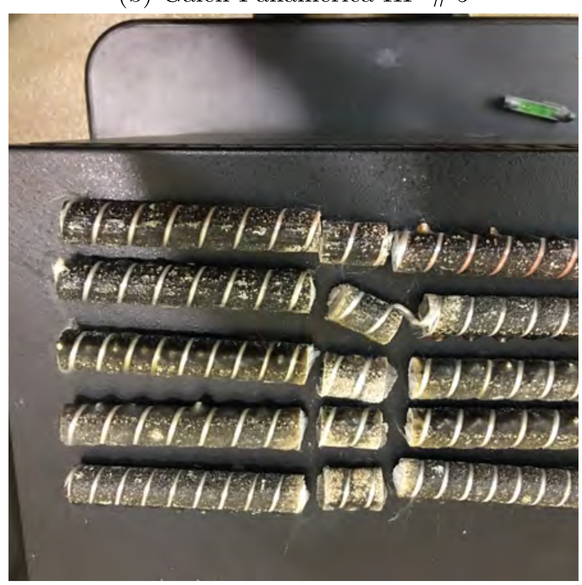

(d) No Rust # 5

Figure 3.17: Failure pattern for tested rebar after horizontal shear test

## 3.10 Summary of Transverse Shear Properties

The statistical values for the transverse shear strength properties of the tested products are listed in the following Table 3.3. A total 30 specimen, five per each manufacture and each size were tested in total. An average of five specimen was calculated and shown in the table. It can be seen in Tables 2.1, and 2.2 that all the BFRP rebar samples are satisfying the minimum required criteria for GFRP transverse shear stress.

Table 3.3: Transverse Shear test statistical values for each sample group (US Customary Units)

| Exposure | | Sample Group | | | | Statistical Values | | | | |
|---|---|---|---|---|---|---|---|---|---|---|
| | | | | | | Shear Stress | | | | |
| Age | T | Manuf. | Resin | Size | Lot | $\wedge$ | $\vee$ | $\mu$ | $\sigma$ | CV |
| d | °C | Type | Type | # | No. | ksi | ksi | ksi | ksi | % |
| 0 | 23 | GalenPanamerica | HE | 3 | 1 | 28.4 | 30.6 | 29.4 | 1.0 | 3.39 |
| 0 | 23 | GalenPanamerica | HP | 3 | 1 | 33.6 | 37.5 | 35.2 | 1.6 | 4.64 |
| 0 | 23 | GalenPanamerica | HP | 3 | 2 | 36.5 | 39.8 | 37.7 | 1.4 | 3.71 |
| 0 | 23 | GalenPanamerica | HP | 5 | 1 | 32.4 | 35.9 | 33.7 | 1.4 | 4.14 |
| 0 | 23 | GalenPanamerica | HP | 5 | 2 | 35.3 | 38.0 | 36.5 | 1.0 | 2.71 |
| 0 | 23 | NoRustRebar | Epoxy | 3 | 1 | 29.1 | 33.2 | 31.4 | 1.9 | 6.00 |
| 0 | 23 | NoRustRebar | Epoxy | 5 | 1 | 25.7 | 26.9 | 26.5 | 0.5 | 1.94 |

## 3.11 Tensile Test

The obtained and processed data during the tensile strength test are explained in this section. The following graphs in Figures 3.18, and 3.19 show the load vs. displacement and stress vs. strain behavior of Galen HP rebar.

### 3.11.1 Load vs. Displacement Behavior

The graphs in the Figure 3.19 compare the load vs .displacement behavior of rebar. The x-axis of graph represents the cross-head extension and the y-axis represents the applied load.

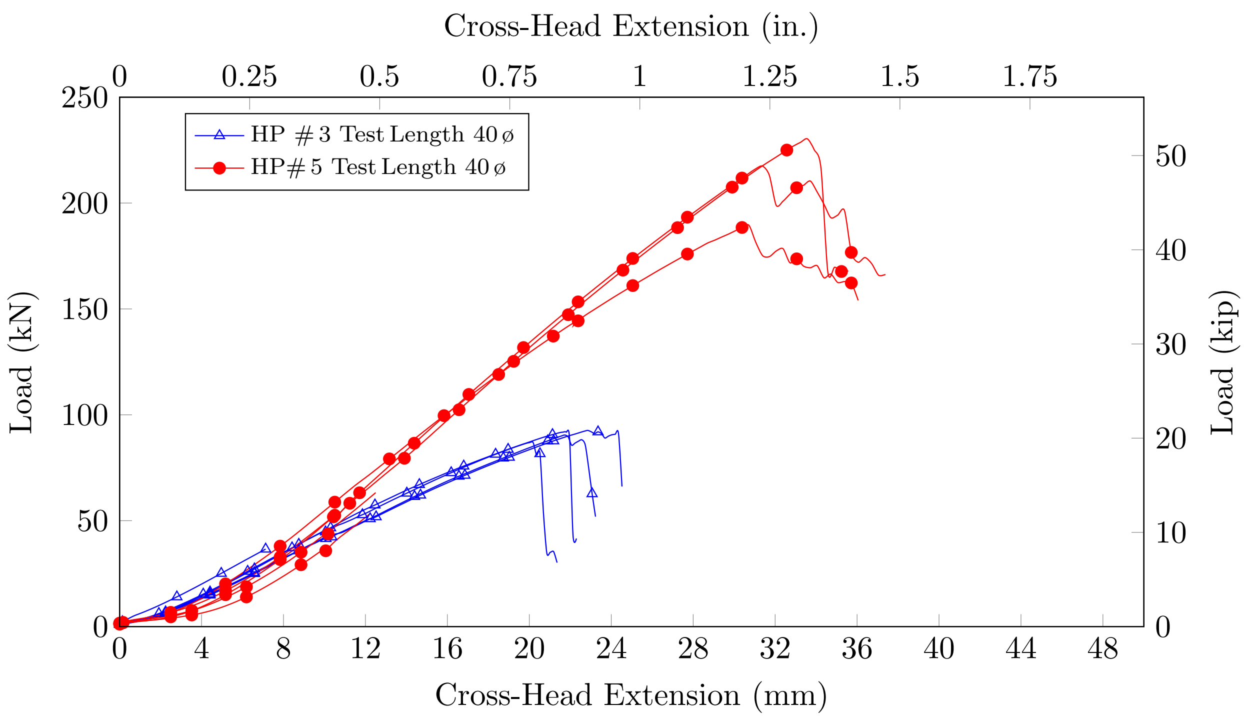


Figure 3.18: Tensile strengt vs. Displacement behavior of Galen Panamerica Lot 1 HP rebar size 3 and 5

### 3.11.2 Stress vs. Strain Behavior

The graphs in the Figure 3.19 compare the stress vs .strain behavior of rebar. The x-axis of graph represents the applied stress and the y-axis represents the strain in rebar.

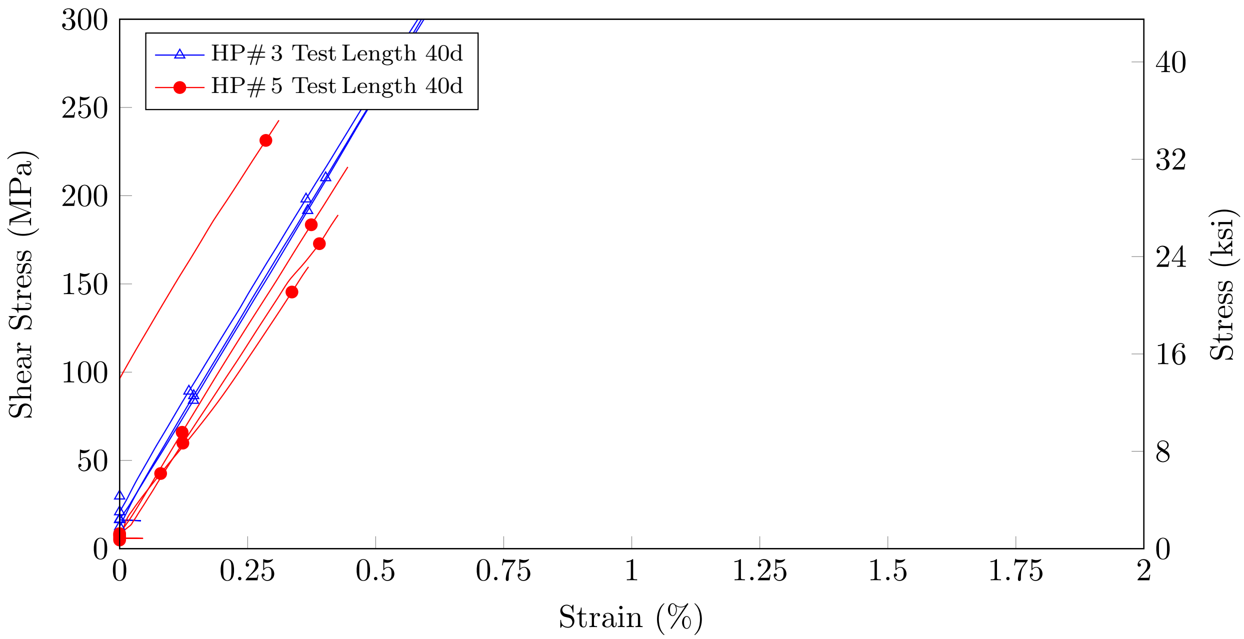


Figure 3.19: Tensile Stress vs. Strain behavior of Galen Panamerica Lot 1 HP rebar size 3 and 5

## 3.12 Modes of Failure

According to ASTM D 7205, three different failure modes may occur during a tensile strength test. The first and expected one is the tensile rupture outside of the anchor pipes. Due to insufficient sample preparation or test procedure issues, two more failure modes may occur. The rebar could slip within the grouted anchor (rebar slippage) or the anchor could slip out of the fixture/grips (anchor slippage). Nevertheless, the last two described failure modes lead to unusable results when defining the material characteristics. However, for this research project, no specimen failed due to rebar or anchor slippage. Hence, tensile rupture of the BFRP rebar was the recorded failure mode for each bar that was tested.

Figure 3.20 show the # 3 rebar specimens from Galen Panamerica for resin type HP. Similarly, Figure 3.21 show the failed specimens for the # 5 rebars, for the same manufacturer and the resin type.

Figure 3.20: GP HP # 3, final failure pattern after tensile test

Figure 3.21: GP HP # 5, final failure pattern after tensile test

All Galen Panamerica specimens, regardless of the resin type, failed in a similar manner. After the peak load was reached a bundle of outer fibers failed and brushed out over the entire free specimen length. After the first load-drop, this behavior continued at each additional sudden load drop until delamination reached the center of the rebar, and the specimen eventually separated into two parts along the rebar axis.

## 3.13 Summary of Tensile Properties

The statistical values for the tensile properties of all products are listed in the following Table 3.4. A total of 10 specimen, 5 per rebar size were tested and the results were analyzed. An average of statistical values of all 5 specimen is shown in Table 3.4

Table 3.4: Tensile strength test statistical values for each sample group (US Customary Units)

| Exposure | | Sample Group | | | | | Statistical Values | | | | | | | | | |
|---|---|---|---|---|---|---|---|---|---|---|---|---|---|---|---|---|
| | | | | | | | Tensile Strength | | | | | Elastic Modulus | | | | |
| Age d | T °C | Manuf. Type | Resin Type | Size # | Lot No. | FreeSpecimenLength Times Dia | $\wedge$ ksi | $\vee$ ksi | $\mu$ ksi | $\sigma$ ksi | CV % | $\wedge$ ksi | $\vee$ ksi | $\mu$ ksi | $\sigma$ ksi | CV % |
| 0 | 23 | Galen Panamerica | HP | 3 | 1 | 40 | 178.2 | 189.3 | 183.8 | 4.8 | 0.03 | 8 | 8 | 8 | 0 | 0.0 |
| 0 | 23 | Galen Panamerica | HP | 5 | 1 | 40 | 139.5 | 171.7 | 161.2 | 12.9 | 0.08 | 7 | 8 | 8 | 1 | 0.1 |

## 3.14 BFRP Rebar Performance

This section summarizes the material performance of the evaluated BFRP rebar samples based on the acceptance criteria for glass FRP rebars as shown in Tables 2.1, and 2.2 based on three different standards. Table 3.5 details the obtained results and the acceptance criteria for # 3 of Galen Panamerica rebar. It can be seen that the cross section properties, and fiber content properties of

Table 3.5: Acceptance criteria for Galen Panamerica rebar # 3

| | | | Per diameter | | FDOT 932-3/2017 | | AC454 | | ASTM D 7957 | |
|---|---|---|---|---|---|---|---|---|---|---|
| Test Method | Test Description | Unit | Nom. | Exp. | Criteria | ✓/✗ | Criteria | ✓/✗ | Criteria | ✓/✗ |
| ASTM D 792 | Measured Cross Sectional Area | $in.^2$ | 0.110 | 0.109 | 0.104 – 0.161 | ✓ | 0.104 – 0.161 | ✓ | 0.104 – 0.161 | ✓ |
| ASTM D 2584 | Fiber Content | % wt. | 82.035 | 82.035 | $\geqslant 70$ | ✓ | $\geqslant 70$ | ✓ | $\geqslant 70$ | ✓ |
| ASTM D 570 | Moist. Absorption short term @50 °C | % | 0.26 | 0.26 | $\leqslant 0.25$ | ✗ | $\leqslant 0.25$ | ✗ | $\leqslant 0.25$ | ✗ |
| ASTM D 570 | Moist. Absorption long term @50 °C | % | 1.77 | 1.77 | $\leqslant 1.0$ | ✗ | n/a | n/a | $\leqslant 1.0$ | ✗ |
| ASTM D 7205 | Min. Guaranteed Tensile Load | kip | 19.68 | 19.68 | $\geqslant 13.2$ | ✓ | $\geqslant 13.2$ | ✓ | $\geqslant 13.2$ | ✓ |
| ASTM D 7205 | Min. Guaranteed Tensile Strength | ksi | 163.38 | 163.38 | n/a | n/a | n/a | n/a | n/a | n/a |
| ASTM D 7205 | Tensile Modulus | ksi | 6,933 | 6,933 | $\geqslant 6,500$ | ✓ | $\geqslant 6,500$ | ✓ | $\geqslant 6,500$ | ✓ |
| ASTM D 7205 | Max. Strain | % | 2.34 | 2.34 | n/a | n/a | n/a | n/a | n/a | n/a |
| ASTM D 7617 | Min. Guaranteed Transverse Shear | ksi | 33.59 | 33.59 | $\geqslant 22$ | ✓ | $\geqslant 22$ | ✓ | $\geqslant 19$ | ✓ |
| ASTM D 4475 | Horizontal Shear Stress | ksi | 6.38 | 6.38 | n/a | n/a | $\geqslant 5.5$ | ✓ | n/a | n/a |
| ACI440. 3 R,B.3 | Bond-to-concrete strength | ksi | TBD | TBD | $\geqslant 1.1$ | n/a | $\geqslant 1.1$ | n/a | $\geqslant 1.1$ | n/a |

the rebar were in the acceptance range, where as the moisture absorption properties of the rebar exceeded. The rebar surpassed all acceptance ranges for all evaluated strength parameters. The following Table 3.6 shows that # 5 rebar of Galen Panamerica were within the acceptance range for cross section, fiber content, and shear properties, where as the modulus of elasticity was lower than the required minimum. Tables 3.7 and 3.8 demonstrate that both No Rust rebar sizes met or exceeded the acceptance criteria. The Tensile strength and bond-to-concrete characteristics for the rebar samples are still to be evaluated. The acceptance criteria for fiber content properties of # 3 and # 5 rebar samples from Pultrall manufacturer is shown in Table 3.9 and Table 3.10 respectively. Both rebar sizes measured fiber content values above the minimum 70 % criteria. A complete performance evaluation of these rebar samples are still underway.

Table 3.6: Acceptance criteria for Galen Panamerica rebar # 5

| Test Method | Test Description | Unit | Per diameter Nom. | Per diameter Exp. | FDOT 932-7/2017 Criteria | FDOT 932-7/2017 ✓/✗ | AC454 Criteria | AC454 ✓/✗ | ASTM D 7957 Criteria | ASTM D 7957 ✓/✗ |
|---|---|---|---|---|---|---|---|---|---|---|
| ASTM D 792 | Measured Cross Sectional Area | $in.^2$ | 0.307 | 0.353 | 0.288 – 0.388 | ✓ | 0.288 – 0.388 | ✓ | 0.288 – 0.388 | ✓ |
| ASTM D 2584 | Fiber Content | % wt. | 81.8 | 81.8 | $\geqslant 70$ | ✓ | $\geqslant 70$ | ✓ | $\geqslant 70$ | ✓ |
| ASTM D 570 | Moist. Absorption short term @50 °C | % | 0.25 | 0.25 | $\leqslant 0.25$ | ✓ | $\leqslant 0.25$ | ✓ | $\leqslant 0.25$ | ✓ |
| ASTM D 570 | Moist. Absorption long term @50 °C | % | 1.17 | 1.17 | $\leqslant 1.0$ | ✗ | n/a | n/a | $\leqslant 1.0$ | ✗ |
| ASTM D 7205 | Min. Guaranteed Tensile Load | kip | 42.82 | 42.82 | $\geqslant 29.1$ | ✓ | $\geqslant 32.2$ | ✓ | $\geqslant 29.1$ | ✓ |
| ASTM D 7205 | Min. Guaranteed Tensile Strength | ksi | 119.6 | 121.16 | n/a | n/a | n/a | n/a | n/a | n/a |
| ASTM D 7205 | Modulus | ksi | 5710 | 5836 | $\geqslant 6,500$ | ✗ | $\geqslant 6,500$ | ✗ | $\geqslant 6,500$ | ✗ |
| ASTM D 7205 | Max. Strain | % | 2.12 | 2.07 | n/a | n/a | n/a | n/a | n/a | n/a |
| ASTM D 7617 | Min. Guaranteed Transverse Shear | ksi | 32.38 | 28.115 | $\geqslant 22$ | ✓ | $\geqslant 22$ | ✓ | $\geqslant 19$ | ✓ |
| ASTM D 4475 | Horizontal Shear Stress | ksi | 5.56 | 4.826 | n/a | n/a | $\geqslant 5.5$ | ✗ | n/a | n/a |
| ACI440. 3 R,B.3 | Bond-to-concrete strength | ksi | TBD | TBD | $\geqslant 1.1$ | n/a | $\geqslant 1.1$ | n/a | $\geqslant 1.1$ | n/a |

Table 3.7: Acceptance criteria for No Rust rebar # 3

| Test Method | Test Description | Unit | Per diameter Nom. | Per diameter Exp. | FDOT 932-3/2017 Criteria | FDOT 932-3/2017 ✓/✗ | AC454 Criteria | AC454 ✓/✗ | ASTM D 7957 Criteria | ASTM D 7957 ✓/✗ |
|---|---|---|---|---|---|---|---|---|---|---|
| ASTM D 792 | Measured Cross Sectional Area | $in.^2$ | TBD | TBD | 0.104 – 0.161 | n/a | 0.104 – 0.161 | n/a | 0.104 – 0.161 | n/a |
| ASTM D 2584 | Fiber Content | % wt. | 75.17 | 75.17 | $\geqslant 70$ | ✓ | $\geqslant 70$ | ✓ | $\geqslant 70$ | ✓ |
| ASTM D 570 | Moist. Absorption short term @50 °C | % | 0.2 | 0.2 | $\leqslant 0.25$ | ✓ | $\leqslant 0.25$ | ✓ | $\leqslant 0.25$ | ✓ |
| ASTM D 570 | Moist. Absorption long term @50 °C | % | 0.55 | 0.55 | $\leqslant 1.0$ | ✓ | n/a | n/a | $\leqslant 1.0$ | ✓ |
| ASTM D 7205 | Min. Guaranteed Tensile Load | kip | TBD | TBD | $\geqslant 13.2$ | n/a | $\geqslant 13.2$ | n/a | $\geqslant 13.2$ | n/a |
| ASTM D 7205 | Min. Guaranteed Tensile Strength | ksi | TBD | TBD | n/a | n/a | n/a | n/a | n/a | n/a |
| ASTM D 7205 | Tensie Modulus | ksi | TBD | TBD | $\geqslant 6,500$ | n/a | $\geqslant 6,500$ | n/a | $\geqslant 6,500$ | n/a |
| ASTM D 7205 | Max. Strain | % | TBD | TBD | n/a | n/a | n/a | n/a | n/a | n/a |
| ASTM D 7617 | Min. Guaranteed Transverse Shear | ksi | 29.07 | n/a | $\geqslant 22$ | ✓ | $\geqslant 22$ | ✓ | $\geqslant 19$ | ✓ |
| ASTM D 4475 | Horizontal Shear Stress | ksi | 5.75 | n/a | n/a | n/a | $\geqslant 5.5$ | ✓ | n/a | n/a |
| ACI440. 3 R,B.3 | Bond-to-concrete strength | ksi | TBD | TBD | $\geqslant 1.1$ | n/a | $\geqslant 1.1$ | n/a | $\geqslant 1.1$ | n/a |

Table 3.8: Acceptance criteria for No Rust rebar # 5

| | | | Per diameter | | FDOT 932-3/2017 | | AC454 | | ASTM D 7957 | |
|---|---|---|---|---|---|---|---|---|---|---|
| Test Method | Test Description | Unit | Nom. | Exp. | Criteria | ✓/✗ | Criteria | ✓/✗ | Criteria | ✓/✗ |
| ASTM D 792 | Measured Cross Sectional Area | in.$^2$ | TBD | TBD | 0.288 – 0.388 | n/a | 0.288 – 0.388 | n/a | 0.288 – 0.388 | n/a |
| ASTM D 2584 | Fiber Content | % wt. | 78.4 | 78.4 | $\geqslant 70$ | ✓ | $\geqslant 70$ | ✓ | $\geqslant 70$ | ✓ |
| ASTM D 570 | Moist. Absorption short term @50 °C | % | 0.18 | 0.18 | $\leqslant 0.25$ | ✓ | $\leqslant 0.25$ | ✓ | $\leqslant 0.25$ | ✓ |
| ASTM D 570 | Moist. Absorption long term @50 °C | % | 0.77 | 0.77 | $\leqslant 1.0$ | ✓ | n/a | n/a | $\leqslant 1.0$ | ✓ |
| ASTM D 7205 | Min. Guaranteed Tensile Load | kip | TBD | TBD | $\geqslant 29.1$ | n/a | $\geqslant 32.2$ | n/a | $\geqslant 29.1$ | n/a |
| ASTM D 7205 | Min. Guaranteed Tensile Strength | ksi | TBD | TBD | n/a | n/a | n/a | n/a | n/a | n/a |
| ASTM D 7205 | Tensile Modulus | ksi | TBD | TBD | $\geqslant 6,500$ | n/a | $\geqslant 6,500$ | n/a | $\geqslant 6,500$ | n/a |
| ASTM D 7205 | Max. Strain | % | TBD | TBD | n/a | n/a | n/a | n/a | n/a | n/a |
| ASTM D 7617 | Min. Guaranteed Transverse Shear | ksi | 25.67 | TBD | $\geqslant 22$ | ✓ | $\geqslant 22$ | ✓ | $\geqslant 19$ | ✓ |
| ASTM D 4475 | Horizontal Shear Stress | ksi | 6.22 | TBD | n/a | n/a | $\geqslant 5.5$ | ✓ | n/a | n/a |
| ACI440. 3 R,B.3 | Bond-to-concrete strength | ksi | TBD | TBD | $\geqslant 1.1$ | n/a | $\geqslant 1.1$ | n/a | $\geqslant 1.1$ | n/a |

Table 3.9: Acceptance criteria for Pultrall rebar # 3

| | | | Per diameter | | FDOT 932-3/2017 | | AC454 | | ASTM D 7957 | |
|---|---|---|---|---|---|---|---|---|---|---|
| Test Method | Test Description | Unit | Nom. | Exp. | Criteria | ✓/✗ | Criteria | ✓/✗ | Criteria | ✓/✗ |
| ASTM D 792 | Measured Cross Sectional Area | in.$^2$ | TBD | TBD | 0.104 – 0.161 | n/a | 0.104 – 0.161 | n/a | 0.104 – 0.161 | n/a |
| ASTM D 2584 | Fiber Content | % wt. | 83.3 | 83.3 | $\geqslant 70$ | ✓ | $\geqslant 70$ | ✓ | $\geqslant 70$ | ✓ |
| ASTM D 570 | Moist. Absorption short term @50 °C | % | TBD | TBD | $\leqslant 0.25$ | n/a | $\leqslant 0.25$ | n/a | $\leqslant 0.25$ | n/a |
| ASTM D 570 | Moist. Absorption long term @50 °C | % | TBD | TBD | $\leqslant 1.0$ | n/a | n/a | n/a | $\leqslant 1.0$ | n/a |
| ASTM D 7205 | Min. Guaranteed Tensile Load | kip | TBD | TBD | $\geqslant 13.2$ | n/a | $\geqslant 13.2$ | n/a | $\geqslant 13.2$ | n/a |
| ASTM D 7205 | Min. Guaranteed Tensile Strength | ksi | TBD | TBD | n/a | n/a | n/a | n/a | n/a | n/a |
| ASTM D 7205 | Tensile Modulus | ksi | TBD | TBD | $\geqslant 6,500$ | n/a | $\geqslant 6,500$ | n/a | $\geqslant 6,500$ | n/a |
| ASTM D 7205 | Max. Strain | % | TBD | TBD | n/a | n/a | n/a | n/a | n/a | n/a |
| ASTM D 7617 | Min. Guaranteed Transverse Shear | ksi | TBD | TBD | $\geqslant 22$ | n/a | $\geqslant 22$ | n/a | $\geqslant 19$ | n/a |
| ASTM D 4475 | Horizontal Shear Stress | ksi | TBD | TBD | n/a | n/a | $\geqslant 5.5$ | n/a | n/a | n/a |
| ACI440. 3 R,B.3 | Bond-to-concrete strength | ksi | TBD | TBD | $\geqslant 1.1$ | n/a | $\geqslant 1.1$ | n/a | $\geqslant 1.1$ | n/a |

Table 3.10: Acceptance criteria for Pultrall rebar # 5

| Test Method | Test Description | Unit | Per diameter | | FDOT 932-3/2017 | | AC454 | | ASTM D 7957 | |
|---|---|---|---|---|---|---|---|---|---|---|
| | | | Nom. | Exp. | Criteria | ✓/✗ | Criteria | ✓/✗ | Criteria | ✓/✗ |
| ASTM D 792 | Measured Cross Sectional Area | $in.^2$ | TBD | TBD | 0.288 – 0.388 | n/a | 0.288 – 0.388 | n/a | 0.288 – 0.388 | n/a |
| ASTM D 2584 | Fiber Content | % wt. | 82.28 | 82.28 | $\geqslant 70$ | ✓ | $\geqslant 70$ | ✓ | $\geqslant 70$ | ✓ |
| ASTM D 570 | Moist. Absorption short term @50 °C | % | TBD | TBD | $\leqslant 0.25$ | n/a | $\leqslant 0.25$ | n/a | $\leqslant 0.25$ | n/a |
| ASTM D 570 | Moist. Absorption long term @50 °C | % | TBD | TBD | $\leqslant 1.0$ | n/a | n/a | n/a | $\leqslant 1.0$ | n/a |
| ASTM D 7205 | Min. Guaranteed Tensile Load | kip | TBD | TBD | $\geqslant 29.1$ | n/a | $\geqslant 32.2$ | n/a | $\geqslant 29.1$ | n/a |
| ASTM D 7205 | Min. Guaranteed Tensile Strength | ksi | TBD | TBD | n/a | n/a | n/a | n/a | n/a | n/a |
| ASTM D 7205 | Tensile Modulus | ksi | TBD | TBD | $\geqslant 6,500$ | n/a | $\geqslant 6,500$ | n/a | $\geqslant 6,500$ | n/a |
| ASTM D 7205 | Max. Strain | % | TBD | TBD | n/a | n/a | n/a | n/a | n/a | n/a |
| ASTM D 7617 | Min. Guaranteed Transverse Shear | ksi | TBD | TBD | $\geqslant 22$ | n/a | $\geqslant 22$ | n/a | $\geqslant 19$ | n/a |
| ASTM D 4475 | Horizontal Shear Stress | ksi | TBD | TBD | n/a | n/a | $\geqslant 5.5$ | n/a | n/a | n/a |
| ACI440. 3 R,B.3 | Bond-to-concrete strength | ksi | TBD | TBD | $\geqslant 1.1$ | n/a | $\geqslant 1.1$ | n/a | $\geqslant 1.1$ | n/a |

# Bibliography


ASTM (2014). *Standard Test Method for Moisture Absorption Properties and Equilibrium Conditioning of Polymer Matrix Composite Materials*, (D5229). ASTM International, West Conshohocken, PA.

ASTM-International (2011). *Standard Test Method for Ignition Loss of Cured Reinforced Resins*, (D2584-11). West Conshohocken, PA.

ASTM-International (2012a). *Standard Test Method for Apparent Horizontal Shear Strength of Pultruded Reinforced Plastic Rods By the Short-Beam Method*, (D4475 - 02 (REAPPROVED 2008)). West Conshohocken, PA.

ASTM-International (2012b). *Standard Test Method for Transverse Shear Strength of Fiber-reinforced Polymer Matrix Composite Bars*, (D7617/D7617M - 11). West Conshohocken, PA.

ASTM-International (2015). *Standard Test Methods for Density and Specific Gravity (Relative Density) of Plastics by Displacement*, (D792-13). West Conshohocken, PA.

# Appendix D

## Deliverable 3: BDV30 986-01 BFRP Material Specifications Recommendations Report

(7 pages)

**Deliverable 3**

# Performance evaluation, material and specification development for basalt fiber reinforced polymer (BFRP) reinforcing bars embedded in concrete

Contract Number BDV30 TWO 986-01
FSU Project ID: 042088

---

*Submitted to:*

**Florida Department of Transportation**
Research Center
605 Suwannee Street
Tallahassee, Florida 32399-0450

**Steven Nolan**
Project Manager
FDOT Structures Office

---


*Prepared by:*

**Raphael Kampmann, Ph.D.**
Principal Investigator
**Francisco De Caso, PhD, LEED A.P.**
Co-Principal Investigator
**Michelle Roddenberry, Ph.D., P.E.**
Co-Principal Investigator

FAMU-FSU College of Engineering
Department of Civil & Environmental Engineering
2525 Pottsdamer Street
Tallahassee, Florida 32310

University of Miami
Department of Civil, Architectural & Environmental Engineering
1251 Memorial Drive — McArthur Engineering Building 308
Coral Gables, Florida 33146


---

02/28/2019

# Recommendations

This report aims to provide recommendations for the mechanical and physical requirements of basalt fiber reinforced polymer (BFRP) rebars to assist the Florida Department of Transportation with the implementation process. BFRP rebar technology is still considered new in civil engineering construction in the United States, but it has been successfully used around the world in demonstration and low-risk projects. Before using any new or emerging material in infrastructure projects, the physical and mechanical properties must be evaluated and compared to acceptance criteria. In case of emerging materials, acceptance criteria might not have been fully established yet and research is needed to characterize a variety of products to determine general market quality and to define adequate limiting values. In this report, recommendations for physical properties such as cross-sectional dimensions, fiber content, and moisture absorption properties for BFRP rebars are proposed. In addition, recommendations for mechanical properties, including the apparent horizontal shear strength, the transverse shear strength, and the tensile properties are suggested. These suggestions are the result of experimental material evaluations and accompanying literature reviews. After the relevant material parameters were obtained for three different commercially available BFRP rebar products — and two different sizes (# 3 and # 5) — the results were analyzed and statistically compared and evaluate. Based on the findings, the following recommendations are provided:

**Cross Section property** The cross-sectional properties were measured according to ASTM D 792 (ASTM-International, 2015b). The cross sectional property is an important characteristics because the true tensile strength of rebar depends on the effective area. The nominal cross sectional area per FDOT specifications, section 932, for # 3 GFRP rebar is 0.11 in., with a minimum measured area of 0.104 in. and a maximum measured area of 0.161 in.. For # 5 rebar nominal cross sectional area, it is 0.31 in., with a minimum measured cross sectional area of 0.228 in. and a maximum of 0.338 in.. All the rebars shall be in the range so as to avoid errors in assumed centroid position for structural resistance calculations, any fit up errors in detailing such as spacing, cover or clearance, and consistency in product approval. It appears that these cross-sectional specification are useful for BFRP rebars as well because the issue of shear lag and load transfer in BFRP rebars is not significantly different from the mechanisms observed in GFRP rebars (Kampmann et al., 2018). Likewise, the production sequence for BFRP rebars and the load transfer is similar to glass fiber based rebars which allows similar definitions for both rebar types.

**Fiber Content** The experiments and the accompanying mathematical procedures to determine the fiber content percentage of FRP rebars are specified in material standard ASTM D 2584 - 11(ASTM-International, 2011). The fiber content percentage of the rebar plays a key role in the load capacity of the rebar because induced stresses are mostly carried by the fibers in the rebar, while the resin matrix must be stiff enough to transfer the loads between the individual fibers. The minimum fiber content percentage required for GFRP rebars according to FDOT specifications, section 932, which follows ASTM D 2584 -11(ASTM-International, 2011) is 70 %. After careful evaluation on the tested samples, it was seen that two of the three BFRP rebar products exceeded the required minimum criteria by at least 10 %. The third manufactured product exceeded the criteria by 5 %. Further decrease in the fiber content percentage may affect the stress transfer capacity of the rebar. However, it appears reasonable to suggest a minimum fiber content percentage for BFRP rebars to be similar to that for GFRP products. Additional research and analyses are required to establish a strong correlation between fiber content percentage and its effects on the rebar strength to support any modifications to the GFRP specifications specifically for BFRP.

**Moisture Absorption of BFRP rebar** ASTM D 5229 (ASTM, 2014) details seven different test procedures (A through E,Y, and Z) for estimating moisture absorption properties for FRPs in different environments. Procedure A is most commonly used, and therefore, was followed for this research project as well. The moisture absorption property plays an important role in retaining the strength of rebar and its long-term durability in harsh environments because high moisture absorption values are indicative of a porous rebar which is more prone to degradation. According to FDOT specifications section 932, which follows ASTM D 5229 (ASTM, 2014) section 7.1, the maximum short-term moisture absorption limit for GFRP rebars is 0.25 % by weight. And long-term moisture absorption shall be less than 1 %. After proper evaluation of the tested specimens, it was found that the long-term moisture absorption of BFRP rebars was less than 1 %. As increased moisture absorption property affects the strength and strength retention of FRP rebars, it is reasonable to suggest that the BFRP rebar shall follow the criteria established for GFRP moisture absorption properties. Furthermore, because the microstructure porosity and the moisture absorption of FRP rebars are closely related, SEM analysis of specimen after long-term moisture absorption tests should be conducted to evaluate the rebar properties at the micro level and to define its vulnerability to degradation. New products should be characterized via SEM and the findings and images stored in a data base for comparison to future iterations of specific product lines.

**Horizontal Shear Strength** The horizontal shear test was conducted according to ASTM D 4475 (ASTM-International, 2012a) standards. It has been noted that the FDOT specifications does not include minimum horizontal shear strength requirements for rebars made from any fiber material. The horizontal shear failure, however, is an indicator of the resin strength and the resin-to-fiber bonding quality and as such important for the load transfer from fiber to fiber. After a manufacturer survey was conducted — as part of the literature review — to identify common practices in the FRP rebar industry, it has been noted that horizontal shear tests are one of the common quality control methods that producers rely on to ensure production quality and consistency. Accordingly, FDOT Section 932 would benefit from limiting minimum values for the acceptance of FRP rebars. Likewise, it would provide a direct benefit to the manufacturing community and the intersection between FDOT and technology implementation because a quality control parameter could be directly targeted during production — and quickly evaluated. The horizontal shear strength of # 3, and # 5 GFRP rebars appears to range around 6 ksi (c.f. Kampmann et al. (2018)). However, because no specified criteria for the minimum horizontal shear strength has been defined, additional research focusing on this property is recommended.

**Transverse Shear Strength** ASTM D 7617 (ASTM-International, 2012b) was followed to test and analyze the transverse shear data obtained from BFRP rebar testing. FRP rebars are weak in the transverse direction or perpendicular to the rebar longitudinal axis. According to FDOT specification, section 932, GFRP rebars are required to reach a minimum shear strength of 22 ksi, before rupture. After a careful testing and analysis process, the tested # 3 BFRP rebars sustained shear stresses at failure ranging from 30 ksi to 36 ksi and # 5 rebars sustained a stress range from

26 ksi to 33 ksi. Based on the results obtained in this study, in comparison to other studies (Kampmann et al., 2018), it appears that BFRP rebars are stronger than GFRP rebars in the transverse direction. For simplicity, this research suggests that the minimum transverse shear strength criteria for BFRP rebars should be similar to the criteria defined for GFRP rebars.

**Tensile Properties** The tensile strength and elastic modulus of BFRP rebars were evaluated based on procedures and methods detailed in ASTM D 7205 (ASTM-International, 2015a) The minimum tensile load requirements for # 3 GFRP rebar according to FDOT specifications, section 932, is 13.2 kip, and for # 5 rebar is 29.1 kip. Based on the findings from this research project and projects targeting glass fiber based rebars (Kampmann et al., 2018), it can be stated that BFRP rebars appear to be measurably stronger in tension with higher elastic moduli — as compared to GFRP rebars. It has been noted that the minimum tensile load sustained by # 3 BFRP rebars is 19.68 kip and that of # 5 rebars is 42.8 kip . The elastic moduli of BFRP rebar were measured with a minimum of 8 ksi. The elastic moduli of GFRP rebar according to Kampmann et al. (2018) was measured to reach average values of approximately 7000 ksi. All tested BFRP rebar strengths superseded the minimum strength criteria for GFRP rebars. A Further detailed testing of a wide range of rebars from several manufacturers is required to fully study the strength properties of rebar and to properly define a minimum required criteria. However, if basalt fiber specific criteria are desirable for the tensile properties, the data in this research suggests that the minimum strength and elastic modulus should be significantly higher for BFRP rebars.

**Further Suggestions** It is noted that no long-term tests were performed throughout this project and that additional durability analyses for BFRP rebars in extreme environments shall be done. It appears vital because of the unique chemical composition of basalt fibers and the interaction they can potentially undergo in saline-rich and high pH environments. This may be one of the most important aspects for a proper life cycle of concrete structures reinforced with BFRP rebars in aggressive environments (e.g.; bridges in Florida) because of the highly basic conditions in cementitious paste.

Lu et al. (2015) compared virgin to aged, pultruded BFRP plates and rebars to measure the effect of thermal aging (at 135 °C and 300 °C for four hours) on the longitudinal tensile strength and the inter laminar shear properties. It was found that the degradation process of aged rebars immersed in alkaline solution and distilled water accelerated due to thermal aging. Altalmas et al. (2015) studied the bond-to-concrete durability properties of sand coated basalt fiber reinforced polymer (BFRP) rebars and glass fiber reinforced polymer (GFRP) rebars via accelerated conditioning in acidic, saline, and alkaline solutions for 30 days, 60 days, and 90 days. The results showed that the bond strength of rebars immersed in acid solution, alkaline and saline environments in comparison to un-aged rebars reduced and that all rebars failed in inter-laminar shear. Wang et al. (2017) tested tensile strength and Young's modulus properties of BFRP and GFRP rebars exposed to seawater and sea sand concrete (SWSSC). The rebars were exposed to normal SWSSC (N-SWSSC), and high performance SWSSC (HP-SWSSC) at room temperature, 40 °C, 48 °C, and 50 °C for 21 days, 42 days and 63 days. When compared to HP-SWSSC, N-SWSSC was more aggressive on both BFRP, and GFRP bars due to the high alkali ion concentration. In high temperature environments, the GFRP rebars were more durable than the BFRP rebars, because of the different resins. Based on the SEM, 3D X-ray, and CT-results, the resin properties of GFRP bars were more stable in SWSSC conditions than the resin used for the tested BFRP rebars. In research projects conducted by Benmokrane et al. (2017) and Kajorncheappunngam et al. (2002), the longterm durability in alkali environments at accelerated temperatures for rebars made with different resins was evaluated. It was seen that the performance of epoxy resins was comparably good and acceptable.

Wei et al. (2011) studied degradation of basalt fiber-epoxy resin and glass fiber-epoxy resin composites in seawater. Wei et al. (2011) found that the bending and tensile strength decreased with increase in immersion time. The chemical stability of BFRP rebars can be improved by lowering the $Fe^{+2}$ ions in basalt rock and durability of rebar in seawater can be increased.

Two of the three tested rebar types for this research included rebars made with epoxy resins. The mechanical performance of the rebars made from epoxy resin was higher than the rebars made from other resin. Most basalt rebar manufacturers across the globe uses epoxy resin in the manufacturing processes. It appears that epoxy resins are suitable for the production of basalt FRP rebars and that such constituent materials should be considered in future updates of standard specifications (Florida Section 932). However, additional research with a focus on physical and mechanical properties in response to chemical durability for rebars made with different resins should be conducted.

Comparing this research to a previous study (Kampmann et al., 2018), it can be seen that the maximum strain and elongation of BFRP rebars surpasses the maximum strains of glass fiber based rebars. Likewise, the elastic lengthening of BFRP tendons is higher than that of steel (Thorhallsson and Jonsson, 2012; Pearson et al., 2013) and it might be beneficial to evaluate basalt fiber materials for the use of prestressing tendons.

# References


Altalmas, A., Refai, A. E., and Abed, F. (2015). "Bond degradation of basalt fiber-reinforced polymer (bfrp) bars exposed to accelerated aging conditions." *Construction and Building Materials*, *81*, 162–171.

ASTM (2014). *Standard Test Method for Moisture Absorption Properties and Equilibrium Conditioning of Polymer Matrix Composite Materials*, (D5229). ASTM International, West Conshohocken, PA.

ASTM-International (2011). *Standard Test Method for Ignition Loss of Cured Reinforced Resins*, (D2584-11). West Conshohocken, PA.

ASTM-International (2012a). *Standard Test Method for Apparent Horizontal Shear Strength of Pultruded Reinforced Plastic Rods By the Short-Beam Method*, (D4475 - 02 (REAPPROVED 2008)). West Conshohocken, PA.

ASTM-International (2012b). *Standard Test Method for Transverse Shear Strength of Fiber-reinforced Polymer Matrix Composite Bars*, (D7617/D7617M - 11). West Conshohocken, PA.

ASTM-International (2015a). *Standard Test Method for Tensile Properties of Fiber Reinforced Polymer Matrix Composite Bars*, (D7205/D7205M – 06 Reapproved 2011). West Conshohocken, PA.

ASTM-International (2015b). *Standard Test Methods for Density and Specific Gravity (Relative Density) of Plastics by Displacement*, (D792-13). West Conshohocken, PA.

Benmokrane, B., Ali, A. H., Mohamed, H. M., ElSafty, A., and Manalo, A. (2017). "Laboratory assessment and durability performance of vinyl-ester, polyester, and epoxy glass-frp bars for concrete structures." *Composites Part B: Engineering*, *114*, 163–174.

Kajorncheappunngam, S., Gupta, R. K., and GangaRao, H. V. (2002). "Effect of aging environment on degradation of glass-reinforced epoxy." *Journal of composites for construction*, *6*(1), 61–69.

Kampmann, R., De Caso Y Basalo, F., and Ruiz Emparanza, A. (2018). *"Performance evaluation of glass fiber reinforced polymer (gfrp) reinforcing bars embedded in concrete under aggressive environments.*" Technical Report BDV30 TWO 977-18, Florida Department of Transportation.

Lu, Z., Xian, G., and Li, H. (2015). "Effects of exposure to elevated temperatures and subsequent immersion in water or alkaline solution on the mechanical properties of pultruded bfrp plates." *Composites Part B: Engineering*, *77*, 421–430.

Pearson, M., Donchev, T., and Salazar, J. (2013). "Long-term behaviour of prestressed basalt fibre reinforced polymer bars." *Procedia Engineering*, *54*, 261–269.

Thorhallsson, E. and Jonsson, B. S. (2012). "Test of prestressed concrete beams with bfrp tendons." *Reykjavik University*.

Wang, Z., Zhao, X.-L., Xian, G., Wu, G., Raman, R. S., Al-Saadi, S., and Haque, A. (2017). "Long-term durability of basalt- and glass-fibre reinforced polymer (bfrp/gfrp) bars in seawater and sea sand concrete environment." *Construction and Building Materials*, *139*, 467–489.

Wei, B., Cao, H., and Song, S. (2011). "Degradation of basalt fibre and glass fibre/epoxy resin composites in seawater." *Corrosion Science*, *53*(1), 426–431.

# Appendix E

## Deliverable 1: BDV34 986-03 BFRP-RC Link-Slab Demonstration Project – Literature Review Report

(31 pages)

**EXHIBIT A – SCOPE OF SERVICE**

Project Title: **BRIDGE DECK WITH LINK-SLAB**

**for FPID: 435390-1-52-01: US 41 from Midway Blvd to Enterprise**

**Contract Number: BDV34 986-02**

**Deliverable 1 - TASK 1 – Literature Review**

Submitted by: Principal Investigator: **Adel ElSafty**, Ph.D., P.E.

University of North Florida

Address: School of Engineering, 1 UNF Drive, Jacksonville, FL 32224-2645

Email Address: adel.el-safty@unf.edu

Phone Number: (904) 620-1398

Submitted to: Steven Nolan

The Florida Department of Transportation

State Structures Design Office

605 Suwannee Street, MS 33

Tallahassee, FL 32399-0450

Dr. Cheresa Y. Boston

Director of Sponsored Research,

University of North Florida, Office of Research and Sponsored Programs

1 UNF Drive, Jacksonville, Florida 32224

Phone: (904) 620-2455, Fax: (904) 620-2457, Email: cheresa.boston@unf.edu

Project Manager: Steven Nolan

Florida Department of Transportation

State Structures Design Office

Email Address: Steven.Nolan@dot.state.fl.us , Phone: (850) 414-4272

February 28, 2019

**BACKGROUND STATEMENT**

Bridge deck joints are costly to buy, install, and maintain. They have provided severe performance and maintenance problems as water and deck drainage contaminated with chemicals leak through the superstructure and onto the pier caps below, thus damaging or eventually completely destroying some vital parts of bridges such as prestressing cable anchorage systems, beams, bearings, substructure seat areas, and end diaphragms. Also, debris accumulation in the joints may restrain deck expansion (ElSafty 1994).

One of the best solutions is to adopt jointless bridges and elimination of expansion joints in bridge decks. That has been an effective method of constructing bridges. It corresponds to reduced maintenance and improved bridge-deck life expectancy. It is possible to replace bearing devices with simple elastomeric pads, or totally integrate the superstructure with the supports without any bearings. With the use of jointless bridge decks, there are no joints to purchase nor bearings to maintain, the riding surface is smoother, the initial and life-cycle cost are lower, and there will be a reduction in span bending moments and deflections. In conclusion, using a link-slab and making the bridge girders (partially continuous) continuous for live load provides lower cost, improved durability, longer spans, improved seismic performance, better resistance to wind loads and storm wave loads, improved structural integrity, and improved riding quality. Current consensus seems to allow elimination of expansion joints on bridges as long as 650 feet. Much longer bridges have occasionally been constructed without reported distress. There is a need for simple guidelines for design and detailing of the popular continuous-for-live-load connection system. An options for jointless bridge deck link-slab is shown in Fig. 1.

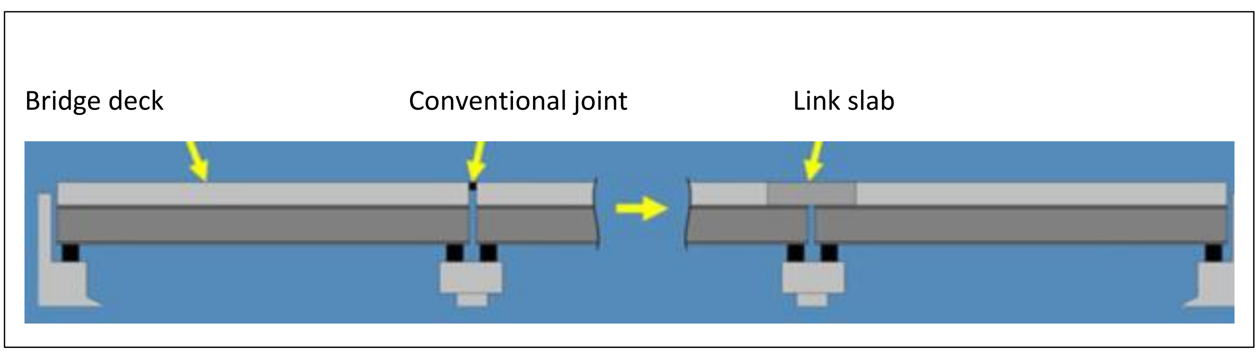


**Fig. 1: Link-slab option**

## LITERATURE REVIEW:

The national bridge inventory indicates that a big percentage of the highway bridges in United States are designed as single or multiple simple-span girders supported at the piers and abutments, and separated by joints (FHWA 2004). These joints are provided at the girder ends of each simple span to allow the movement of the deck and superstructure due to temperature changes, shrinkage, creep, and other effects. These deck joints generally lead to water, sometimes contaminated with chlorides, leaking through the joints causing deterioration and corrosion of the bridge deck, girders, bearing, and supporting systems. Joints can also get filled with debris and fail to allow expansion and contraction of the superstructure. Therefore, the joint systems affect the durability of bridge structures and do not provide a reliable and leak-proof performance. In addition, joints and bearings can be expensive to install and maintain.

A growing trend in bridge design has been toward the elimination of joints and bearings in the bridge superstructure. Yet, the behavior of jointless bridge deck is not precisely known and the designs could have some uncertainties. Despite the numerous benefits of jointless bridge decks, there is no standardized design procedures for these bridges and there is only a list of specifications and design recommendations available. Therefore, there is a need to further investigate the feasibility of an innovative system for reducing or eliminating the number of bridge deck joints. The alternatives include using a concrete or ultra-high-performance concrete (UHPC) link-slab reinforced with steel or fiber-reinforced polymer (FRP) rebar to join adjacent bridge decks without imposing girder continuity.

Over many years, the use of jointless bridges has proven to be an excellent alternative to preserve bridges from the adverse effects of debris, leaking water, and salt induced corrosion damage.  The jointless bridge option had also proven to be an economical option that provided several inherent design advantages. In the AASHTO LRFD Bridge Design Specifications, there are no requirements for maximum bridge length allowed without expansion joints. Most state highway agencies allow eliminating joints for bridges whose lengths are less than 350 feet for bridges with steel beams and 650 feet with concrete beams; however, there are some bridges over 1000 ft long that have performed well without expansion joint (Tadros 2016).

Several researchers indicted the effect of deck continuity over the piers on the moment developed in the spans, the reduction in deflection and vibration than simple span bridge girders, the improved durability and riding quality after eliminating the joints. Gastal and Zia (1989) performed an analysis of bridge beams with jointless decks. ElSafty (1994) conducted an analysis and investigation of jointless bridge decks with partially debonded simple span beams. Zia et al. (1998) investigated casting fully-continuous deck over simply supported girders with partial debonding of the deck from the girders ends at supports, using both numerical and experimental analysis, as shown in Fig. 2. Okeil and Elsafty (2005) investigated the partial continuity in bridge girders with jointless decks and the effect of the system's support configuration on the axial force developed in the link-slab. Caner and Zia (1998) presented the results of a test program to investigate the behavior of link-slabs connecting two adjacent simple-span girders, and proposed a simple method for designing the link-slab. ElSafty and Okeil (2008) also investigated extending the service life of bridges using continuous decks, as shown in Fig. 3 and Fig. 4.

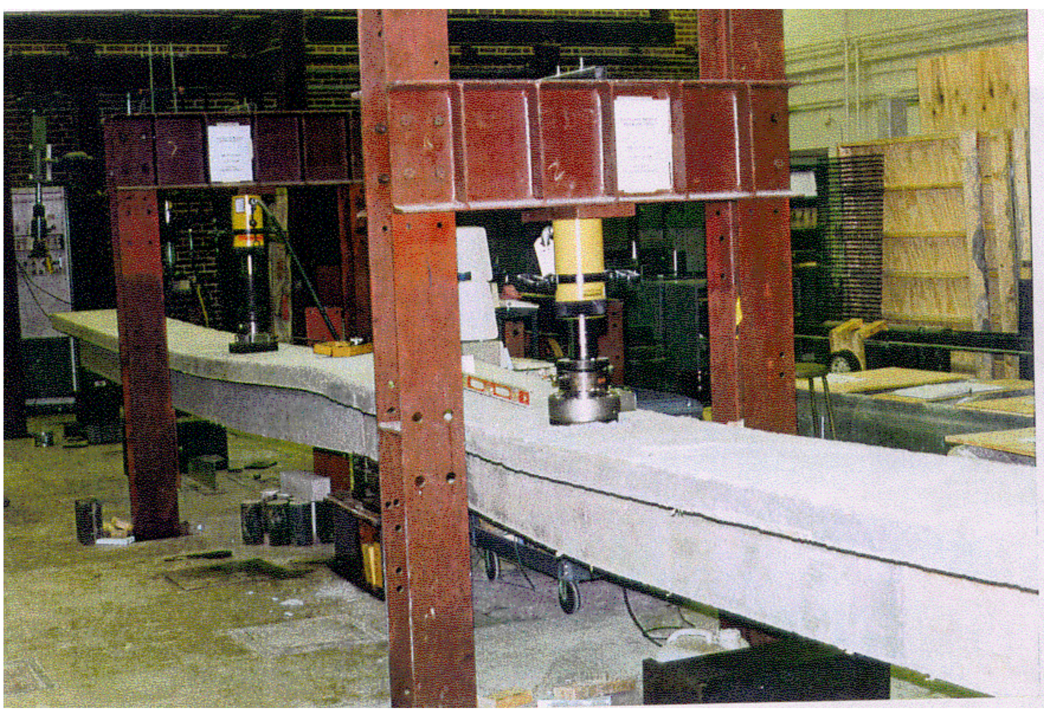

**Fig. 2: Testing of a 2-span bridge model - Zia et al. (1998)**

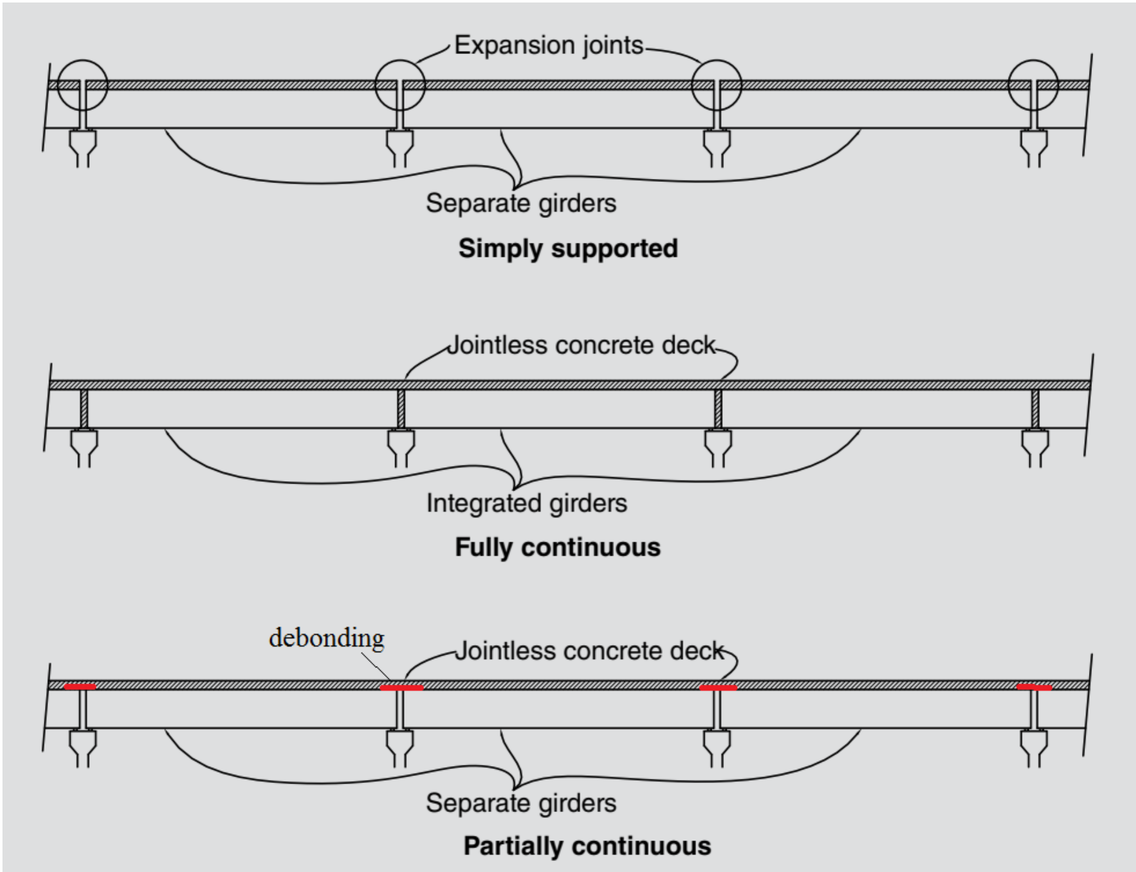


**Fig. 3: Some types of jointless bridge decks**

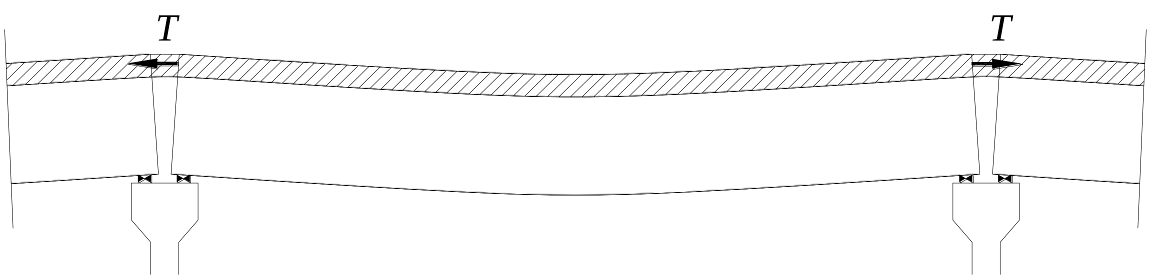


**Fig. 4: Continuity caused by linking concrete decks in adjacent spans**

Thippeswamy et al. (2002) conducted an investigation on jointless bridges to study the behavior of jointless bridges supported on piles and spread footings and subjected to varying load conditions. In addition, time-dependent material properties have also been investigated. In their study, Thippeswamy et al. (2002) presented synthesized analytical data to understand the performance under varying load combinations, field testing and monitoring results of a jointless bridge West Virginia, and effects of primary versus secondary loads, boundary conditions, and system flexibility on induced stresses at various bridge locations.

Reyes and Robertson (2011) investigated the use of high-performance fiber-reinforced cementitious composite (HPFRCC) reinforced with glass fiber reinforced polymer (GFRP) bars as link-slabs to replace the bridge expansion joints. Several small-scale specimens were tested. Then, a full scale test specimen with a full scale bridge expansion joint was investigated to characterize the performance of HPFRCC with GFRP reinforcing bars. The full-scale bridge expansion joint specimen emulated an expansion joint condition of a composite steel girder to concrete deck slab section. The link-slab was subjected to cyclic axial strains in both tension and compression and later in direct tension until failure. It was found that the cast-in-place link-slab had the advantage of providing good continuity with the bridge deck. The failure was due to rupture of the anchorage at the ends of the link-slab.

Virginia DOT also suggested the shown link-slab detail, Fig. 5.

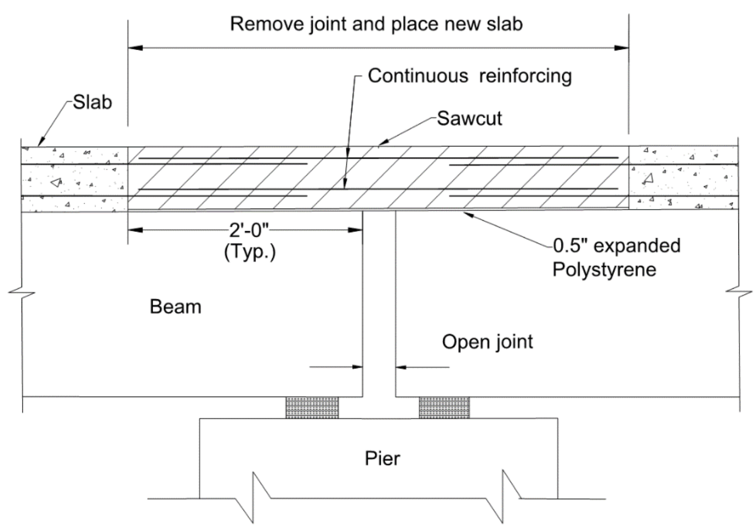


**Fig. 5: Use of link-slab by VDOT for rehabilitation work to eliminate expansion joint**

Virginia DOT also listed the following types of joint systems used in Virginia, as shown in Figs. 6-13:

- **Armored Joints – Open or Sealed**

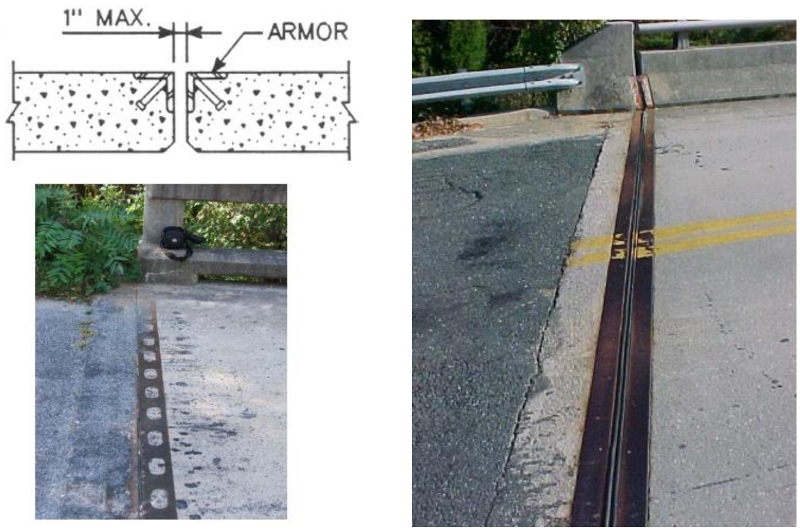


**Fig. 6: Armored Joints**

- **Hot Poured Sealer /Expansion Material**

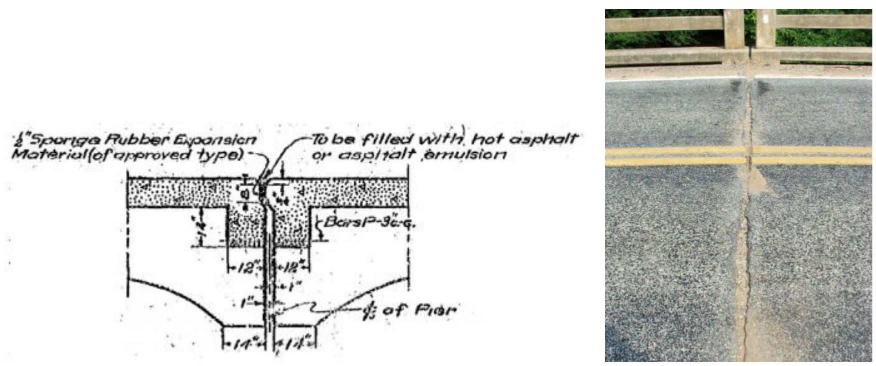


**Fig. 7: Hot Poured Sealer**

- **Preformed Elastomeric Compression Seals**

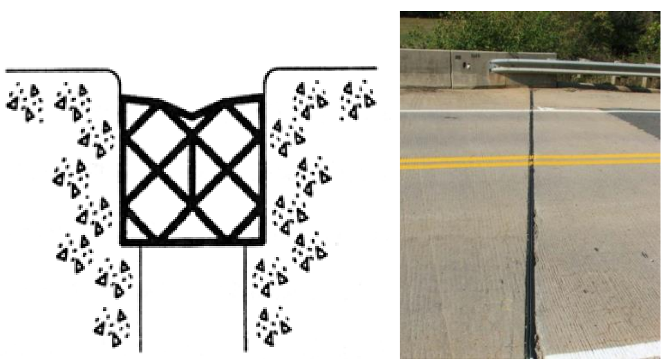

**Fig. 8: Preformed Elastomeric Compression Seals**

- **Poured (Silicone) Seals**

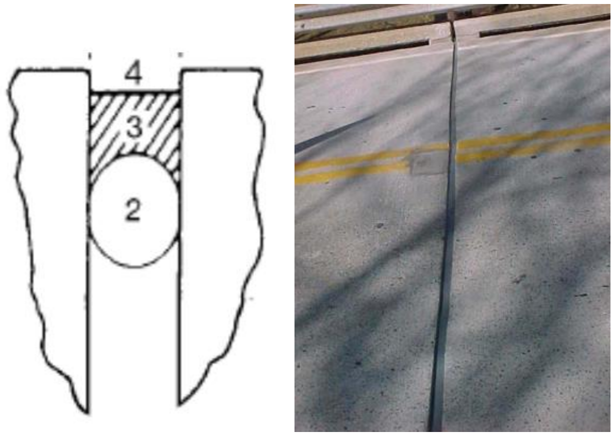


**Fig. 9: Poured (Silicone) Seals**

- **Asphalt Plug Joints**

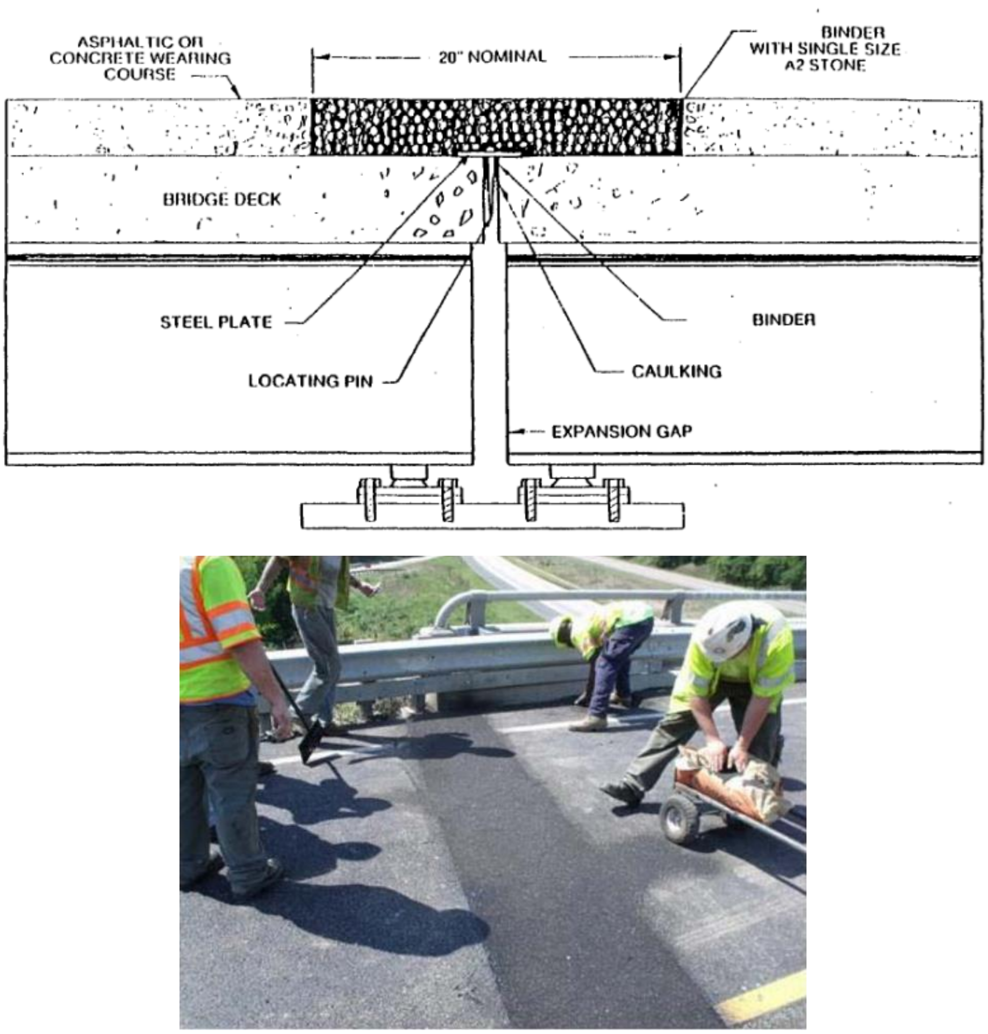


**Fig. 10: Asphalt Plug Joints**

- **Strip Seals**

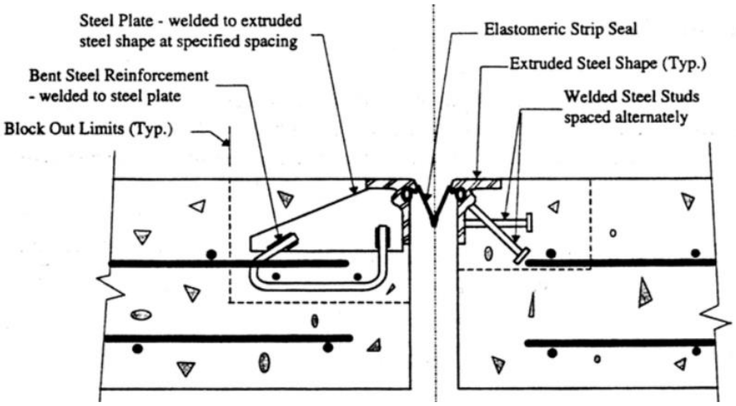


**Fig. 11: Strip Seals**

- **Sliding Plate Joints**

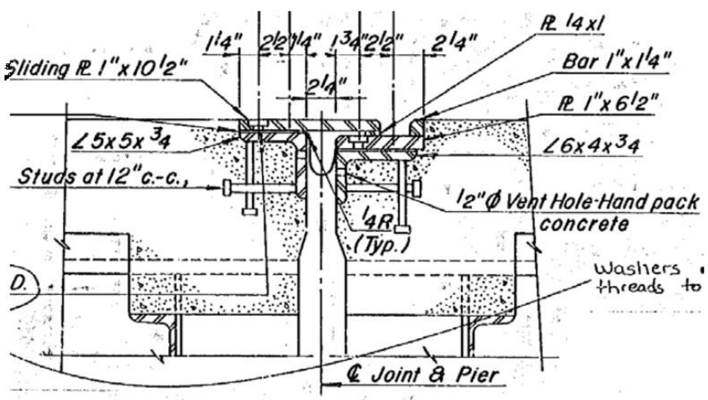


- **Finger Joints**

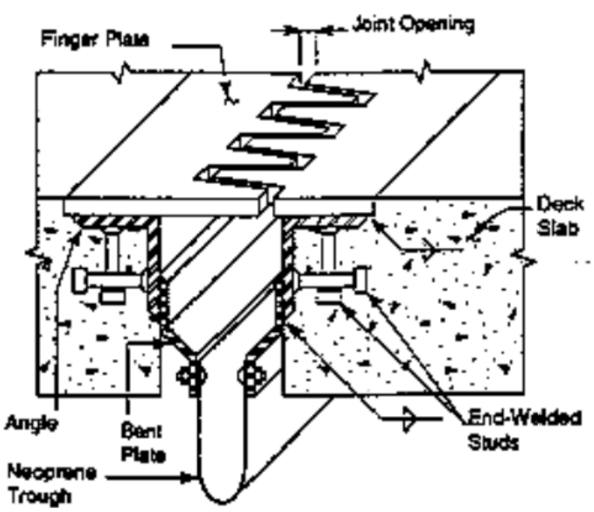


**Fig. 12: Finger Joints**

- **Cushion Seal (Elastomeric Expansion Dam)**

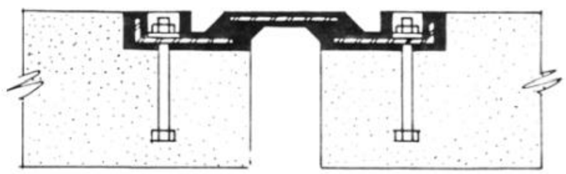

**Fig. 13: Cushion Seal (Elastomeric Expansion Dam)**

Xu et al. 2018 discussed an approach taken to rehabilitate the Shili Bridge by eliminating expansion joints and retrofitting the structure from simply-supported concrete box girders into a continuous bridge. Condition assessments were performed before retrofitting. In addition, several design options and construction procedures were considered and analyzed. Static and dynamic load tests were carried out after the completion of rehabilitation. The lessons learned in this project are presented and discussed. This practical and novel methodology was a step forward toward improving safety, sustainability, reliability, and quality of such existing bridges in China and elsewhere. It was concluded that Continuity of side-by-side box girders not only eliminated joints between the spans, but also reduced the positive moment at midspan by introducing negative dead load bending moment over the supports. Removal of joints over the abutments enhances bridge durability and eliminates the typical bump at the ends of a bridge. These factors would contribute to improved bridge durability, better ride quality, and reduced maintenance costs. The rehabilitation and strengthening of Shili Bridge provides a basis for the retrofitting of similar existing bridges to address durability and deterioration problems. Providing continuity can also reduce the amount of strengthening materials (CFRP and metal plates) that may be needed along the bottom of the girders. This is because the length of the positive bending moment region would be shortened after continuity of girders is achieved, thus reducing construction quantities and achieving overall cost savings. Steps must be taken to limit any restraints to the free sliding of the approach slab. A separation is needed between the sliding approach slab and the curbs to ensure that the approach slab can slide as freely as possible.

Groli et al. (2014) conducted an experimental campaign aimed at validating a previously published simplified serviceability design method of the columns of long jointless structures. The proposed method was also extended to include tension stiffening effects which proved to be significant in structures with a small amount of reinforcement subjected to small axial loading. This refinement allowed significant improvement of predictions for this type of element. The campaign involved columns with different reinforcement and axial load ratios, given that these parameters had been identified as crucial when designing columns subjected to imposed displacements. Experimental results were presented and discussed, with particular regard to cracking behaviour and structural stiffness. Considerations on tension stiffening effects were also made. Finally, the application of the method to typical bridge and building cases was presented, showing the feasibility of jointless construction, and the limits which should be respected.

Mothe (2006) investigated the behavior of the link-slab and its effect on the behavior of the bridge system as a whole. The scope of the study was to develop FE models to analyze the variation of forces, stresses and moments in the link-slab as well as the level of continuity generated in the girder system. The analysis was carried out for different bridge parameters which are likely to affect the behavior of link-slab; namely, bearing stiffness, skew angle, span lengths and debonding length ratio of link-slab. The study helped in understanding the effects of the aforementioned factors on the behavior of the link-slab and the system. The study also proposed development of a modified three moment equation for different parameters. The parameters which influence the three moment expression are the bearing stiffnesses, material properties and geometric information. A thorough parametric study is required to validate the expression. The results can be used for development of a design procedure for the link-slab and the expression can be used for analysis of the link-slab. The results obtained showed that the link-slab behaves more like a tensile member rather than a bending member with the increase in bearing stiffness and debonding length ratios. This observation was consistent in all the bridge types and skew angles considered for the study.

Ho and Lukashenko (2011) described the available design methodologies and provide an example of its application for a bridge retrofit. Link-slabs are currently being installed in new bridge construction, and also used to replace expansion joints in the rehabilitation of existing structures. The applicable use of link-slabs in the field is limited by variables such as girder end rotation from applied loads, bridge skew, and girder depth. Link-slabs are designed to flex, however excessive deflection causes potential for the development of wide cracks, exposing the interior steel reinforcement to susceptibility of corrosion. The concrete deck is typically composite with the supporting steel or concrete girders, but is debonded in the link-slab region to increase the link-slab curvature length, resulting in a reduced slab flexure and minimizing cracking. Although flexural cracking cannot be completely eliminated, water ingress into the cracks can be controlled by the following design considerations: limiting deck crack opening width by limiting end girder rotation; application of waterproofing membrane on top of concrete deck; and use of fiber reinforced concrete in the link-slab. It was indicated that examples of successful link-slab applications have been implemented in Ontario, Canada and Michigan, USA. The benefits of the use of link-slabs include reduced costs for maintenance of expansion joints, and less reinforcing steel in the deck resulting in less construction time and cost. Also with the elimination of expansion joints, there is less likelihood of chlorides permeating through the joint and causing corrosion and damage to the reinforced deck and substructure components. The use of link-slabs are slowly gaining acceptance as Canadian Ministries of Transportation learn more about their benefits of reduced maintenance costs over the lifespan of new or rehabilitated structures. It is recommended that these link-slabs be monitored over their service lives to better determine their long-term effectiveness.

Kendall et al. (2008) developed and applied an integrated life-cycle assessment and life-cycle cost analysis model to enhance the sustainability of concrete bridge infrastructure. The objective of that model was to compare alternative bridge deck designs from a sustainability perspective that accounts for total life-cycle costs including agency, user, and environmental costs. A conventional concrete bridge deck and an alternative engineered cementitious composite link-slab design were examined. Despite higher initial costs and greater material related environmental impacts on a per mass basis, the link-slab design results in lower life-cycle costs and reduced environmental impacts when evaluated over the entire life cycle. Traffic delay caused by construction comprises 91% of total costs for both designs. Costs to the funding agency comprise less than 3% of total costs, and environmental costs are less than 0.5%. These results showed life-cycle modeling is an important decision-making tool since initial costs and agency costs are not illustrative of total life-cycle costs. Additionally, accounting for construction-related traffic delay was vital to assessing the total economic cost and environmental impact of infrastructure design decisions.

***New York DOT***

New York DOT has been building integral bridges as well as jointless decks since the late 1970s. They performed well from the beginning, but a recent study evaluated their performance to identify details possibly needing improvement in future construction. Ratings obtained during a field survey of numerous integral bridges and jointless bridge abutments were analyzed, as well as condition ratings assigned by bridge inspectors during their biennial inspections (Alampalli and Yannotti 1998). Results indicate that these bridges have been functioning as designed and showed superior performance when compared with conventional bridges. These types thus should be used whenever possible to eliminate joints in bridge construction. Details needing improvement were identified. On the basis of these observations, design changes have been recommended for future construction. Integral bridges will be limited to structures having skews less than 30 degrees pending further study. A research project was initiated for further examination of construction practices and assumptions made during the design process.

***North Carolina DOT***

Gastal and Zia (1989) performed an analysis of bridge beams with jointless decks. ElSafty (1994) conducted an analysis and investigation of jointless bridge decks with partially debonded simple span beams. Zia et al. (1998) investigated casting fully-continuous deck over simply supported girders with partial debonding of the deck from the girders ends at supports, using both numerical and experimental analysis, as shown in Fig. 2. Okeil and Elsafty (2005) investigated the partial continuity in bridge girders with jointless decks and the effect of the system’s support configuration on the axial force developed in the link-slab. Caner and Zia (1998) presented the results of a test program to investigate the behavior of link-slabs connecting two adjacent simple-span girders, and proposed a simple method for designing the link-slab. ElSafty and Okeil (2008) also investigated extending the service life of bridges using continuous decks. Wing and Kowalsky

(Wing 2005) evaluated the link-slab concept proposed earlier by Caner and Zia (1998), constructed, and instrumented a full-scale jointless bridge and its link-slabs for performance evaluation. This study has concluded that although the design rotation of the link-slab, obtained by assuming simply-supported deck, was 0.002 radian, actual rotation was far below this value. However, to control crack width, link-slabs were still heavily reinforced, thus stiffening the slab and decreasing its ability to act as a hinge between the adjacent decks. In addition, the study suggested that the performance of reinforced concrete link-slabs was highly affected by the construction quality, which most often results in large crack width.

***Michigan DOT***

***ECC:*** To overcome the problem of heavily reinforced link-slabs, Engineered Cementitious Composites (ECC) were proposed to replace conventional concrete slabs. ECC are high performance fiber reinforced cementitious composites that have high durability and strain capacity over 400 times that of a normal concrete. The tensile strain of ECC material was associated with a large number of microcracks that have a limited crack width between 50 μm and 70 μm at 1% tensile strain. These cracks do not increase in width with increasing the tensile strain even up to failure (4% strain) (Lepech and Li - 2009). Kim et al. (2004) have evaluated the performance of bridge deck link-slabs designed with ductile ECC experimentally using full-scale slabs. The results of these experiments have shown significant enhancements in deflection capacity and crack width control of link-slabs when constructed using ECC material.

Li et al. (2003 and 2005) conducted a research project with Michigan DOT describing the development of durable link-slabs for jointless bridge decks based on strain hardening cementitious composite - engineered cementitious composite (ECC). Specifically the superior ductility of ECC was utilized to accommodate bridge deck deformations imposed by girder deflection, concrete shrinkage, and temperature variations, providing a cost-effective solution to a number of deterioration problems associated with bridge deck joints. Current design concept of link-slabs was first examined to form the basis of design for ECC link-slabs. Microstructurally optimized ECC material, with good workability and satisfactory mechanical properties was then developed. After the material design, the shrinkage, shrinkage crack resistance and the freeze-thaw behavior of the pre-selected mix proportion was investigated and revealed excellent for the durability concern. Improved design of ECC link-slab/concrete deck slab interface was confirmed in numerical analysis and further strengthened by excellent reinforcement pullout and shear stud pushout behavior in ECC. Based on the above findings, monotonic and subsequent cyclic tests of full-scale ECC link-slab specimens were performed and compared with those of a conventional concrete link-slab. It was revealed that the inherent tight crack width control of ECC decouples the dependency of crack width on the amount of reinforcement. This decoupling allows the simultaneous achievement of structural need (lower flexural stiffness of the link-slab approaching the behavior of a hinge) and durability need (crack width control) of the link-slab. Overall investigation supported the contention that durable jointless concrete bridge decks may be designed and constructed with ECC link-slabs. Finally, a simple design guideline was presented. Also, the results of full scale mixing trials and demonstrations were summarized and recommendations were made along with batching sequences and mix designs for large scale mixing. A summary of construction practices and procedures was also included, followed by the results of full scale load testing on the completed ECC link slab demonstration bridge. The load tests concluded that the ECC link-slab functions as designed under bending loads.

The Michigan DOT incorporated link-slabs during deck replacements and deep resurfacing. Field performance assessment documented full-depth cracking of most of the link-slabs. These cracks allow surface water infiltration, which leads to accelerated deterioration. Ulku et al. (2009) conducted a study to address link-slab design and performance issues. The literature is inconsistent with the influence of design parameters on link-slab performance. The objective was to document the link-slab behavior of its design parameters, to propose a method to calculate the link-slab moment and axial force, and to propose recommendations for updating current design details and construction procedures. Single-girder, two-span, finite element assemblage models under various types and levels of loads in conjunction with the link-slab design parameters were used to evaluate the moments and axial forces developed in the link-slab. Analysis showed that support conditions underneath the link-slab greatly influence the link-slab moment and axial force. Use of moment interaction diagram is recommended for the design. A detailed analysis and design example is presented incorporating live load, temperature gradient load, and the support configurations.

Lepech and Li (2009) investigated the application of ECC in a bridge deck link-slab. The unique ultra-high tensile ductility and tight crack width of self-consolidating ECC was exploited in this application to improve bridge deck constructability, durability, and sustainability. Design guidelines and material specifications were developed for implementation of this ECC link-slab technology. A construction project implementing these guidelines and specifications was conducted in 2005 on an ECC-concrete bridge deck in southeast Michigan, USA. A full scale load test was conducted to explore the structural response of the constructed ECC link-slab. These load tests validated that the incorporation of an ECC link-slab in placement of a conventional expansion joint did not alter the simply supported nature of the bridge spans, and that ample strain capacity of the ECC is reserved for temperature induced straining as designed. Two years after this ECC link-slab was placed, the performance of this link-slab remains unchanged. With further long term performance monitoring and additional demonstration experience, ECC link-slab can be an effective replacement of conventional expansion joints resulting in significantly reduced bridge deck maintenance needs.

***Georgia DOT***

Snedeker et al. (2011) evaluated the performance history of continuous bridge decks in the State of Georgia, to determine why the current design detail works, to recommend a new design detail, and to recommend the maximum and/or optimum lengths of continuous bridge decks. The continuous bridge decks have continuous reinforcement over the junction of two edge beams with a construction joint for crack control. It was indicated that the current technical literature and current practices and design procedures were synthesized and summarized. GDOT maintenance reports were reviewed, and preliminary field evaluations were conducted to determine the performance of the continuous deck detail. The effects of bridge movement due to thermal strains, shrinkage, and live loads were considered in simplified analytical studies to better understand the demands placed on the GDOT continuous deck detail. A summary of the preliminary design and length recommendations were provided upon completion of Part 1 of the research.

***Europe***

In recent years, the so called jointless or integral bridge design has seen a significant rise in popularity in Europe. Whereas in the last decades, designers preferred clearly defined statical systems and only adopted jointless design principles for small structures, the new generation of engineers pushes for integral design wherever possible. This development is to some degree motivated by a paradigm shift towards life-cycle cost-orientated design. Integral bridge structures lack joints and bearings, which typically are the least durable elements and thus remove the need for costly inspections and replacements. However, the obvious advantage of reduced direct and indirect maintenance costs entails novel and complex design solutions, especially for the transition area between structure and soil body. Furthermore, their statically indeterminate nature leads to increased importance of the soil–structure interaction. Both aspects are associated with significant uncertainty.

Wendner and Strauss (2015) focused on the probabilistic performance assessment of an inclined approach slab solution for integral bridge structures of up to 150 m of total length. Findings are presented by the example of a recently constructed and ever since monitored 67-m-long prototype structure. Monitoring data recorded by a multisensor monitoring system during the first 30 months after construction serves as inputs for a probabilistic, extreme value-based assessment of critical design assumptions. In particular, (1) the modeling of boundary conditions, (2) the activated degree of earth pressure against the abutment wall, and (3) the strain distribution in the fiber-reinforced soil above the inclined approach slab were investigated. It was concluded that the combination of short and long extensometers represents a robust and cost-effective monitoring approach for relative and absolute abutment movements that has already been adopted by Austrian bridge owners. The obtained information can be used to investigate the soil–structure interaction in terms of actual boundary conditions and developing earth pressure, in case no other sensor system is available. Based on the observed linear relationship between temperature within the deck slab and recorded abutment movements, it was found that the recorded displacements account for only 42% of the expected displacements, assuming free thermal expansion. Hence, the assumption of free thermal expansion during the design of the dilatation area is highly conservative by itself. In the current engineering practice, the assumption of free thermal expansion compensates for the lack of experience regarding the actual performance of the approach slab that represents a hidden safety margin. The observed strain field is in agreement with the theoretical assumptions, showing a high strain concentration near the tip of the slab and indicating an inclined area of localized deformation going up to the surface.

Charuchaimontri et al. (2008) investigated the influence of lap reinforcement in link-slabs of highway bridges under four independent boundary conditions by using a three-dimensional nonlinear finite element code based on the microplane model. Numerical solutions for load–deflection relationships, internal force distribution and failure cracking planes are presented for link-slabs with different details of lap reinforcement. A full-scale test was performed on three reinforced concrete long span link-slabs with various lap reinforcement details subjected to mid-span loading. The comparison indicated a good agreement between the results from finite element analysis and the experiment. The model can be used to predict the effective moment of inertia of the link-slab under mid-span loading, end rotation and end translation for the development of design criteria for a link-slab.

***MTO***

To address this problem of joints in bridges, the Ministry of Transportation of Ontario (MTO) has recently rehabilitated a number of bridge decks using a debonded link-slab system to replace the deck joints at the pier locations. MTO recently carried out an experimental research study of the long-term performance of the system on scale test models that were subjected to extensive cyclic loading in the laboratory. It also conducted a load test of a recently rehabilitated structure to study its structural behavior both before and after the link-slab was constructed. The test structure was instrumented with sensors that measured deflections and strains in the link-slab and girders.

Au et al. (2013) described the experimental research study on link-slab and the behavioral load tests that were carried out, and discusses the results obtained. The experimental study showed that the long-term performance of the link-slab was not affected by the extensive cyclic loading to which the model was subjected, and the load testing of the test structure showed that it satisfied the serviceability limit state requirements of the Canadian Highway Bridge Design Code, thus validating the design methodology of the system.

***PCI***

Details of jointless bridge superstructures are available in the PCI publication, “The State-of-the-Art of precast/Prestressed Integral Bridges,” authored by the Subcommittee on Integral Bridges of the Committee on Bridges.

## THE USE OF FRC and FRP REBAR IN LINK-SLABS

Several researchers have investigated the use of Fiber-Reinforced Polymers (FRP) for bridge deck reinforcement (NCHRP – 2003) as alternatives to conventional steel reinforcement to provide corrosion resistant reinforcement that increases bridge service life and achieve economic and environmental benefits

### *FRC*

Materials with high tensile strain capacity, such as fiber-reinforced concrete (FRC), can be used for application in the link-slab to improve the strength, durability, and cracking characteristics of the link-slab. Hong (2014) established a computational model of an existing bridge (Camlachie Road Underpass). It is found that the model and modelling approach in SAP2000 closely predicted the field test results obtained by the Ministry of Transportation of Ontario (MTO). Additionally, it is established that the horizontal stiffness of the elastomeric bearings is very low and therefore the supports are representative of roller supports. Therefore, axial forces are not generated when there are no horizontal restraints in the supports.

Hong (2014) examined the properties of FRC from experimental tests. Four-point bending tests are used to estimate the ultimate and service stresses of FRC using procedures from the fib Model Code (2010). It is found that the results from the fib Model Code are in agreement with the experimental beam tests by Cameron. Therefore, it is concluded that the fib Model Code procedures are valid for calculating the ultimate and service stresses in FRC, and are used in the computational and analytical models. Hong 2014 conducted a parametric study to provide a better understanding of link-slab bridge behavior to assess the impact of design decisions on the bridge response. It is found that the use of hooked steel fibres minimized the crack width of the link-slab, and a debonded length a 5% to 7.5% is found to be optimal based on cost and serviceability. Moreover, it is found that fibres are more effective when less steel reinforcements are used in the link-slab. Lastly, a parametric study is conducted on the computational model using non-linear analysis by including FRC in the computational model in the form of plastic hinges. It is concluded that the computational model has shown signs of cracking at the pier supports, which is consistent with the site observations during the MTO field test for the Camlachie Road Underpass. Hong 2014 developed an analytical model (i.e., design guideline) on the analysis and design of link-slab bridges with FRC. It is found that the proposed analytical model is able to closely represent the link-slab bridge behavior with very small difference (2-3%), whereas the current method of analysis using Caner and Zia's approach shows a larger prediction error (16%). For the link-slab design with FRC, it is found that fibres in reinforced concrete helped increase the bending moment capacity of the link-slab by more than 10% compared to normal reinforced concrete (without fibres). The use of polypropylene fibres and hooked steel fibers in the link-slab reduces the required steel reinforcement by 3.5% and 21%, respectively, and the crack width of the link-slab reduces by more than 3 times with the addition of fibres. Okeil et al. (2013) conducted a field study in Louisiana investigating the performance of a skewed prestressed concrete bulb-tee girder bridge made continuous. The study presented details of the monitoring system developed for this project, which has been in service for more than two years. Temperature, strain, rotation, and elongation readings are presented. It was concluded that positive moments develop in bridges employing the new continuity detail. They are caused by creep and thermal effects that cause upward camber at midspans, which leads to positive moments at continuous girder ends. Seasonal and daily temperature variations can induce large restraint moments in the bridge, especially temperature gradients. The level of restraint moment due to the combined seasonal and daily temperature effects is probably the most important factor in the design of this detail because the designer has no influence on the temperatures at the bridge site. The other positive-moment-inducing factor (girder creep caused by prestressing forces) can be greatly reduced by not establishing continuity until after a large portion of the creep takes place.

***Hawaii DOT***

Reyes and N. Robertson (2011) in the report of the State of Hawaii Department of Transportation indicated that a cast-in-place link-slab has the advantage of providing good continuity at the ends of the FRCC section to the concrete or bridge deck, meaning it can be built to be flush with the bridge deck. However, because of the limitation of permanent strain in the link-slab, the effectiveness of the slab in compression is reduced. Therefore, a precracked link-slab would be more appropriate in most applications. The study also indicated that because HPFRCC concrete requires a long setting and curing time to reach its optimal strength, it may not be practical to cast-in-place especially when time is a construction consideration. The study also suggested that pre-cast slabs has the advantage of pre-cracking but are limited by the bond of the link-slab to the existing concrete. It suggested bonding through vertical dowels installed at an angle so that the slab is essentially pulled downward during tension loads, or a combination of vertical dowels and horizontal GFRP bars that would be more effective than either acting alone

## TYPES OF BEAM CONTINUITY AT PIERS

There are several alternatives to create a link-slab and or jointless superstructure over the piers. AASHTO LRFD specifications (2009), Article 5.14.1.4 allows designers to use any one of the shown methods of design. Some examples of these jointless superstructure are listed as follows:

### (a) Continuous deck slab or link-slabs supported by simple span beams

Most of the concrete beam bridges in Florida are currently built using continuous deck over the joint between beams/girders at a pier. A typical detail is shown in Fig. 14. The details do not include beam end diaphragms or debonding between the deck and beam. The absence of end diaphragms in these details significantly simplifies construction, but may not be feasible in states subjected to significant seismic activities. Some of the details include a saw-cut or tooled crack control joint in the deck over the pier that may be filled with sealant.

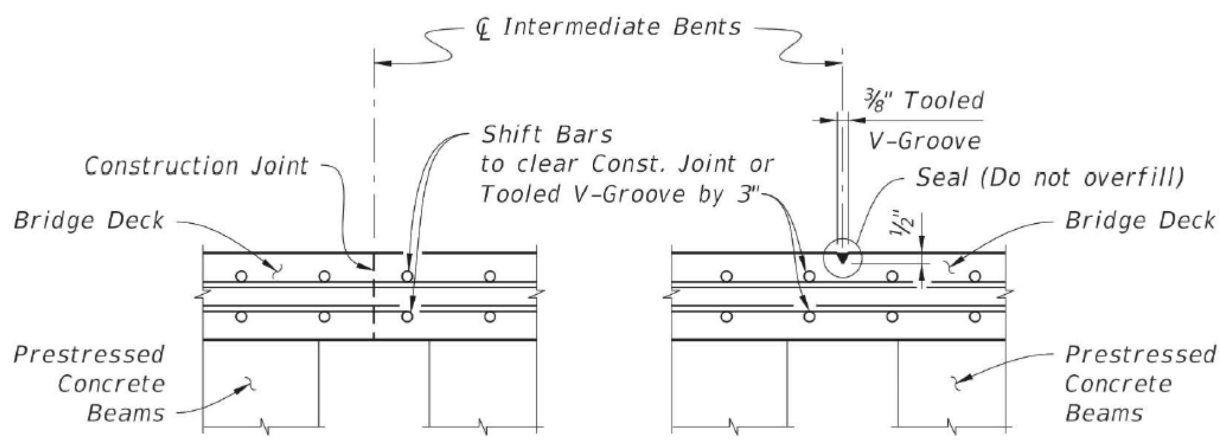


**Fig. 14: Florida Department of Transportation details for continuous slab over joint between simple spans. Figure: Florida Department of Transportation Structures Detailing Manual**

A similar method is also adopted using a link-slab to connect the simply-supported girders/beams with a continuous deck, while part of the slab is debonding from the girder ends at both sides of the joint. This detail of the link-slab with debonding results in a reduction in developed strains and cracking in the continuous deck slab since it distributes the deformations over a greater length. This method has a simpler construction than a fully continuous superstructure and is considered as a cost effective way of developing a jointless deck. To control cracking, a groove is formed, preinstalled or cut transversely in the deck at the pier centerline and may be filled with a sealant. Several researchers [ElSafty (1994); Zia et al. (1995)] provided early recommendations for design and construction of link-slabs. They recommend debonding the end 5% of the deck slab from the ends of the beams to reduce strains and control cracking in the link-slab region. Recommended analysis is to impose the end rotations of the beams on the slab. The resulting stress in the deck reinforcement should be limited to 40 ksi and cracking should be checked with current AASHTO LRFD specifications crack control provisions.

***Virginia DOT***

An example of a link-slab system used to remove expansion joints when rehabilitating bridges in Virginia is shown in Fig. 15. In this detail, which is used for relatively short spans, the debonded length is a constant 2 ft (VDOT 2013).

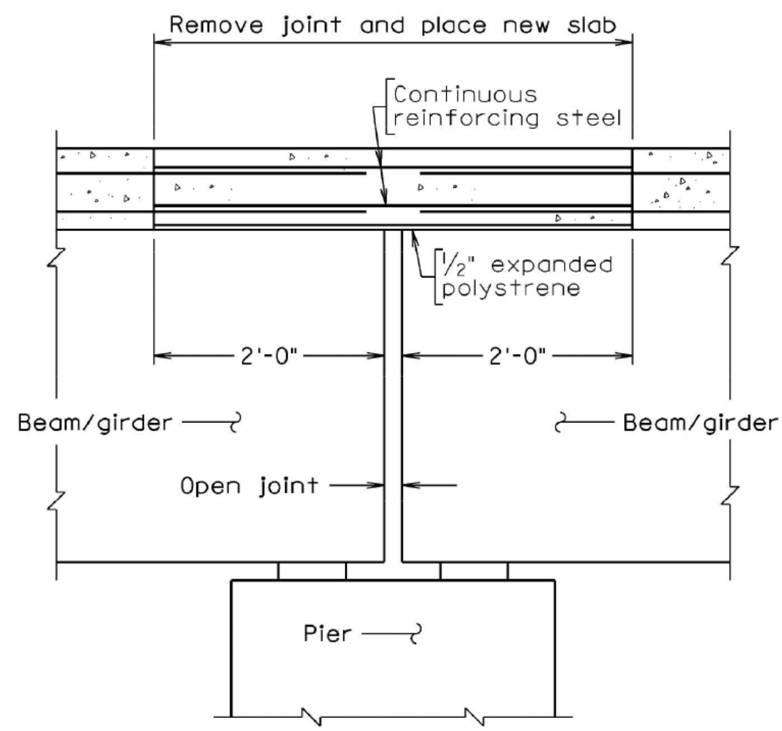


**Fig. 15: Link-slab detail used by Virginia Department of Transportation to eliminate expansion joint in rehabilitation projects**

### (b) Continuous-for-Live-Load Beams

The prestressed concrete beams are set on bearings as simple spans and the diaphragm concrete may be placed partial height (Fig. 16). The deck concrete is then placed on the simple-span beams. Longitudinal deck reinforcement that extends over the pier region is designed to resist all subsequent loads, such as live load, as a continuous span composite superstructure. This system has been performing well for more than 40 years.

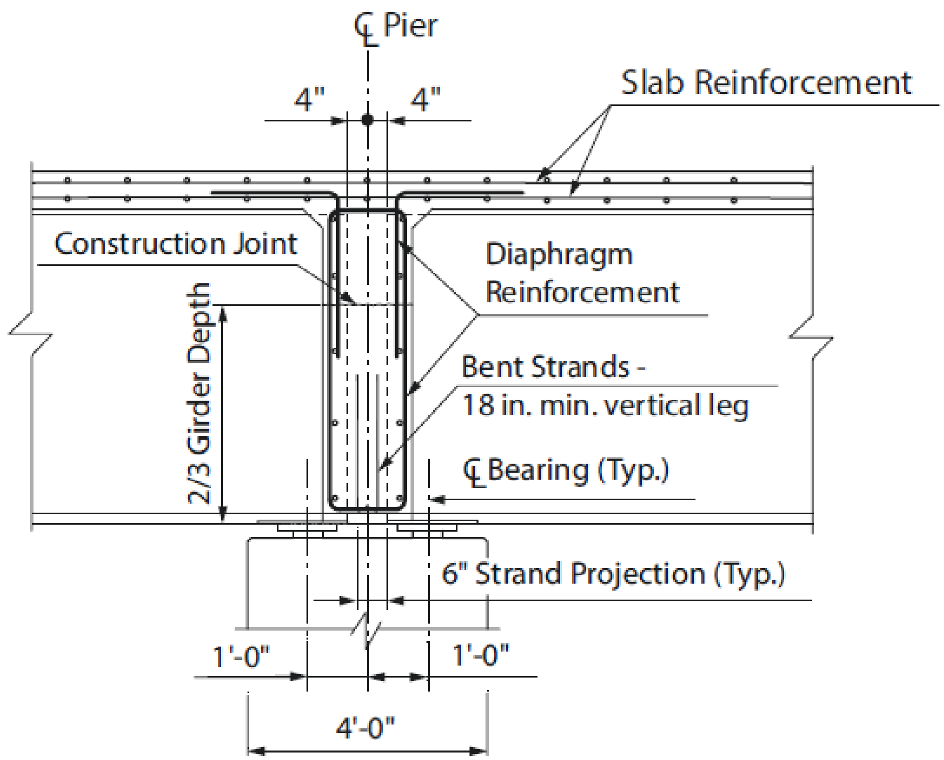


**Fig. 16: Example of pier diaphragm details with either fixed or expansion bearings (Tadros 2016)**

### (c) Threaded Rod Continuity System

A method called threaded rod continuity was reported by Sun et al. (2016), where beams were made continuous using high-strength threaded rods placed on top of the beams in the negative moment zone over the piers. The rods were embedded in a concrete placement on the top flange of the beam that is constructed at the same time as the continuity diaphragm, as shown in Fig. 17. The result is a continuous beam for deck weight as well as all subsequent loads. This system, while slightly more complicated than the continuous-for-live-load system, allows for further optimization of the capacity of the beams. Also, as an additional benefit, the negative moment due to deck weight generally offsets the long-term positive restraint moment at the pier, eliminating the need for bars or strands extending from girders to provide a positive moment connection.

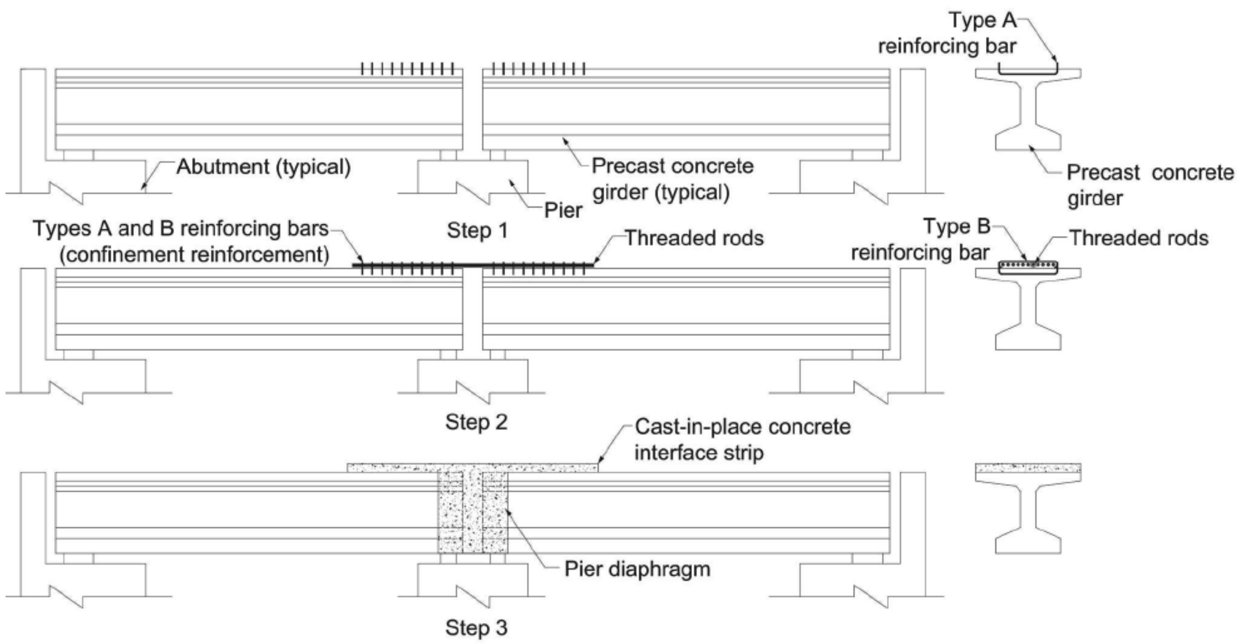


**Fig. 17: Construction steps of implementing threaded rod continuity system prior to deck placement (Sun et al. 2016)**

### (d) New Link-slab System Details

Louisiana Transportation Research Center proposed a link-slab to be designed with enough FRP reinforcement to withstand the loads placed on the slab. Also, when possible, the link-slab was designed to be uncracked while under typical service loads. Design has been in accordance with the newest ACI 440 criterion. When creating the FRP link-slab, special measures should be considered to anchor the FRP reinforcement to the existing bridge deck during the installation of a link-slab in an existing deck. Using FRP grating or FRP bars for the creation of a link-slab in a new bridge or a complete bridge deck replacement was considered.

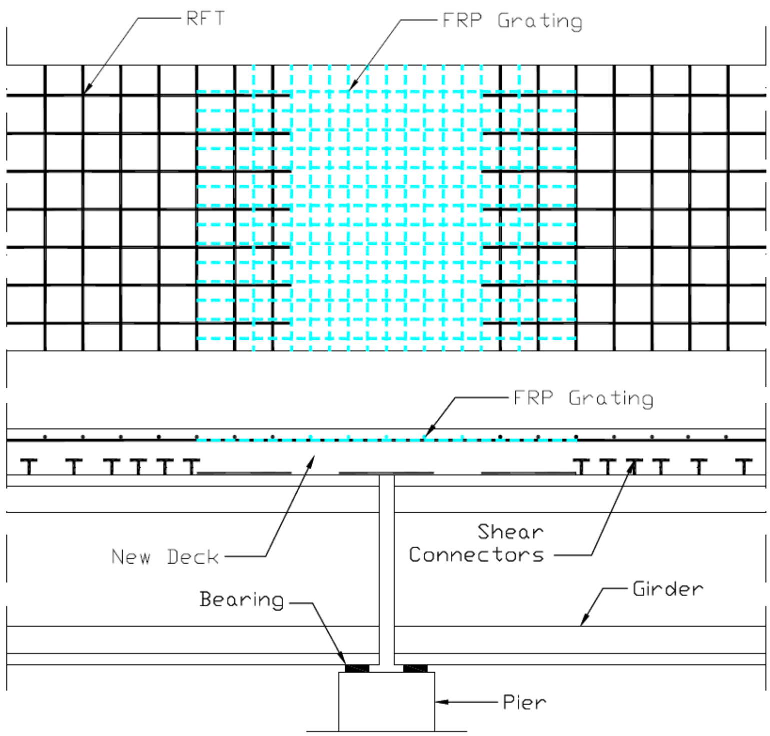


**Fig. 18:** FRP grating as reinforcement for new link-slab.

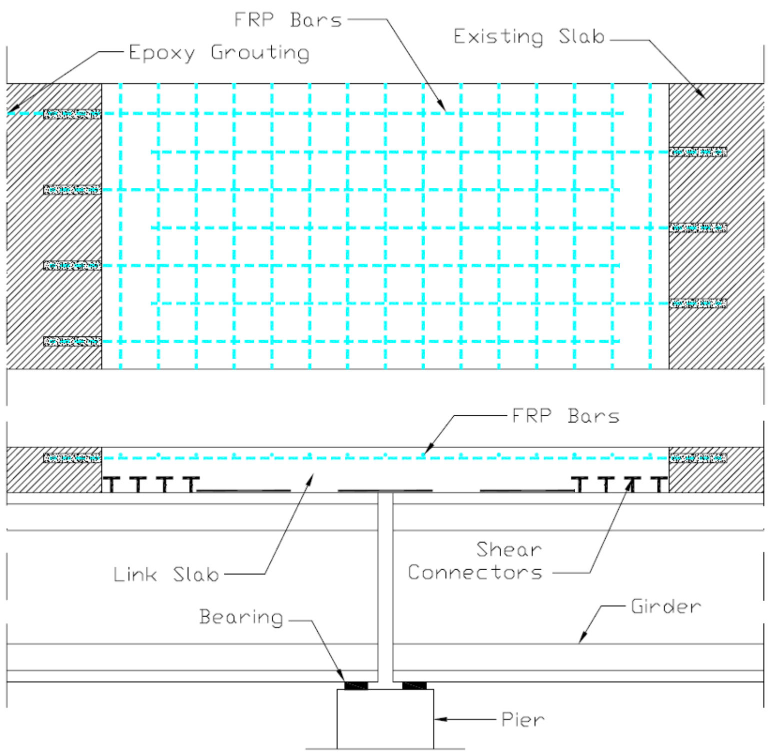


**Fig.19: FRP rebars for use in link-slab installed in existing deck**

## INSTRUMENTATION OF THE LINK-SLAB

Researches have indicated that the link-slabs were instrumented using real-time strain inducers, thermocouples, and pH meters. Data was collected during field tests and service. The data logger has record when certain strains were reached in the FRP reinforcement.

Okeil, et al. (2013) investigated a precast prestressed-concrete simple-span girders that were made continuous by pouring a continuity diaphragm between the girders ends. Special reinforcement was extended from the girders’ bottom flanges into the diaphragm to ensure continuity under positive moments that result from time-dependent effects such as creep, shrinkage, and temperature gradient. The bridge has been instrumented with embedded and surface-mounted sensors and was monitored for over 2 years to evaluate the performance of the new continuity detail. A live-load test was carried out to evaluate the response of the new detail under truck loads. A bridge segment was monitored that was a three-span continuous superstructure, 242 ft (73.8 m) long with a 45-degree skewed layout. American Association of State Highway and Transportation Officials (AASHTO) bulb-tee girders (BT-72) were used for the construction of this segment. Because of the bridge’s symmetry, only one of the identical intermediate bents was monitored. A 96-channel monitoring system was designed to record essential performance measures for evaluating the continuity detail. Several sensor types were chosen to measure temperatures, strains, rotations, crack widths, and gaps. All sensors used the vibrating wire technology, which is known to be more suitable for long-term monitoring projects because they do not suffer from drifting. Embedded as well as surface-mounted sensors were employed.

Six types of sensors were used and the monitoring system included 66 active sensors. The sensors were strategically located at midspan and on both sides of the continuity diaphragm to capture the important measures that are most influenced by continuity, such as strains in hairpin bars and the gap between adjacent girder ends. The relative movement between the bottom flanges at the ends of the adjacent girders on both sides of the continuity diaphragm was investigated using the gapmeters installed at girders. Rotations on both sides of the continuity diaphragm were recorded. All measurements were corrected for temperature changes per recommendations of the gauge manufacturer. Figure 20 shows a schematic of the sensor locations. Okeil et al. (2013) provide more details about the instrumentation. Figure 21 shows instrumentation options and details.

Live load test on the monitored segment was conducted to assess the continuity detail's performance under truck loads. Dump trucks weighing 54.1 and 57.0 kip (24.5 and 25.9 tonnes) were used to load the bridge in nine static loading cases.

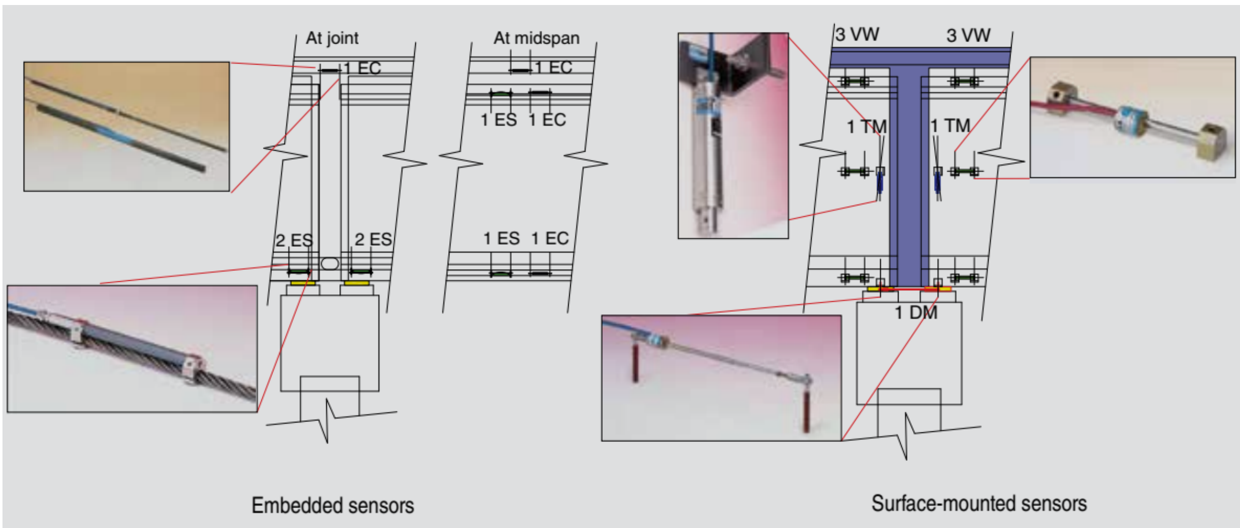


**Fig. 20: Distribution of sensors at each monitored location. Note: DM = gapmeter gauge; EC = sisterbar gauge; ES = strandmeter gauge; TM = tiltmeter gauge; VW = vibrating wire strain gauge.**

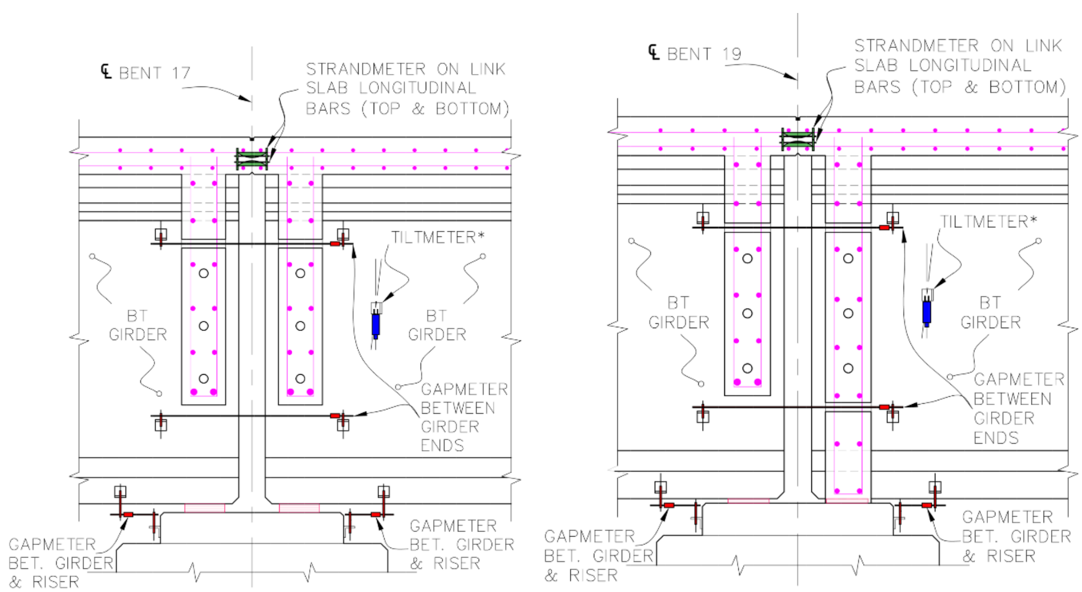

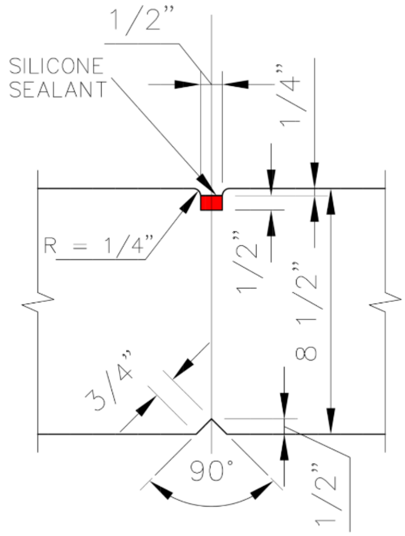


**Fig. 21: Details of typical instrumentations**

The monitoring of the tested bridge indicated that the continuity detail has the ability to transfer forces from one girder to the adjacent girder across the continuity diaphragm, as evidenced by the recorded data under long-term effects as well as live loads.

The authors concluded that seasonal and daily temperature variations can induce large restraint moments in the bridge, especially temperature gradients. The level of restraint moment due to the combined seasonal and daily temperature effects is probably the most important factor in the design of this detail because the designer has no influence on the temperatures at the bridge site. The other positive-moment-inducing factor, such as girder creep caused by prestressing forces, can be reduced by not establishing continuity until after a large portion of the creep takes place. The results from the instrumentation and monitoring also indicated that the live load test revealed that the continuity detail transferred negative and positive moments across the diaphragm. The strains from the live load test were lower than long-term effects. Even if the actual design load was to be applied (approximately twice the test live load), the strains would still be small. Therefore, the live load case should be considered in the design; however, it is not the most demanding action on the detail.

## REFERENCES


- AASHTO. (2009). AASHTO LRFD bridge design guide specifications for GFRP-reinforced concrete bridge decks and traffic railings, 1st Ed., Washington, DC.
- Alampalli, S. and Yannotti, A. P. (1998) "In-Service Performance of Integral Bridges and Jointless Decks" Transportation Research Record Journal of the Transportation Research Board 1624(1):1-7
- Au, A., Lam, C., Au, J., and Tharmabala, B (2013) "Eliminating Deck Joints Using Debonded Link Slabs: Research and Field Tests in Ontario" J. Bridge Eng., ASCE, 2013, 18(8): 768-778.
- Caner, A., and Zia, P. "Behavior and Design of Link Slabs for Jointless Decks" PCI Journal, Vol. 43, No. 3, pp. 68-80, May-June 1998.
- Caner, A., and Zia, P. (1998) "Behavior and Design of Link Slabs for Jointless Bridge Decks" PCI Journal, Page 68-80.
- Charuchaimontri, T., Senjuntichai, T., Oˇzbolt, J., and Limsuwan, E., (2008) "Effect of lap reinforcement in link slabs of highway bridges" Engineering Structures 30 (2008) 546–560.
- El-Safty, A. K., "Analysis of Jointless Bridge Decks with Partially Debonded Simple Span Beams," Ph.D. Dissertation, North Carolina State University, Raleigh, NC, 1994.
- ElSafty, A., and Okeil, A. M., (2008). "Extending the Service Life of Bridges Using Continuous Decks, PCI Journal - Precast/Prestressed Concrete Institute." PCI, Vol. 53, No. 6, pp. 96-111. 30.
- Gastal, A.L. and Zia, P. (1989). "Analysis of Bridge Beams with Jointless Decks." In: International Symposium on Durability of Structures, LISBON, Conference Report, Zurich, IABSE, ETH Honggrberg.
- Groli, G., Caldentey, A.P., Soto, A.G., Marchetto, F., and Parrotta, J.E. (2014) "Simplified serviceability design of jointless structures. Experimental verification and application to typical bridge and building structures" Engineering Structures 59 (2014) 469–483.

- Ho E. and Lukashenko, J., (2011) “LINK SLAB DECK JOINTS” 2011 Annual Conference of the Transportation Association of Canada, Edmonton, Alberta.
- Hong, Y. (2014) “Analysis and Design of Link Slabs in Jointless Bridges with Fibre Reinforced Concrete” PhD. Thesis, University of Waterloo, ON, Canada.
- Kendall, A., Keoleian, G, A., and Helfand, G.E., (2008) “Integrated Life-Cycle Assessment and Life-Cycle Cost Analysis Model for Concrete Bridge Deck Applications” J. Infrastruct. Syst., ASCE, 14(3): 214-222.
- Kim, Y. Y., Fischer, G., and Li, V. C. “Performance of Bridge Deck Link Slabs Designed with Ductile Engineered Cementitious Composite”, ACI Structural Journal, V. 101, No. 6, pp. 792-801, Nov-Dec 2004.
- Lepech., M. D. and Li. V.C. (2009) “Application of ECC for bridge deck link slabs” Materials and Structures, 42:1185–1195.
- Li, V. C., Fischer, V.C., Kim, G., Lepech, Y., Qian, M., Weimann, S., and Wang, S. (2003) “Durable Link Slabs for Jointless Bridge Decks Based on Strain-Hardening Cementitious Composites” Michigan Department of Transportation, Research Report RC-1438.
- Li, V.C., Lepech, M., and Li, M. (2005) “Field Demonstration of Durable Link Slabs for Jointless Bridge Decks Based on Strain-Hardening Cementitious Composites” Michigan Department of Transportation, Research Report RC- 1471.
- Mothe, R.N. (2006) “Partial continuity in prestressed concrete girder bridges with jointless decks” MSc. Thesis, Louisiana State University and Agricultural and Mechanical College.
- Okeil, A. M. and ElSafty, A. (2005). “Partial Continuity in Bridge Girders with Jointless Decks, Practice Periodical on Structural Design and Construction.” ASCE Journal, Vol. 10, No. 4, pp 229-238, doi:10.1061/(ASCE)1084-0680(2005)10:4(229).
- Okeil, A. M., Hossain, X., and Cai, C. S. (2013) “Field monitoring of positive moment continuity detail in a skewed prestressed concrete bulb-tee girder bridge” Spring 2013, PCI Journal, Page 80-90.
- Reyes, J. and Robertson, I.N., (2011). “PRECAST LINK SLABS FOR JOINTLESS BRIDGE DECKS.” Technical Report, Hawaii Department of Transportation

- Snedeker, K., White, D., and Kahn. L., (2011) “Evaluation of Performance and Maximum Length of Continuous Decks in Bridges – Part 1” GDOT Research Project No. 09-07, Task Order No. 02-64. Report, Page 130.
- Sun, C., N. Wang, and M. K. Tadros, M.K (2016). “Threaded Rod Continuity for Bridge Deck Weight.” PCI Journal, Precast/Prestressed Concrete Institute, Chicago, IL. V. 61, No. 3, pp. 47-67.
- Tadros, M.K. (2016), Eliminating Expansion Joints in Bridges, Concrete Bridge Technology, Aspire, pp. 32-35
- Thippeswamy, H.K., GangaRao, H.V.S., and Franco, J.M. (2002) “Performance Evaluation of Jointless Bridges” J. Bridge Eng., ASCE, 7(5): 276-289.
- Ulku, E., Attanayake, U., and Aktan, H., (2009) “Jointless Bridge Deck with Link Slabs Design for Durability” Transportation Research Record: Journal of the Transportation Research Board, No. 2131, Transportation Research Board of the National Academies, Washington, D.C., 2009, pp. 68–78.
- Virginia Department of Transportation (VDOT), Jeff Milton, (March 2013), 2013 Virginia Concrete Conference Joint Maintenance and Best Practices in Deck Joint Replacement
- Wendner, R. and Strauss, A. (2015) “Inclined Approach Slab Solution for Jointless Bridges: Performance Assessment of the Soil–Structure Interaction” J. Perform. Constr. Facil., ASCE, 29(2): 04014045.
- Wing, K. M. and Kowalsky, M. J. “Behaviour, Analysis, and Design of an Instrumented Link Slab Bridge” ASCE Journal of Bridge Engineering, Vol. 10, No. 3, pp. 331-344, May 2005.
- Xu, Z., Chen, B., Zhuang, Y., Tabatabai, H., and Huang, F. (2018) “Rehabilitation and Retrofitting of a Multispan Simply-Supported Adjacent Box Girder Bridge into a Jointless and Continuous Structure” J. Perform. Constr. Facil., ASCE, 32(1): 04017112.
- Zia, P., Caner, A., and ElSafty, A. (1995). “Jointless Bridge Decks.” Technical Report, FHWA/NC/95-006, North Carolina Department of Transportation (NCDOT).

# Appendix F

## BEI-2019 Mini-Symposium on BFRP Emerging Standards for Marine and Coastal Structures: Accepted Abstracts

a. *Basalt FRP-RC Standardization for Florida DOT Structures*
b. *Evaluation of Bond-to-Concrete Characteristic of Basalt Fiber-Reinforced Polymer Rebars for Design Code Implementation*

(2 pages)

# Basalt FRP-RC Standardization for Florida DOT Structures

Steven Nolan[1*], Chase Knight[2], Raphael Kampmann[3]

[1]: Florida Department of Transportation – State Structures Design Office, Tallahassee,FL. USA; email: Steven.Nolan@dot.state.fl.us
[2]: Florida Department of Transportation – State Materials Office, Gainesville FL. USA; email: Chase.Knight@dot.state.fl.us
[3]: FAMU-FSU College of Engineering, Tallahassee FL. USA; email: kampmann@eng.famu.fsu.edu

[*]: corresponding author

**BEI Membership**: Yes

**Keywords**: Basalt, BFRP, composite reinforcing, corrosion-resistant, standards

**Abstract**:

Fiber-reinforced polymer bars are emerging as a viable economical solution to eliminate corrosion degrading of reinforced concrete (RC) structures caused by chloride attack in both coastal and cold weather locations. The corrosion mechanism is similar in these divergent environments due to the presence of chlorides: within seawater along the coastal fringe of 20 states; and within deicing chemicals used in most of the other US states.

Significant improvements in manufacturing techniques and resin matrix materials have occurred in recent years enabling exploitation of the superior properties of Basalt FRP reinforcing bars that is now available. The Canadian Standards Association will shortly be adopting BFRP reinforcing for concrete structures in their next update to the Canadian Highway Bridge Design Code.

FDOT under their Transportation Design Innovation initiative is committed to providing resilient, sustainable, cost effective and scalable solutions to the aging infrastructure challenge. The provision of multiple material options for corrosion-resistant reinforcing is foreseen as a positive development to encourage competition, further innovation and provide a redundant supply chain for FRP materials, especially as wider deployment occurs.

Additionally, a significant amount of inferior BFRP products are reportedly now available on the world market due to the lack of standards, underlying the need and urgency for establishing robust standards in the US. This project is developing standard (guide) design specifications, and standard material and construction specifications for basalt fiber-reinforced polymer (BFRP) bars for the internal reinforcement of structural concrete for use by Florida Department of Transportation.

# Evaluation of Bond-to-Concrete Characteristic of Basalt Fiber-Reinforced Polymer Rebars for Design Code Implementation

Raphael Kampmann[1*], Tim Schneider[2]

[1]: Department of Civil & Environmental Engineering, Florida A&M University - Florida State University, College of Engineering, Tallahassee FL. email: kampmann@eng.famu.fsu.edu

[2]: ?? email: ??

[*]: corresponding author

**BEI Membership**: Yes

**Abstract**:

Due to historical developments, fiber reinforced polymer (FRP) materials in the United States are mostly based on glass (GFRP) or carbon (CFRP) and the majority of reinforcing bars (rebars) for concrete structures are GFRPs. Recently, Basalt based composites gained traction as these materials have been successfully used in Russia and China, and because US based FRP manufacturers and distributers have started to use basalt fibers for various rebar products. BFRP rebars are now considered because of the low production cost compared to CFRP rebars and due to improved chemical resistance, a higher tensile strength, and a higher modulus of elasticity compared to GFRP rebars. As the production of BFRP rebars is yet to be standardized, manufacturers around the world have produce various BFRP rebar types with different surface enhancements that affect the bond-to-concrete performance in various ways. For the study presented in this paper, it was the goal to evaluate the design-critical bond-to-concrete property for dissimilar BFRP rebar types through pullout tests according to ACI440.3R, B.3.in an effort to characterize the bond performance of various surface conditions. The evaluated independent test variables included the rebar diameter (# 3 and # 5) and the bond interface created by the various rebars (sand coated, helically grooved, and with surface lugs), and the measured dependent variables focused on the free-end slip, load-end slip, bond stress development, and interface stiffness. The results showed that the bond stiffness and rebar slip behavior are dependent on the surface enhancement features; while rebars with sand coating presented a ductile rebar slip behavior, all other surface featured lead to sudden slip preceded by a higher bond stiffness. Likewise, the strength capacity of BFRP rebar-concrete interface was affected by the surface enhancement features as well, and sand coated rebars attained the highest capacity. Each rebar type lead to a distinctive failure interface and the failure modes suggested that a limitation of the bond stiffness would be beneficial for future design code implementations.